2019

Mass Spectrometry-Based Quantitative Proteomic Analysis of Biological Fluids

Patience Akosua Afedi
South Dakota State University

MASS SPECTROMETRY-BASED QUANTITATIVE PROTEOMIC ANALYSIS OF BIOLOGICAL FLUIDS

BY

PATIENCE AKOSUA AFEDI

A dissertation submitted in partial fulfillment of the requirements for the

Doctor of Philosophy

Major in Chemistry

South Dakota State University

2019

MASS SPECTROMETRY-BASED QUANTITATIVE PROTEOMIC ANALYSIS OF BIOLOGICAL FLUIDS

PATIENCE AKOSUA AFEDI

This dissertation is approved as a creditable and independent investigation by a candidate for the Doctor of Philosophy in Chemistry degree and is acceptable for meeting the dissertation requirements for this degree. Acceptance of this does not imply that the conclusions reached by the candidate are necessarily the conclusions of the major department.

Douglas E. Raynie, Ph.D. Date

Dissertation Advisor

Head, Department of Chemistry and Biochemistry

Dean, Graduate School Date

ACKNOWLEDGEMENTS

This work is foremost dedicated to my Lord and Savior, Jesus Christ from whom I owe my very breath, strength and the grace to have come thus far.

Many thanks to my husband, Samuel Noonoo and son, Joshua Noonoo in recognition of their unflagging support, sacrifice and understanding through the often lonely years of graduate work. They made the burden bearable. I would like to thank my parents and siblings for their support and steadfast believe in me. I am grateful to my Dad, Nicholas K. Afedi for giving me an education he never had.

Special thanks to my advisor, Dr. Douglas Raynie. He graciously stepped-in midway through the program when my first advisor had to leave the school. During this difficult time, he provided the needed academic and professional guidance. He truly has been an academic foster parent. I would like to thank Dr. Linhong Jing, my first advisor. I am grateful for the opportunity to work with her.

I am indebted to my graduate committee members, Dr. Brian Logue, Dr. Suvobrata Chakravarty, Dr. Lan Xu, and Dr. Jim Rice. They have been with me from the get go and have helped in providing academic guidance these many years. Thank you. Special thanks to Dr. George Perry for his immense contributions and collaboration. Indeed, I look forward to future collaborations.

I thank all my friends for their support and encouragement especially those here in Brookings, SD who through our fellowship also provided laughter and warmth. You all made a home away from home.

TABLE OF CONTENTS

ABBREVIATIONS

2-DE	Two-dimensional electrophoresis
CAD	Coronary artery disease
DDA	Data-dependent acquisition
FDR	False discovery rate
ICAT	Isotope-coded affinity tags
iTRAQ	Isobaric tag for relative and absolute quantitation
LC	Liquid chromatography
MRM	Multiple reaction monitoring
PAGE	Polyacrylamide gel electrophoresis
PQD	Pulsed Q collision-induced dissociation
PTM	Post-translational modification
SDS	Sodium dodecyl sulfate
SILAC	Stable isotope labeling by amino acids in cell culture
TMT	Tandem mass tag
VSMC	Vascular smooth muscle cells

LIST OF FIGURES

LIST OF TABLES

ABSTRACT

MASS SPECTROMETRY-BASED QUANTITATIVE PROTEOMIC ANALYSIS OF BIOLOGICAL FLUIDS

PATIENCE AKOSUA AFEDI

2019

Proteomics is a high-throughput approach to study protein expression, structure, function, interaction, post-translational modifications, and localization in a cell or tissue. Proteomic shotgun approach was used to analyze changes in proteins in bovine follicular fluid (FF) and plasma (PL) from cows with high estradiol (HE2) or low E2 (LE2) during the pre-ovulatory period. FF creates a unique microenvironment in follicles necessary for follicle growth and oocyte maturation, and pre-ovulatory concentrations of E2 have been reported to impact several processes involved with fertility. Initial steps in the analysis involved development of an immunodepletion protocol for high abundant proteins (HAPs) in bovine PL, FF, epididymis sperm and ejaculated sperm. The determined depletion rates for the HAPs albumin, IgG, and IgA ranged from 98.7 to 99.9%. Similar depletion rate was observed for alpha-1-antitrypsin based on its gel band. Peptides were labeled with iTRAQ reagents and quantified using 2-dimentional liquid chromatography (LC) electrospray (ES)-based mass spectrometry. E2 was associated with protein changes in PL and FF. Protein expression changes between FF HE2 and FF LE2 were higher than PL HE2 and PL LE2. There were 15 up-regulated proteins and ten down-regulated

proteins in FF HE2 compared to FF LE2. Seven proteins were up-regulated and nine proteins down-regulated in PL HE2 compared to PL LE2. Proteins were more predominant in PL than in FF but the extent of protein changes with HE2 was greater in FF than in PL. Several of the differentially expressed proteins function in follicle development and were mainly categorized under cellular process and metabolic process. Pathway analysis identified the up and down-regulated proteins were predominantly associated with the complement and coagulation cascades which support the view that folliculogenesis and ovulation are hemorrhagic events. The data demonstrates E2 regulates a wide range of reproductive associated proteins in bovine PL and FF and forms the basis for further investigation of specific processes involved in such regulation. This work was also interested in characterization and quantification of atherosclerotic lesions in three regions of aortic root of *ApoE*$^{-/-}$ mice.

Atherosclerosis is the underlining cause of heart attack and stroke, the two leading cause of cardiovascular death worldwide. The three regions of the aortic root examined were the ascending aorta region (AAR), region showing the orifices of the coronary arteries marking the start of the ascending arch (OCAR) and aortic sinus region (ASR) in *ApoE*$^{-/-}$ male and female mice at different ages. 67 *ApoE*$^{-/-}$ and 27 wild type C57BL/6J mice (controls) were fed with a high fat diet (HFD) until age 8, 12, 18, or 24 weeks. Through systematic classification and quantification of lesions in each region and statistically data analysis, we found that the complexity and total atherosclerotic lesion areas in *ApoE*$^{-/-}$ mice was location and age dependent. It was slowest in the AAR with lesions progressing from dominant type I at 8 weeks, type II at 12 weeks, types III at 18 and types III and IV at 24 weeks of age. Lesion development was comparable in the OCAR and ASR regions;

types II and III lesions dominated in mice at 8 and 12 weeks of age respectively while types IV and types IV and V dominated at 18 and 24 weeks of age, respectively. Average percentage of atherosclerotic lesions typically increased from the AAR to the OCAR to the ASR at a specific age, and from 8 to 24 weeks of *ApoE*$^{-/-}$ mice at each region, correlating with the histological data. These findings would be beneficial in experimental design and targeting of lesion types in aortic roots of the popular *ApoE*$^{-/-}$ murine atherosclerosis model.

CHAPTER 1

1 LITERATURE REVIEW

1.1 Mass-spectrometry Based Proteomics

Proteomics is a high-throughput approach to study protein expression, structure, function, interaction, post-translational modifications, and localization in a cell or tissue[1]. Proteomic field involves collection of varied disciplines including molecular biology, biochemistry, bioinformatics, cell imaging by light and electron microscopy, array and chip experiments, and genetic readout experiments[1, 2]. This makes proteomics a versatile tool for studying numerous biological systems. The ability of proteomic to analyze thousands of proteins and post-translational modifications (PTMs) in a single experiment with good quality makes it advantageous over traditional methods such as western blots which often analyze one protein at a time[3].

Mass spectrometry is now the de facto method for analyzing proteomic samples, contributed greatly by advancement in mass spectrometry instrumentation including advancement in LC systems (e.g. ultra-high-pressure reversed-phase systems) and development of commercial and public software tools able to identify and quantify proteins from the numerous data generated from the MS and MS/MS analysis. Advancement in current mass spectrometry for proteomics [(e.g. quadrupole time-of-flight (QTOF), linear trap quadroupole (LTQ) and Orbitrap technology)] include improved sensitivity (ten to 50 times), data acquisition and speed (five to ten times), and number of proteins identified and quantified from a proteome (5,000–10,000 proteins)[4].

Because mass spectrometry is central to proteomics and is used in this dissertation, a theoretical background to the technology and principles is discussed below.

1.2 Mass Spectrometer

Mass spectrometric measurements are carried out in the gas phase on ionized analytes. The basic components of a mass spectrometer (Figure 1.1) are an ion source, a mass analyzer that measures the mass-to-charge ratio (*m*/*z*) of the ionized analytes, and a detector that registers the number of ions at each *m*/*z* value and displays the results in a chart form called the mass spectrum.

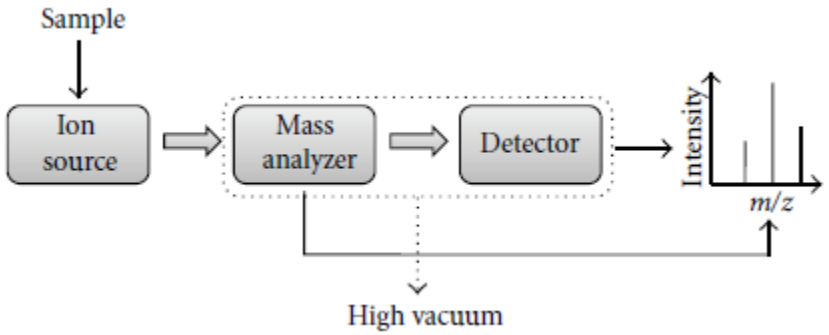

Figure 1.1. The basic components of a mass spectrometer**.** Shown in Banerjee and Mazumdar[3]. The ion source ionizes the analytes, the mass analyzer measures the mass-to-charge ratio (*m*/*z*) of the ionized analytes, and a detector registers the number of ions at each *m*/*z* value, displayed in the mass spectrum.

1.2.1 Ionization Techniques

Electrospray ionization (ESI) and matrix-assisted laser desorption/ionization (MALDI) are the two techniques most commonly used to volatize and ionize the proteins

or peptides for mass spectrometric analysis. MALDI method involves subliming and ionizing the analyte out of a dry crystalline matrix via laser pulses. ESI ionizes analytes out of a solution. MALDI is relatively used to analyze simple peptide mixtures compared to ESI method which is preferred for complex matrices[2]. ESI technique is used in this dissertation and is thus further discussed.

ESI is a soft ionization process, i.e. very little residual energy is retained by the analyte which generally results in no fragmentation of the analyte or breakage of very weak interactions like electrostatic interactions, van der Waals interactions, and hydrophobic interactions upon the ionization process. ESI also produces multiple charged ions thereby giving ions with m/z values within the mass range of all common mass analyzers. These factors make ESI a powerful and reliable tool for ionizing non-volatile thermally labile large-molecular weight biomolecules (10^5 Da), such as proteins in the gaseous states and their subsequent mass spectrometric analysis for rapid identification and structural characterization on the basis of molecular mass of the analyte. Although ESI is primarily used for biomolecules, its application has been extended to a broad range of analytes including polar organic, inorganic, and metal-organic complexes[3]. The ESI method is robust and sensitive and can detect peptides at femto levels in microliters volumes. Because ESI ionizes analytes out of a solution, it is readily coupled to liquid-based separation tools such as chromatography techniques, which allows for prefractionation of the peptides in complex mixtures thereby reducing the number of different precursors that enter the mass spectrometer at a time.

Under ESI operation, a dilute solution of the analyte is drawn to the tip of a capillary tube where a high voltage (2-6 kV) is applied. The applied voltage creates a

strong electric field which causes the dispersion of the sample solution into an aerosol of highly charged electrospray (ES) droplets with the same polarity as the applied voltage. A coaxial nebulizer gas (dry N_2) flows around the capillary and enhances the nebulization, directs the emerging charged droplets towards the mass spectrometer and helps in the solvent evaporation of the charge droplets. The charged droplets diminishes in size by solvent evaporation as it moves towards the mass spectrometer until it reaches the point (Rayleigh limit) where the surface tension can no longer sustain the Coulomb force of repulsion and results in disintegration into much smaller offspring droplets (Coulomb fission). Solvent evaporation and Coulomb fission repeats until nanodroplets are obtained from which gas-phased charge analyte molecules is formed[3].

Different models have been proposed for the mechanism for forming the gas-phase ions of the analyte from the highly charge droplets. According to the Charge Residue Model (CRM), this is proposed for large macromolecules like proteins, series of solvent evaporation and Coulomb fission result in extremely small charged droplet that contains only one analyte molecule. Desolvation of this droplet causes its charges (on the surface) to land on the analyte. Based on the Ion Evaporation Model (IEM), series of solvent evaporation and Coulomb fission decrease the radii of the charged droplets to a size when the electric field due to the charges at the surface of the droplet is strong enough to cause direct emission of the solvated ion. Thus formation of extremely small droplets is not required. Applied positive potential or positive-ion mode results in positively charged ions and applied negative potential or negative-ion mode results in negatively charge ions[3].

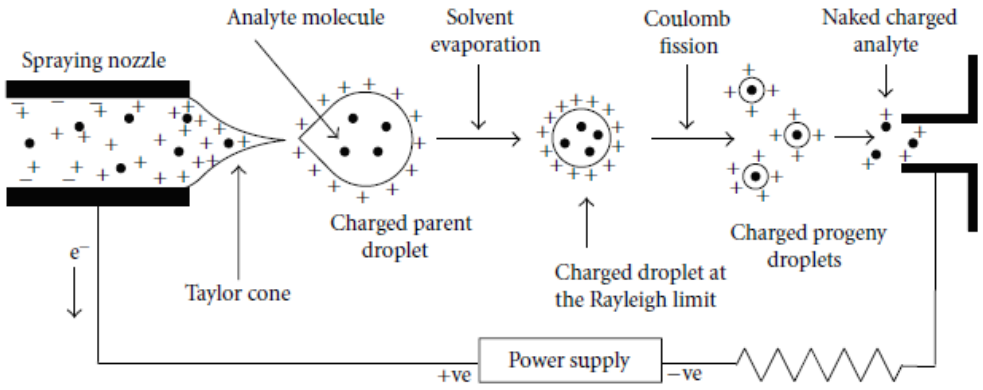

Figure 1.2. Schematic representation of the electrospray ionization (ESI) process. Shown in Banerjee and Mazumdar[3]. ESI is a soft ionization process often used to ionize proteins for mass spectrometry analysis.

To reduce flow rate which subsequently reduce space charge effect and increases ionization efficiency, small capillary electrospray emitter tips are employed (nano-electrospray). Nano-electrospray is able to achieve a constant signal for 10-30 minutes for a 1 µl sample. The nano-electrospray is more tolerable to high aqueous solvents and salt contamination compared to conventional electrospray. Because less sample volume is used in nano-electrospray, sample lasts longer enabling multiple experiments to be performed[3].

1.2.2 Mass Analyzers

The mass analyzer is central to the mass spectrometer. There are four basic types of mass analyzers currently used in proteomics research. These are the ion trap, time-of-flight (TOF), quadrupole, and fourier transform ion cyclotron (FT-MS) which is currently being replaced by the orbitrap analyzer. These vary in design and in key parameters that characterize a mass analyzer, namely sensitivity, resolution, mass accuracy, and the ability to generate information-rich ion mass spectra from peptide fragments. Mass

analyzers can be stand alone or, in some cases, put together in tandem to take advantage of the strengths of each. This dissertation used the Finnigan Linear Trap Quadropole (LTQ) (Thermo Fisher Scientific). It consists of a 2-dimentional (2-D) quadrupole ion trap analyzer.

Ion trap analyzers are typically composed of four rod-shaped electrodes, to which DC and AC are applied to produce electric fields that confine ions of interest in space prior to subsequent MS or MS/MS analysis. AC of same amplitude but opposite sign (i.e. positive and negative polarity) within the radio frequency (RF) range is applied to pairs of electrodes (This is referred to as the 'main RF') helps to confine ions radially and induce ion motion. The applied DC helps to confine ions axially. Ions of interest are isolated (i.e. trapped) and unwanted ions are simultaneously ejected via resonance ejection. Simultaneous resonance ejection is achieved by applying a superimposed AC wave containing secular frequency values (q) matching each of the unwanted ion's secular motion to the exit rod[5]. In two dimensional (2-D) trap, also called linear ion tap (LIT) (Figure 1.3), the forces act on the ions only in the x and y dimensions. This allows them to spread out axially and increases the ion capacity compared to conventional three dimensional (3-D) traps. Therefore LIT has increased resolution, sensitivity, and mass accuracy than the 3-D trap and is more commonly used[2, 6]. Accordingly, the Finnigan LTQ mass spectrometer is robust, has high sensitivity, and provides rapid and reproducible mass spectrometric analysis of complex samples.

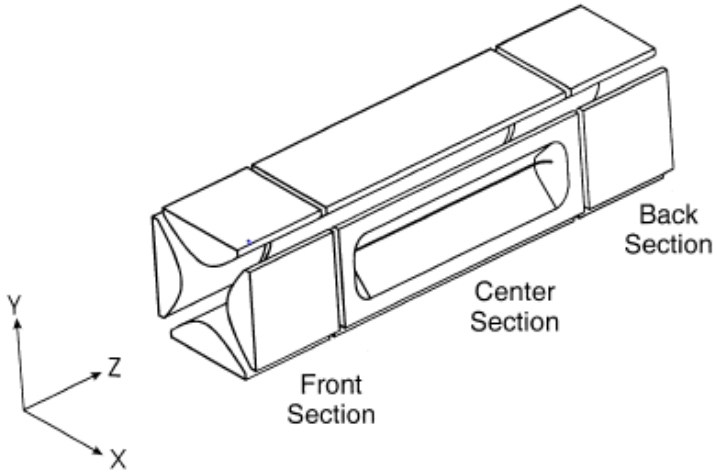

Figure 1.3. Basic design of the two-dimensional quadrupole ion trap. Shown in Schwartzet et al.[6] The Finnigan LTQ mass spectrometer used in this dissertation consists of this type of analyzer.

1.2.3 Fragmentation Techniques for Proteomics

There are a number of techniques used to generate the fragment ions of precursor ions. These include collision-induced dissociation (CID), electron-capture dissociation (ECD), electron-transfer dissociation (ETD), surface-induced dissociation (SID), and infrared multiphoton dissociation (IRMPD). CID is the most widely used method to generate fragment ion. In CID, the gaseous precursor ion is allowed to collide with an inert and neutral target gas (e.g. N_2, He, Ar) in the collision cell. Upon the collision, the precursor ion gains some of the kinetic energy which is converted into internal energy. Thus, an unstable excited state precursor ion is produced which then decompose into the product ions. CID mainly forms N-terminal a- and b-fragments, and C-terminal y-fragment**.** Among the ion types, b and y are the most common, formed from the breakage of the amide bonds of the peptide backbone[3]. Figure 1.4 shows formation of b- and y-

ions. a-ion can be formed from neutral loss of carbon monoxide from b-ion. CID was used in the identification of proteins in high abundant proteins (HAPs) and low abundant proteins (LAPs)/depleted fractions in plasma and FF in this dissertation.

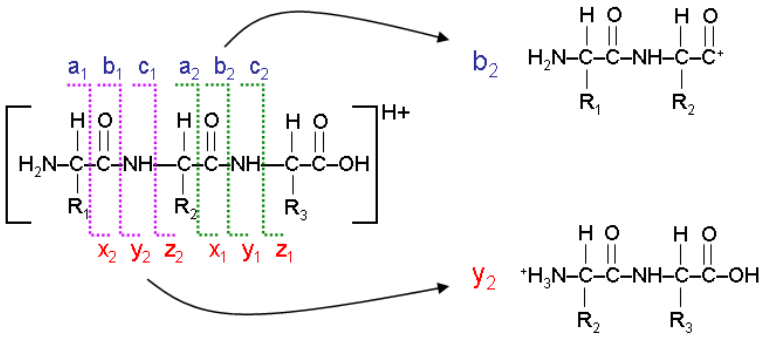

Figure 1.4. Formation of fragment ions from a peptide backbone. b- and y-ions are commonly formed with CID and are formed via breakage of the peptide bond. a-ion can be formed from neutral loss of carbon monoxide from b-ion. (http://www.alchemistmatt.com/mwthelp/peptidefragmodelling.htm).

1.2.3.1 Pulsed Q Collision-Induced Dissociation (PQD)

Pulsed Q Collision-Induced Dissociation (PQD) was developed by Thermo Fisher Scientific and implemented exclusively for their LIT mass spectrometers. PQD involves activating the precursor ion at a high activation (Q) value (0.6-0.8 eV) and using a short (~100 μs), high amplitude resonance excitation pulse. In this step, the ions with *m/z* resonant to this excitation pulse absorb energy and become kinetically excited. Next, ions are held at the high Q value for a short period (delay time ~ 100 μs), which is long enough for the kinetic energy of the ions to be converted into internal energy through collisions, but not long enough for significant dissociation to occur. Subsequently, the

precursor ions' Q value is pulsed to a low value by rapidly dropping the RF amplitude and then allowing the precursor ions to undergo fragmentation at this low Q value[7].

PQD generates spectra qualitatively similar to CID but additionally allows the observation of low *m/z* fragments that are usually excluded from CID spectra due to the "1/3 rule". PQD therefore eliminates the need for MS^3 which is often required with CID in ion trap instruments in order to detect low *m/z* fragments[7, 8]. Because of its ability to detect product ions of low *m/z*, it has been applied successfully to detect the signature low-mass reporter ions (ranges from 114.1 to 121.1) of Isobaric Tag for Relative and Absolute Quantification (iTRAQ) labels for the quantification of peptides[9]. PQD was also successfully employed with iTRAQ labeling in this dissertation.

1.2.4 Tandem Mass Spectrometry

Tandem mass spectrometry (MS/MS) is a method where the gaseous ions are subjected to two or more sequential stages of mass analysis (which may be separated spatially or temporally) according to quotient mass/charge[3]. In MS/MS analysis, a precursor ion (parent ion) is selected by a mass analyser (Q1) and then focused into a collision cell (q2) where it undergoes gas-phased reactions to generate different fragment ions (daughter/product ions) of different masses. Another analyser (Q3) scans the masses of the product ions and generates the product ion spectrum. The MS/MS technique is selective, accurate, reproducible, and enhances the lower limit of detection for peptides by up to 100-fold compared to unbiased MS analysis. It also has multiplex capability in that it can analyze and quantitate hundreds of proteins per run, thereby increasing the throughput.

1.2.5 Data Dependent Acquisition and Data Independent Acquisition

LC-MS/MS experiments in Data Dependent Acquisition (DDA) mode[10, 11] is the standard method for proteomic profiling, biomarker discovery, and relative quantification of proteins through the use of stable-isotope labels. DDA is a method of choice due to its flexibility, breadth of detection, and the simplicity of its setup and analysis. In DDA, the instrument cycles through first a short MS1 survey scan of currently eluting peptides which serves to monitor peptides intensities and identifies the most intense ions and potential sites to fragment. In the sequential MS2 scans, the most abundant precursor ions are individually isolated and fragmented in order of decreasing precursor ion intensity. The number of MS2 scans (or number of the top precursors) can be predefined by the user up to ten MS2 scans. Both MS scan and MS2 scans can occur in a duty cycle of approximately 1s up to 2 s with 10 MS2 scans. DDA can be limited in reproducibility and precision if too many peptides co-elute and appear in a single MS scan and only the most abundant peptides are selected thereby missing the rest. Also, it can prevent the measurements of low abundant proteins. Therefore, prior protein and peptide fractionations can be critical to successful application of DDA. Data generated in this dissertation used DDA and the optimized DDA parameters[12] used are stated at the relevant sections.

Data Independent Acquisition (DIA) involves repeatedly selecting all peptides within a large predefined mass ranges for MS2 scans. This generates highly complex MS2 spectra which can be analyzed aided by spectral libraries derived from prior DIA experiments or auxiliary DDA data. The complexity of the DIA MS2 data makes it

difficult to analyze and this is currently the main disadvantage of using this method. Recently however, DIA is gaining more attention with the development of bioinformatics softwares such as DIA-Umpire, OpenSWATH, and SWATHProphet, able to analyze DIA data[10]. DIA is also limited in reproducibility and measurement of low abundant proteins as their signals can be dwarfed by more abundant proteins.

1.3 Shotgun/Bottom-up Proteomic Workflow

Advances in all areas of LCMS analysis including LC instrumentation and bioinformatics for handling MS/MS generated data, generation of complete gene sequences for a wide variety of organisms, and robust sample preparation and quantification techniques are increasingly making proteomics a reliable tool for investigating the proteome[13]. Proteomic workflows typically follow either the 'bottom-up approach' or top-down approach[14]. In bottom-up, the analysis is performed on proteolytic peptides of the protein while in top-down, the intact protein is analyzed. When bottom-up analysis is performed on a mixture of proteins it is called shotgun proteomics. Shotgun proteomics is superior for the analysis of complex matrices. In this dissertation, the shotgun proteomics approach was optimized and the main steps in our in-house workflow are shown in Figure 1.5.

1.3.1 Protein Prefractionation

Biological samples are complex matrices that contain wide dynamic range in protein concentrations. The dynamic range in protein concentrations in plasma is said to span 10 to 12 orders of magnitude[15, 16]. Albumin and IgG, the top two high-abundant

proteins (HAPs) in plasma constitute about 60% of the total plasma proteome[17, 18] and the top 12 abundant proteins make-up ~95% of the total protein mass[15, 19]. Proteomic analysis of complex biological samples is therefore limited in the limit of detection (LOD), limit of quantification (LOQ), and the linear range of response. Shotgun workflows can incorporate prefractionation methods for separation of proteins mixture to reduce these limitations. Available prefractionation methods include 1- and 2-dimensional polyacrylamide gel-electrophoresis, depletion, and isoelectric focusing (IEF)[14]. Depletion is done to separate the HAPs from the low-abundant proteins (LAPs). Removal of the HAPs enhance the detection of LAPs which otherwise are masked by the HAPs. Immunodepletion involves the use of antibodies in the separation. Our lab optimized sodium dodecyl sulfate polyacrylamide gel electrophoresis (SDS-PAGE) and immunodepletion for the separation of protein mixtures in bovine plasma (PL), follicular fluid (FF), ejaculated sperm, and epididymal sperm samples. Detailed description of the depletion protocol development and optimization is discussed in chapter 2.

SDS-PAGE is a common, simple, rapid, and sensitive fractionation method to separate intact proteins[20]. The sodium dodecyl sulfate (SDS) denatures and disrupts the structure of proteins and confer uniform negative charge to the proteins such that the proteins separate primarily based on molecular weight. Separated protein gel bands can be detected by Coomassie Brilliant Blue or silver staining but the former is preferred for shotgun proteomics due to better linearity of signal and amenability to LC-MS/MS[14]. For LC-MS/MS, gel bands are excised and digested by the in-gel trypsin digestion method[21] prior to analysis. In this dissertation, SDS-PAGE was used to separate crude, bound, and depleted fractions of PL, FF, and epididymal and ejaculated sperm samples.

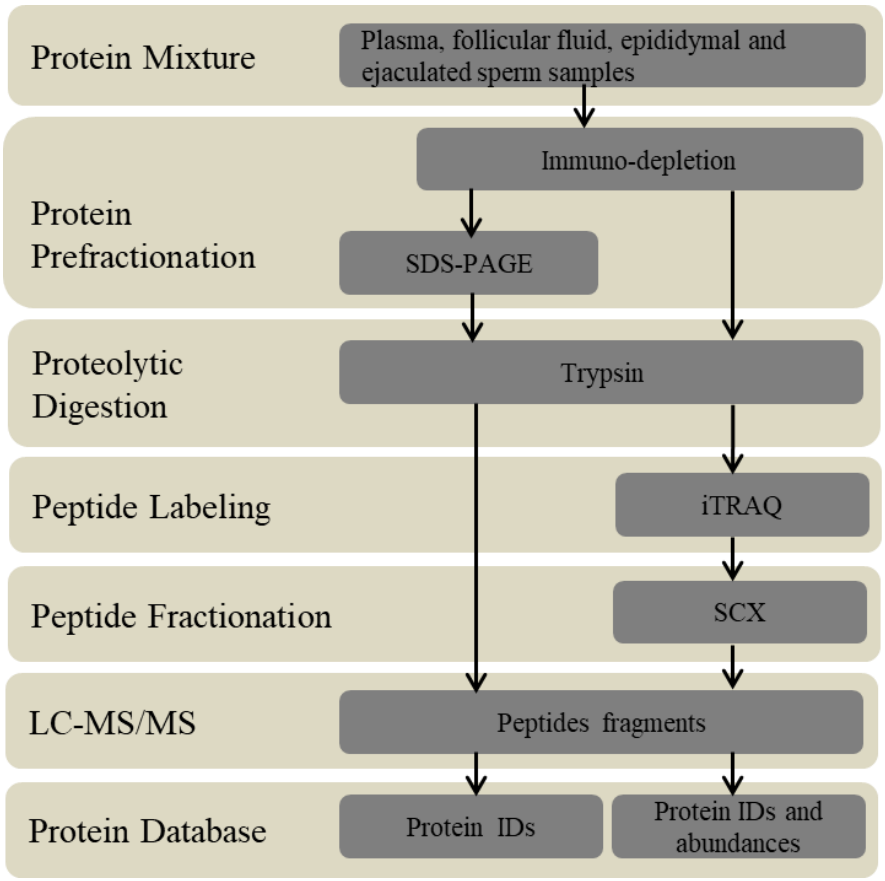

Figure 1.5. Shotgun proteomic workflow used in-house.

1.3.2 Proteolytic Digestion

Proteolytic digestion of intact proteins generates peptides with masses able to be analyzed by mass spectrometry. Trypsin has become the gold standard for protein digestion to peptides for shotgun proteomics[13, 14] and is used in this dissertation. Trypsin cleaves the carboxyl side of arginine and lysine. This sequence specific information is utilized in the identification of peptides and proteins during database search on LC-MS/MS data. Apart from its high specificity, trypsin is also preferred because it generates

suitable size peptides (10-15 amino acids residue long) and produces double charged precursor ions which fragment efficiently in CID[12].

1.3.3 Peptide Fractionation

The mixture of peptides from proteolytic digests of protein mixture is often too complex for current mass spectrometers to deal with all at once despite the recent progress in mass spectrometry. An optimized peptide fractionation method prior to MS analysis therefore becomes necessary to increase peak capacity (i.e. the number of peaks that can be resolved in a unit resolution) and to assure that the number of peptides that simultaneously enter the mass spectrometer stays within analyzable limits. This will enable more proteins to be identified and quantified[22]. Among peptide fractionation methods, liquid chromatography (LC) is often a method of choice because differences in charge and hydrophobicity of peptides can be exploited to assure high resolution of peptides. Adequate resolution of peptides of similar masses is crucial for obtaining distinct no-mixed fragmentation spectra. LC is also commonly used because of its amenability to mass spectrometry, high throughput, and sensitivity. Coupling nano-electrospray to reverse-phase nanoflow liquid chromatography (RPnLC) has been shown to give the largest gain in sensitivity from peptide separation[14, 22]. Typically, one or more chromatographic techniques, such as strong cation exchange (SCX) or hydrophilic interaction chromatography (HILIC), are coupled to RPnLC to further enhance peptide separations. Multidimensional liquid chromatography techniques are now routinely being coupled to tandem mass spectrometry to provide a robust method to identify proteins in complex mixtures.

Strong-cation exchange-reversed phase (SCX-RP), HILIC-RP, and RP-RP 2D systems have been shown to provide suitable orthogonality, i.e. the separation properties in first dimension do not affect that in the second dimension[22]. Orthogonality is crucial for maximizing peak capacity. The SCX-RP has become a popular method in shotgun proteomics, known as multidimensional protein identification technology (MudPIT)[23], due to high sensitivity resulting from the high capacity of strong cation-exchange (SCX) resin and the high resolution of SCX and RP[24]. In SCX, peptides are displaced from the SCX resin by increasing salt concentration. Each collected fraction is then loaded onto a RP column where it is separated using an organic gradient. The SCX separation can be done offline or online in which case the eluted fraction is loaded directly onto the RP column. SCX-RP was successfully used in this dissertation.

1.3.4 Protein identification

Proteins identification with mass spectroscopy is commonly by database search via a number of approaches. Peptide mass fingerprint or peptide mass map analysis approaches[25] involve determining the masses of experimental peptides derived from proteolytic digests of the proteins. Proteins are then identified based on comparison of the experimental masses with theoretical masses of peptides produced *in silico* by digestion of sequences in a target database by the same digestion enzyme as used in the experiment. Because peptide mass fingerprinting basically requires purified target protein, prior fractionation of proteins is necessary and often 1D and 2-D gel electrophoresis is used.

Protein identification using MS/MS data offer greater degree of specificity than peptide mass fingerprinting as it combines fragment ion patterns with peptide masses. This approach is more suitable for analysis of complex mixtures and is steadily replacing peptide mass fingerprinting. It involves scanning the product ion spectra against comprehensive protein sequence databases using one of a number of different algorithms. The 'peptide sequence tag' approach extracts a short, unambiguous amino acid sequence from the peak pattern that, when combined with the mass information, is a specific probe to determine the origin of the peptide. A common approach is to calculate a score based on comparison of calculated fragments from peptides sequences in the database with observed peaks. The calculated score reflects the statistical significance of the match between the spectrum and the sequences contained in a database. In another approach called the cross-correlation method, the search algorithm uses peptide sequences in the database to construct theoretical mass spectra and the overlap or 'cross-correlation' (known as xcorr) of these predicted spectra with the measured mass spectra determines the best match[2, 13]. The xcorr value is thus a statistical measure of the extent of correlation between measured and theoretical fragment spectra and shows the peptide sequence with the best match or score.

The cross-correlation approach is used in one of the most popular peak-finding search engine, SEQUEST™ (Thermo-Fisher Scientific). This work utilized SEQUEST embedded in Proteome Discoverer (Thermo-Fisher Scientific) and searched the bovine protein FASTA database. The Proteome Discoverer application extracts relevant MS/MS spectra from the raw file and determines the precursor charge state and the quality of the fragmentation spectrum. SEQUEST searches the raw data and generates a peak list and

relative abundances. The peaks represent the fragments of peptides for a given mass and charge. SEQUEST then used the cross-correlation scoring system and assigns xcorr values for peptide candidates. To help increase confidence and validate protein identifications, the Proteome Discoverer application also uses a probability-based scoring system to independently rate the relevance of the best matches identified by the SEQUEST algorithm. The output of this is the false discovery rates (FDRs) or false positive rates values. FDR value estimates the number of false positive identifications among all identifications found by a peptide identification search. Determination of FDR involves searching spectra against a database of decoy (fake) peptides, typically derived from digesting *in silico* the inverted or scrambled sequences of expected proteins.

As discussed above, the bulk of proteomic data is generated by database search using search algorithms. All search engines allow for the setting of a number of variables such as molecular mass range, polarity, precursor mass tolerance, fragment mass tolerance, scan type, activation type, proteolytic enzyme used and the maximum allowed missed cleavage sites by the enzyme, number of charges, maximum number of peptides considered for a peptide match, maximum protein references per peptide, type of fragment ion (e.g. b- and y- ions), and possible modifications (either static or dynamic) to certain residues such as alkylation of cysteine, oxidation of methionine or phosphorylation of residues including serine, threonine and tyrosine. Search parameters for database search should be chosen carefully and some parameters such as precursor and fragment mass tolerance may need to be optimized to generate relevant data. Summary of search parameters used in this dissertation are stated at the relevant sections.

1.3.5 Quantitative Proteomics

Protein quantitative data is important for modeling the cellular and metabolic response of an organism and also help in the designing of inhibitors for specific target in disease conditions[26]. Methods for protein quantification by mass spectrometry can be grouped into two: label-free methods and stable isotope labeling methods. In either quantitation approach, protein quantity can be estimated by measuring of peptide quantities.

Label-free methods for quantitation are often used when the introduction of stable isotopes is impractical (e.g., in many animal studies) or the cost is prohibitive. In label-free quantitation workflows[11, 27] usually the peptide ion peaks or peptide fragment ion(s) are integrated and used as a measure of quantity. The absolute quantity can be calculated using a standard curve. Quantitation using fragment ions (as in multiple reaction monitoring; MRM) is more specific as it requires the masses of the precursor ion and the fragment ions to be close to the predicted masses. Also, because peptides fragment in a sequence specific manner, it requires that the relative intensities of the fragment ions do not deviate from the expected intensities which increase specificity.

Other label free quantitation methods not based on peak integration involves searching the fragment mass spectra against a protein-sequence collection and quantitation is subsequently attained using a number of approaches. These include i) Spectra counting where the number of different fragment spectra that identifies peptides derived from a given protein is used as a measure of protein quantity. This method is based on the rationale that peptides from more abundant proteins will be more selected

for fragmentation and will thus produce a higher number of MS/MS spectra. ii) Calculate exponentially modified protein abundance index (emPAI), a measure based on the number of identified peptides of a protein**.** emPAI is based on the fact that generally more peptides are detected for larger proteins and is directly proportional to the protein content in the sample. Label-free quantitation not based on peak integration is generally less accurate when a small fraction of fragment spectra or peptide is observed for a given protein[11, 27].

To compare samples quantitatively in label-free proteomic workflows, LC-MS/MS analysis is performed on each sample separately and the calculated peptides and proteins quantities in the different samples are compared. Label-free methods are therefore susceptible to variations in time-instrument response due to the lack of multiplexity. High reproducibility in sample preparation, high reproducibility of chromatographic separation, the exact alignment of chromatograms from different samples, the use of high-scanning rate, high resolution power of the MS, and highly accurate mass measurement are thus prerequisite for statistical significant results[11]. The high-reproducibility requirements in label-free quantitation can put restraints on prefractionation. Also, analysis time can be greatly increased when the number of samples to be analyzed is large due to the lack of multiplexity.

Labeling methods involving the use of stable isotopes can be classified into two main groups: chemical labeling and metabolic labeling. Labeling strategies are based on the fact that both labeled and unlabeled peptides exhibit the same chromatographic and ionization properties but can be distinguished from each other by a signature mass-shift[11].

Introduction of labels can help optimize reproducibility of the proteomic workflow. In metabolic labeling, the label is introduced to the whole-cell organism through the growth medium. Metabolic labeling therefore provides the earliest possible introduction of stable-isotope labels into the sample but is not always feasible and can be costly and time-consuming particularly when applied to the study of complex organisms. Available metabolic labeling approaches include Stable Isotopic Labeling with Amino Acids in Cell Culture (SILAC) and 14N/15N Labeling[22].

In chemical labeling, proteins or peptides are tagged with the label through a chemical reaction. Available chemical labeling approaches include Isotope-Coded Affinity Tags (ICAT), Tandem Mass Tag (TMT), Isotope-Coded Protein Labelling (ICPL), and Isobaric Tags for Relative and Absolute Quantification (iTRAQ). The different chemical-labeling approaches differ in the site of reaction, the mechanism of reaction and the method of quantitation under the mass spectrometer platform[11, 22]. TMT share similar characteristics with iTRAQ but the number of identified peptides and proteins are higher with iTRAQ (4-plex or 8-plex) than TMT 6-plex[28, 29]. The iTRAQ technology was used in this dissertation and is thus further discussed.

1.3.5.1 iTRAQ Labeling

iTRAQ is a popular chemical-labeling technique that allows four to eight samples to be multiplexed in a single run. The iTRAQ technique is a form of isotope labeling in which the tags are isobaric in nature. The tags contain a peptide reactive group N-hydroxysuccinimide (NHS) ester derivative, a balancer group (carbonyl group), and a reporter group (based on *N*-methylpiperazine). For 4-plex reagent, the reporter groups of

masses 114.1, 115.1, 116.1 and117.1 Da are balanced by corresponding 28, 29, 30 and 31 balancer group to give a total constant mass of 145.1 Da (Figure 1.6). 8-plex reagent has four additional reporter groups of masses 113.1, 118.1, 119.1, and 121.1 and corresponding balance masses of all eight reporter masses range is 192-184 Da, giving a total constant mass of 305.1Da[26, 30]. The different masses of the reporter groups and balancer group are achieved by using combinations of ^{13}C, ^{14}N and ^{18}O isotopes. The iTRAQ derivatization is achieved by reaction of the NHS ester derivative with the N-terminus and ε-amino group of the lysine side-chains to form an amide bond. This makes it possible to label all peptides in a sample.

The iTRAQ protocol often involves reducing, alkylating, and digesting proteins in individual samples prior to iTRAQ labeling. Reduction and alkylation blocks any possible reaction of the reagent with cysteine residues. Digested peptides of a sample are then labeled with an iTRAQ reagent at room temperature and the individual-labeled samples are mixed together in 1:1 ratio. Often iTRAQ-labeled peptides are separated by performing strong cation exchange (SCX) followed by reverse-phase liquid chromatography.

Quantitation with iTRAQ has several advantages over other chemical labeling techniques. Because the tags are isobaric, individual differentially labeled peptides at a given *m/z* elute as a single combined peak in MS, which greatly enhance the signal. This is an important contrast to non-isobaric labeling techniques such as ICAT in which the

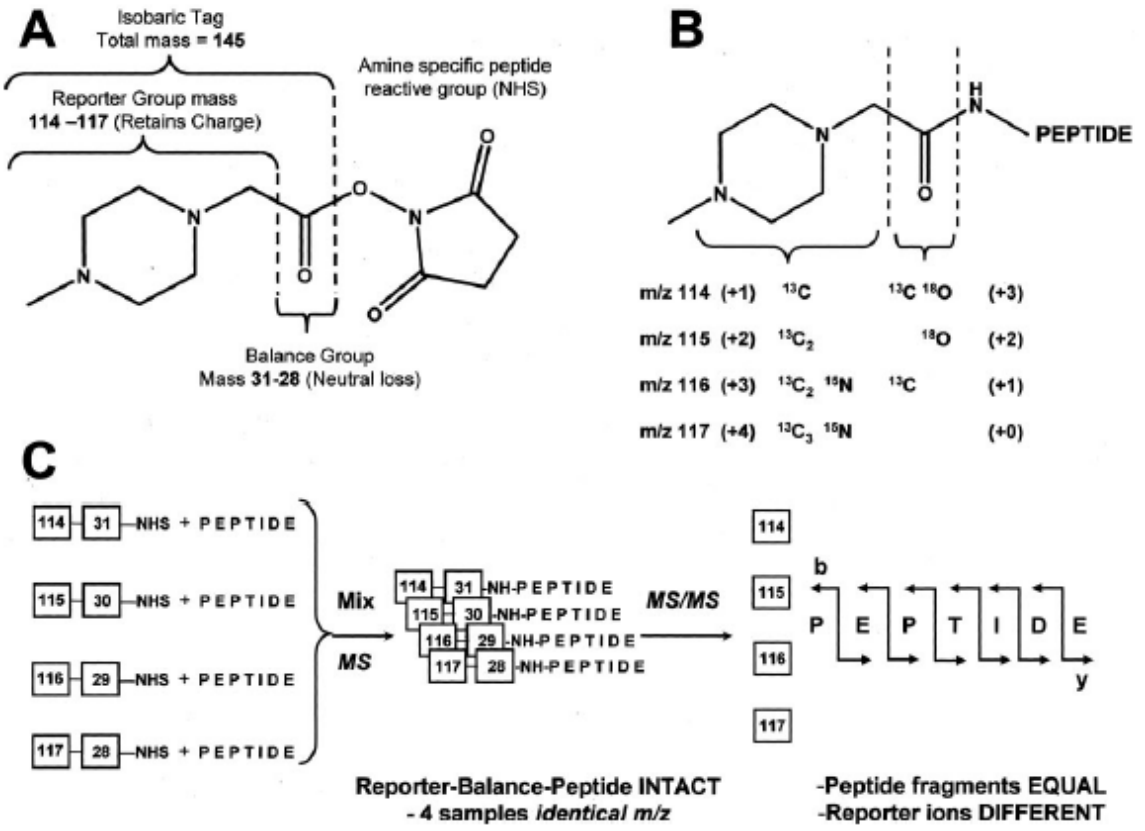

Figure 1.6. Multiplex quantitation using 4-plex iTRAQ reagent. Shown in Ross et al[31]. (A) Structure of 4-plex iTRAQ reagent; (B) Combination of isotopic enrichments used to achieve constant mass (145.1 Da) for each of the four reagents; (C) Illustration of using 4-plex reagents in an LC-MS/MS experiment.

MS (precursor) signal is split due to mass shift and results in decreased signal. Also, there is less complexity of the MS spectra, a benefit arising from the same mass of labeled peptides. At the MS/MS stage, balancer group is loss via neutral loss and the reporter ion which retains a charge is released and observed in the low mass region of the MS/MS spectrum. All other fragment ions remain isobaric, and their individual signal intensities are additive which also increases sensitivity at the MS/MS level[26, 30]. Figure

1.7 is an example of the reporter region in MS/MS spectrum observed for a peptide from a protein digest in our lab.

Because of the multiplexing nature of the iTRAQ tags, variation in time instrument response is eliminated. Additional benefit of iTRAQ technology is that proteins can be identified by their signature peptides and fragment ions via database search using appropriate algorithm in a parallel workflow. The quantification and identification data are emerged using appropriate algorithm e.g. Proteome Discover, ProteinPilot, and i-Tracker[26]. Protein-identification search parameters for iTRAQ labeled peptides include indicating iTRAQ as a fixed modification at the N-terminal and ε-amino group of lysine residues and iTRAQ as a variable modification at tyrosine residues.

The peak intensities or areas of the reporter ions of different masses are used to calculate the relative quantities of peptides of proteins. More than one spectrum can be obtained for a single peptide due to the peptide having more charge states and corresponding different m/z and retention times. Additionally, this could be because the peptide has better ionization efficiency and is more abundant. Therefore more than one peptide ratio and error can be calculated for a single peptide. Spectra ratios are calculated often using the lowest reporter ion as the reference (114.1 in 4plex or 113.1 in 8 plex experiment). Spectra ratios corresponding to the same peptide are merged by i) taking the average of all the representing spectra ratios or the median to represent the peptide or ii) scoring the spectra and the spectrum that most defines a given peptide is chosen to represent the peptide. The average (or weighted average) or median of the calculated peptide ratios of an identified protein is taken to represent the relative quantity of that

protein. Absolute quantification with iTRAQ can be achieved by labeling a reference peptide belonging to the protein with one of the iTRAQ reagent and upon mixing with the other iTRAQ labeled samples and subsequent MS analysis, the intensity or area of the reporter ion of the reference peptide is used to calculate the absolute value.

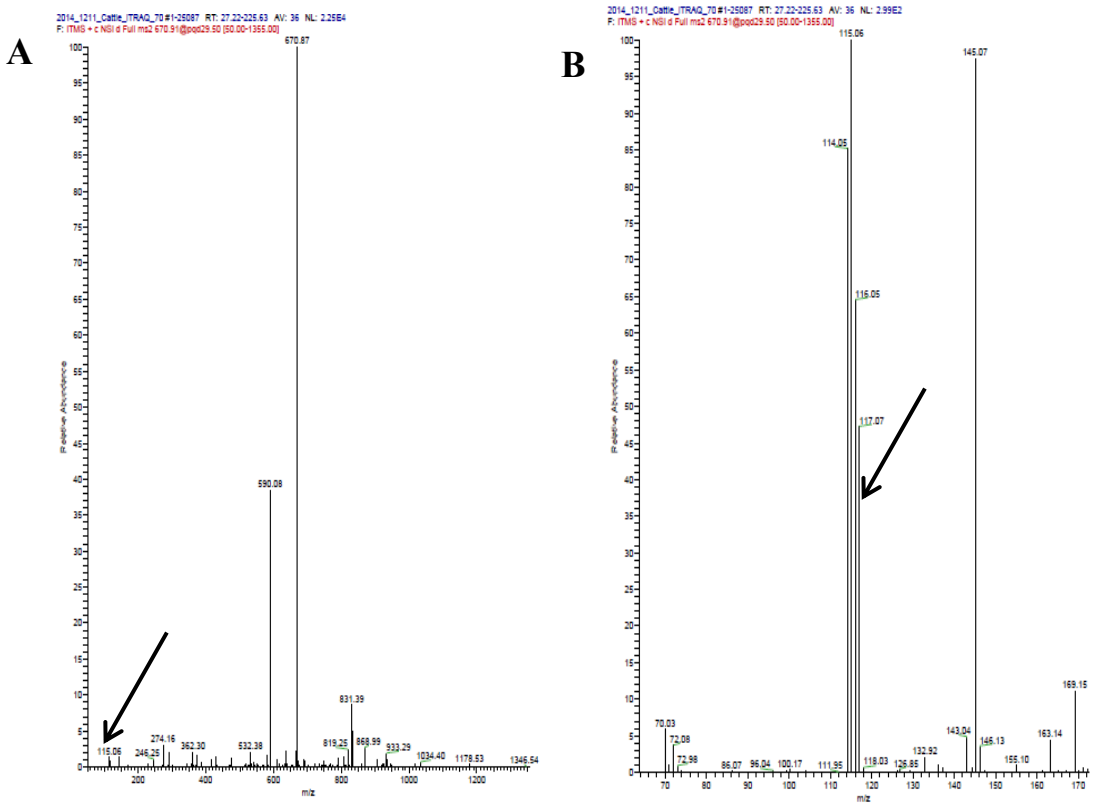

Figure 1.7. Exemplary MS/MS spectrum of an electrospray ionized peptide fragmented by pulsed q collision induced dissociation (PQD) in Finnigan LTQ. iTRAQ reporter ions (arrows) in low mass region in A is zoomed in and shown in B. Reporter ions 114, 115, 116 and 117 are observed.

1.4 Applications of Proteomics in Reproduction Research in Bovine

Mass spectrometry-based proteomics is continuing to provide insights into several biological systems in human and several species. An important area of its application is

molecular research in reproduction. The potential benefits from this area of research are enormous and include uncovering and broadening the understanding of a variety of molecular events in reproductive important tissues such as testis, ovary, endometrium, oviduct, and placenta as well as gametes and embryos; improved understanding of the effects of reproductive toxicants particularly disease states (e.g. polycystic ovary syndrome (PCOS), infertility, subfertility, endometrial disorders, and miscarriage) or hormones and cytokines; and identification of potential protein biomarkers and/or treatment targets for successful reproduction and fertility interventions[32, 33]. While significant proteomic research has been dedicated to human reproduction and fertility[33], very few have focused on that of other species including bovine. A significant contributor to this drawback is the lack of available comprehensive sequence database for protein identification in these species. Also, in bovine, established traditional methods for assessing and improving reproduction and fertility remain the standard practices among farmers.

Cow-reproductive performance (fertility) is very important as it defines the attained biological and economic benefits. Traditionally, cow productivity, i.e. the number of calves produced per lifetime or per unit land area is estimated by a number of factors including age at first calving, calving (fertility rate), calving interval, number of services per conception (NSC), age at puberty, and nutrition[34]. First calving marks the beginning of a cow's productive life and age at first calving is closely related to generation interval (the average age of parents at birth of their offspring that in turn will produce the next generation of breeding animals). Late first calving has been associated with increasing longer calving intervals. Also, NSC has also been reported to increase in

increasing age at first calving. In general, earlier first calving increases lifetime productivity of cows. The commonest estimate of fertility rate is the percentage of mated or inseminated cows that become pregnant (pregnancy rate) or finally calve (calving rate). Fertility rates can also be estimated prior to calving as the percentage non-return rate. This is the number of cows bred that do not come back in heat and are thus assumed to have conceived. Differences in calving rate between years have been associated with the quality and quantity of available forage. Calving interval is probably the best index of a cattle herd's reproductive efficiency. Calving interval is the amount of time (days or months) between the birth of a calf and the birth of a subsequent calf, both from the same cow. Calving interval is estimated to be affected by factors such as genetics, age, sex of the calf, suckling duration, and feeding after calving. Calving interval decreases with shorter suckling duration, high feeding after calving, and having female calves instead of males at calving. The shorter calving interval with female calves is attributed to shorter suckling duration with females than males. Shortest calving interval is observed with cows of intermediate age (6-9 years) compared to young age (3-6 years) and old age (12-16 years). Effective recognition, measurements and management of the reproductive estimates is essential to the productivity of the cow. Artificial insemination (AI) is a common practice also used to increase pregnancy rate and cow productivity. In this respect, accurate detection of oestrus is essential for achieving high pregnancy rate.

Although these traditional reproductive estimates are still being practiced, it is increasing being recognized that the application of proteomics can provide parallel information that will enhance reproduction in cattle. Proteomic application potential benefits include identification of biomarkers (i) predictive of early pregnancy detection,

fetus, and maternal survival[35, 36]; (ii) for evaluation and selection of quality sperm, oocyte, and embryo[37, 38]; (iii) monitoring of genetic/physiological and environmental causal diseases affecting reproduction; and (iv) suitable for use as treatment targets for successful artificial insemination, pregnancy, and offspring. Accordingly, a number of studies have been conducted[39-43].

Folliculogenesis is the process in which recruited primordial follicle grows and undergoes stages from primary, secondary, tertiary (pre antral follicle and mid-antral follicle), dominant to ovulatory follicle with the potential to ovulate its oocyte to be fertilized or die by atresia[44]. Follicular fluid (FF) accumulates into the follicle antrum starting with the early stage of follicle development and becomes the natural environment of the developing oocyte (Figure 1.8). FF consists of a wide variety of dynamically changing proteins responsible for growth and development that ultimately affect the quality and fertilization potential of the oocyte. Therefore, FF is a useful substrate for proteomic reproduction and fertility research. Moreover, FF is an easily accessible biological fluid as it is aspirated in abundance from follicles[33].

Ferrazza et al.[40] recently investigated protein expression profile of bovine FF at key stages of follicular development. The group identified a total of 143 proteins, twenty-two of which were differentially expressed between stages indicating intrafollicular changes over development. The group also found that the complement and coagulation systems, acute-phase response signaling, liver/retinoid X receptor activation, and biosynthesis of nitric oxide and reactive oxygen were the most significant pathways associated with the proteins. Another group investigated the effect of bovine FF proteins

and their acidic and basic groups as maturation media supplements for *in vitro* embryo development. They found oocyte maturation rate, the development to the blastocyst stage rate, and blastocyst cell number were not significantly differing in 10% bovine FF supplemented *in vitro* maturation (IVM) medium and controls (supplemented with fetal bovine serum and hormones). However, inteferon tau (INFτ) and insulin-like growth factor-2-receptor (IGF-2r) expression levels in the 10% bFF were significantly higher than in the control. Supplementing the IVM medium with basic bovine FF protein fraction resulted in significantly higher oocyte maturation rate and blastocyst cell number and greater expression levels for almost all developmentally important genes, especially INFτ and HSP70 when compared to supplementing with acidic fraction. INFτ is the primary factor responsible for maternal recognition of bovine pregnancy[45]. Binding of IGF-2r to the growth factor enable pathway for the growth factor regulation of fetal growth[46, 47]. The upregulation of both proteins shows the importance of FF proteins in the establishment of pregnancy and fetal growth. Proteomic approach was also used to identify eight differentially expressed proteins in FF from preovulatory follicles of less fertile cows that are important to follicular function[48].

These studies show the potential of proteomic analysis of FF to provide better insights into key factors involved in folliculogenesis, establishment of pregnancy, embryo development, and the identification of therapeutic targets in bovine. The applications of the outcomes of such research stand to improve the productivity of the cow. In this dissertation, proteomic analysis of bovine FF and plasma (PL) was performed and the effect of high and low estradiol (E2) on protein expressions during the preovulatory stage was investigated. Detail of this work is discussed in Chapter 3.

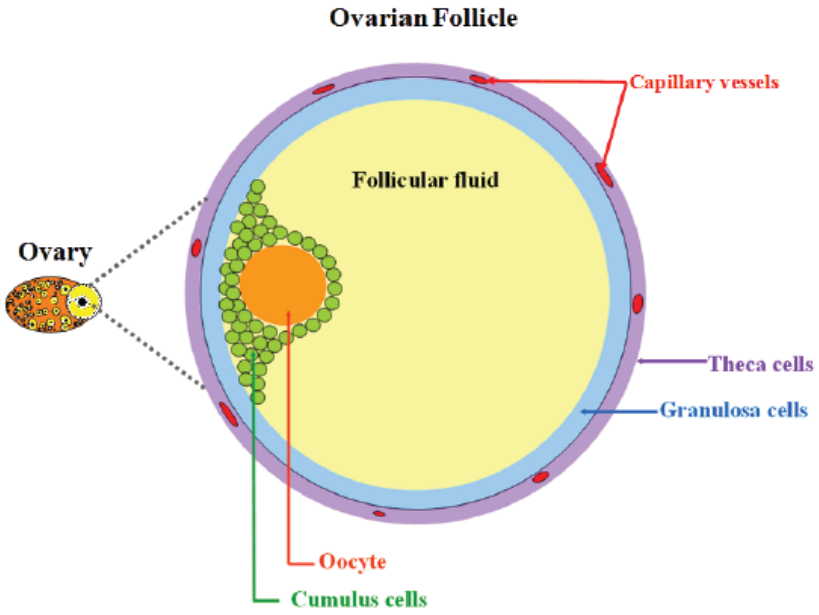

Figure 1.8. Schematic picture of an ovarian antral follicle in mono-ovulant species. Shown in Fahiminiya *et al*[49]

1.5 Atherosclerosis

Atherosclerosis is a multifactorial progressive disease characterized by the narrowing and hardening of arteries caused mainly by build-up of cholesterol, lipids, cellular debris, and calcium to form plaque in the intima of large- and medium-sized arteries[50]. The plaque formation and subsequent narrowing and hardening of the arteries result in chronic luminal obstruction, abnormalities of blood flow, and diminished oxygen supply to target organs[51]. Complications of atherosclerosis lead to coronary artery disease (CAD; heart attack), cerebrovascular disease (CeVD; stroke), and diseases of the aorta and arteries, including peripheral vascular diseases (PVD) and hypertension. Globally, CAD and CeVD are the leading causes of cardiovascular deaths[50]. Risk factors for atherosclerosis include diabetes mellitus, obesity, hypertension, tobacco use, harmful use

of alcohol, high levels of low density lipoprotein (LDL) cholesterol, low level of high density lipoprotein (HDL) cholesterol, advancing age, male gender, unhealthy diet (rich in salt, fat and calories), psychological factors, physical inactivity, poverty, low education status, and family history of premature CAD[50, 52].

Atherosclerosis is viewed as an inflammatory disease[53, 54] with initial events involving dysfunction of the endothelium (lining of the artery)[55, 56]. Endothelia injury is initiated by a variety of events/substances including dyslipidemia (particularly high levels of LDL cholesterol), hypertension, infection, presence of free radicals, and low shear stress. The damaged endothelium allows migration of lymphocytes, monocyte, and lipids, particularly LDL cholesterol, into the arterial intima. Dysfunction of the endothelium also promotes expression of cellular adhesion molecules ICAMs (e.g. ICAM-1), vascular cell adhesion molecules (VCAMs) (e.g. VCAM-1), chemokines, and selectins such as P- and E selectin. These processes are partially mediated by nuclear factor κB (NF-κB), one of the transcriptional controllers in vascular inflammation and an integrator in atherogenesis[55-57]. Leucocytes and monocytes adhere to the endothelium via VCAM-1 binding and enter the intima by diapedesis between endothelial cells at their junctions. This process is mediated through chemokines, such as monocyte chemoattractant protein 1 (MCP-1) and IL-8 as leukocyte chemoattractant. LDL cholesterol, upon migration into the arterial intima undergoes oxidation to become oxidized LDL (OxLDL) which are subsequently engulfed by monocyte-derived macrophages via receptors such as scavenger receptor A (SR-A) and CD36. A lipid laden macrophage is called a foam cell and is the first type of atherosclerotic lesion[55] (Figure 1.9). The monocytes/macrophages promote the local inflammatory response secreting cytokines, degrading enzymes [(matrix metalloproteinases (MMPs)] as

well as growth factors that stimulate smooth-muscle cell (SMC) migration from the media (deeper layer of the artery) into the site of plaque formation and SMC proliferation. As the atherosclerosis development continues, a fibrous cap consisting of smooth muscle cells and collagen forms. Also, the necrotic lipid core is formed when macrophages involved in the initial reaction begin to die and accumulate and a fibrous cap is formed around the lesion location. The atherosclerotic lesion (atheromatous plaque) enlarges as cells and lipids accumulate. The enlarging lesion causes the inner surface of the artery to become irregular and also bulges into the arterial lumen resulting in narrowing of the lumen. These make it harder for blood to flow through the artery, resulting in the artery becoming less pliable[50, 55].

The continuous influx of cells into the sub-intimal space elicits chronic inflammatory response by the adaptive immune system. Also, the microenvironment of the plaque could elicit adaptive immune response which in such case is coordinated by lymphocytes rather than macrophages. The selective recruitment and activation of T-helper type 1 (Th1) T lymphocytes represents a key point in the transition from stable plaque to unstable plaque. In particular, selective recruitment of Th1 T lymphocytes promotes plaque destabilization/disruption eliciting vascular inflammation and downregulating extracellular matrix production by SMCs. Other contributors to the thinning of the fibrous cap resulting in plaque rapture include activated macrophage secreted procoagulant proteins and MMPs proteases that can degrade collagen, interferon (IFN)-γ that strongly inhibit the proliferation of SMCs and the production of interstitial collagens by vascular SMCs, and ligation of CD40 (expressed by macrophages) which increases the production of matrix-degrading proteases. Thinning of the fibrous cap and

subsequent rapture of the plaque releases lipid fragments and cellular debris into the vessel lumen. Of importance is the exposure of procoagulant factors expressed within lesions to circulating clotting factors initiating the coagulation cascade responsible for thrombosis. If the thrombus develops in a coronary artery it can cause heart attack and if it develops in the cerebral (brain) artery, it can cause stroke[50, 55].

Six types of atherosclerotic lesions have been identified, and are differentiated by morphological features and clinical significance[58-60]. Types I to III lesions (early types) are usually clinically silent whereas types IV-VI lesions (advanced forms) are often associated with the symptoms and complications of the disease[61]. Description of these lesions is discussed in section 4.4.4 of Chapter 4.

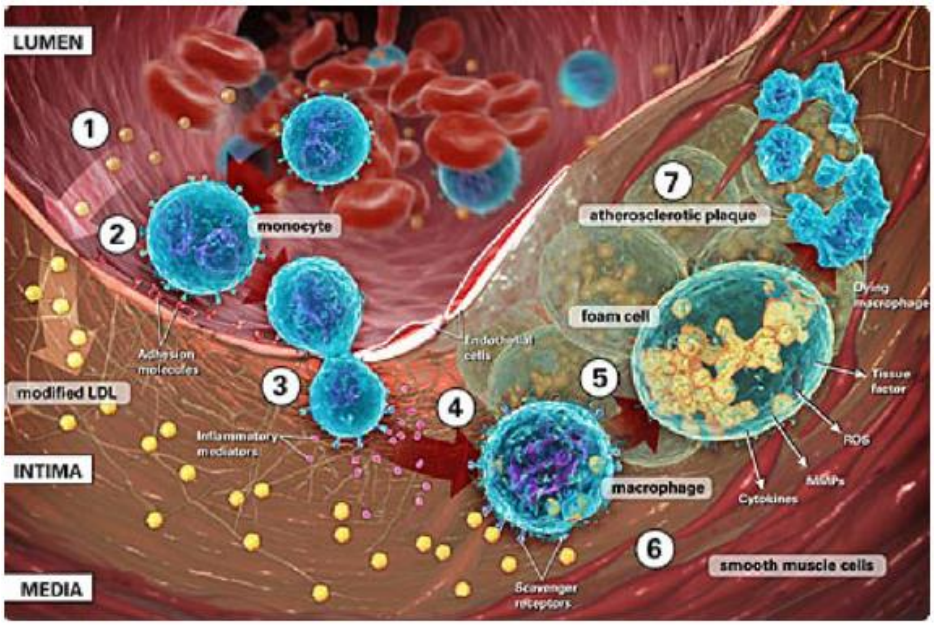

Figure 1.9. Atherosclerotic plaque development. The numbering and arrows indicate events leading to plaque development.
(http://www.resverlogix.com/product_development/nexvas_platform/nexvas_vascular_inflammation.html)
Shown in Glaudemans *et al*, 2010[55]

1.6 The Apolipoprotein E Knock-Out (*ApoE*$^{-/-}$) Mouse Model of Atherosclerosis

Mice are the most popular experimental animals because of their small size, wide availability, easy of genetic manipulation, short generation time allowing less time duration for research projects and the relatively low cost in feeding and housing compared to other experimental animals[62, 63]. Wild-type mice however have a different serum-lipid profile of elevated levels of HDL in contrast to elevated levels of LDL in humans which makes it resistant to developing atherosclerosis unless on a high-saturated fat and cholesterol diet for prolonged periods. The C57BL/6 wild-type mouse strain was found to be the most susceptible on such diet but only developed early types of lesions which were not comparable to that found in humans[64]. This presented a need for a more efficient mouse model for studying atherosclerosis.

Among the available mice-atherosclerosis models, the apolipoprotien E knock-out (*ApoE*$^{-/-}$) mouse model[65, 66] is popular because of its susceptibility to spontaneously develop atherosclerotic lesions in a progressive manner and with lesion morphological features observed in humans[63, 67]. The *ApoE*$^{-/-}$ mouse model is based on the function of apolipoprotein E (ApoE) protein. ApoE is a glycoprotein synthesized in the liver, brain, and by monocytes and macrophages in vessels. It is a constituent of all lipoproteins except low-density lipoprotein (LDL). It mediates the cellular uptake of several different lipoproteins, most notably, cholesterol, atherogenic triglycerides, and very low-density lipoproteins (VLDL). It also functions in biliary excretion of cholesterol[63, 68, 69]. Deletion of the apoE gene thus dramatically increases the serum cholesterol levels mostly in the form of VLDL remnants and chylomicrons and makes it susceptible to developing atherosclerotic lesions. The atherogenic process is accelerated when on a high saturated

fat and cholesterol diet[65, 66]. Because C57BL/6 mouse strain is more susceptible in developing atherosclerosis[64, 70], it is often the background for *ApoE*$^{-/-}$ mice[71].

The *ApoE*$^{-/-}$ atherosclerotic model allows for studies on lesion size and composition and the identification of possible therapeutic targets; nutritional interventions aimed at the effects of changes in micro- and macronutrients on lesion size and on atherosclerotic cells/molecules (e.g. monocytes, macrophages, oxLDL) or mechanisms (e.g. LDL oxidation, uptake of oxLDL by macrophages); the effects of therapeutic agents on atherosclerotic molecules, lesions, and events; and the genes related to atherosclerosis[62, 63, 68].

1.7 Lesion Analysis in Mice

Atherosclerotic studies in mice often involve estimating the extent of lesions by histological methods. Two methods widely used are the *en face* method[72] and the serial cross section method[73]. The *en face* method involves removing the entire aorta and opening it longitudinally to expose the intimal surface by dissecting from the heart to the iliac arteries. The primary incision follows the ventral side of the aorta and the inner curvature of the aortic arch. A second incision is made along the outer curvature of the aortic arch to the subclavian branch to obtain a flat tissue for imaging. Minor branches are cut off and the aorta, from the heart to approximately 3mm distal to the iliac bifurcation, is pinned out on a black surface using 0.2mm diameter stainless steel pins. Staining with, e.g., Sudan IV is performed to enable visualization of lipid-laden lesions and measurement of lesion surface areas. Lesion area is usually represented as a percent of the total intimal surface that is covered by atherosclerotic lesions. The *en face* is a

rapid method that provides a two-dimensional assessment of lesion size on the entire aorta but is limited in the assessment of lesion thickness[71, 72].

The serial cross-sectioning method involves sequential sectioning of the heart and the aortic root onto histological slides and subsequent histopathological analysis including staining (e.g. oil red O) and image analysis by appropriate software is used to examine and quantify lesions. Analysis of the aortic sinus region requires serial sectioning 400µm total area starting from the appearance of the aortic sinus cusps and spanning distal towards the ostia of the coronary arteries. Histological analysis of the aortic root and the ascending aorta requires serial sectioning spanning about 900µm stretch of the aortic root[60, 73, 74]. The serial cross-sectioning method, although labor and time consuming, enables examination of lesion thickness and composition.

Atherosclerosis studies with the *ApoE*$^{-/-}$ mouse model have enabled the identification of predilection sites (Figure 1.10) of atherosclerosis development in mice[67, 75] which include the aortic root, carotid arteries, lesser curvature of the aortic arch, pulmonary artery and the principal branches of the thoracic aorta. These predilection sites have been the focus for probing of the disease. Of these, the quantification of the aortic root is considered the standard in many laboratories due to the high susceptibility of this site to atherosclerosis in mice and lesions develop in mice at earlier age than the other predilection sites. Also, the aortic sinus cups serve as an anatomical landmark to keep the area under study constant[76]. This dissertation characterized and quantified lesions in the aortic root of *ApoE*$^{-/-}$ mice at different ages using the serial cross sectioning method and this is discussed in detailed in Chapter 4.

1.8 Proteomic in Atherosclerosis Biomarker Discovery

Although clinical assessments remain the primary tool for atherosclerosis and associated cardiovascular disease management, they pose limitations particularly in predicting individual risk and risk of recurrence[77]. A biomarker is defined as "a characteristic that is objectively measured and evaluated as an indicator of normal biological processes or pharmacologic responses to a therapeutic intervention"[78]. Identification and measurements of atherosclerosis biomarkers, which were originally introduced to improve existing clinical assessments and to enable the identification

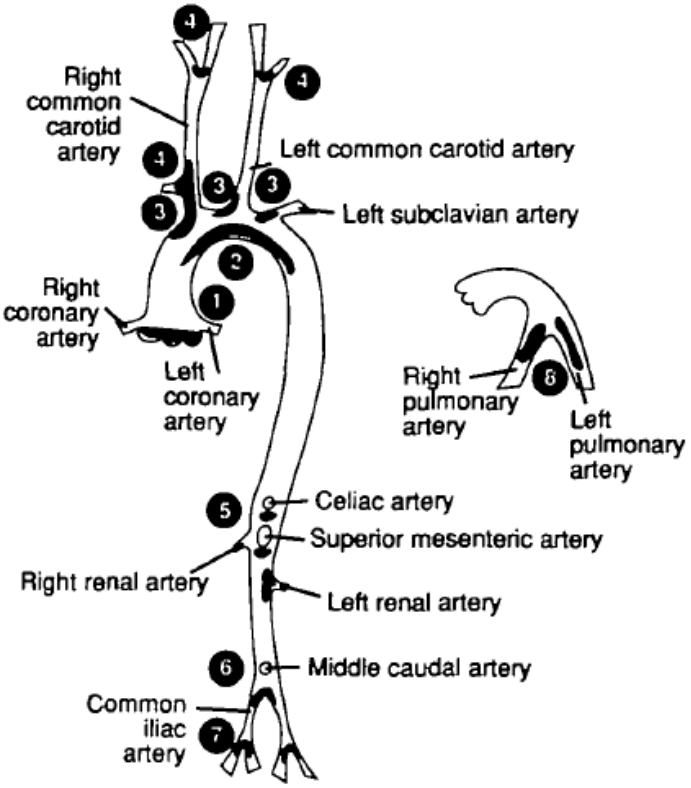

Figure 1.10. Predilection sites of atherosclerosis development on the aorta and pulmonary arteries of *ApoE*$^{-/-}$ mice. Predilection sites are shaded black. 1. Aortic root; 2. Lesser curvature of the aortic arch; 3. Principal branches of the thoracic aorta; 4. Carotid arteries; 5. Principal branches of the abdominal aorta; 6. Aortic bifurcation; 7. Iliac artery; and 8. Pulmonary arteries (From Nakashima et al.,[67])

of vulnerable patients[79] continue to hold great promise. A suitable biomarker would have the advantage of identifying high risk individuals, accurately and quickly diagnose disease conditions and effectively predict and treat patients with the disease[79].

Mass-spectrometry-based proteomics technologies are powerful tools that can be employed in the search for novel biomarkers for atherosclerosis and related diseases due to the ability of such technologies to identify thousands of proteins in a single experiment. By these methodologies, several biomarker candidates have been identified. A comprehensive list compiled by de la Cuesta *et al*, 2015[80] include fibrinogen fragment D, annexins (e.g. A4, A5, A10), cathepsin D, alpha 2 macroglobulin, S100 proteins, myeloperoxidase (MPO), gelatinase, matrix metalloproteinases (e.g. MMP-3, MMP-9), vinculin, apo B100, thrombospondin-2 (TSP-2), manganese-dependent superoxide dismutase (MnSOD), and caspase-9 as potential markers of atherosclerosis; death-inducer obliterator 1 **(**DIDO 1), fibrinogen, cardiac troponin I and T (cTnI, cTnT), inosine, alpha 2 macroglobulin, and serine as potential biomarker for myocardial infarction; haptoglobin (hp) and serum amyloid A (SAA) as candidate markers for ischemic stroke; proline, arginine, alanine, ornithine, creatinine, and trimethylamine N-oxide (TMAO) as potential markers for coronary artery diseases (CAD).

Many of the candidate biomarkers have however not been incorporated into clinical assessments mainly because they fail to meet all the requirements of a true biomarker. Protein biomarkers that have been incorporated into clinical assessments such as oxidized low-density lipoprotein (oxLDL), C-reactive protein, fibrinogen, lipoprotein-associated phospholipase A2 (Lp-PLA2), Lp(a), osteopontin (OPN), osteoprotegerin (OPG), .MMP-3, MMP-9, myeloperoxidase (MPO) , homocysteine, cardiac troponin I

and T (cTnI, cTnT), and tissue factor (TF)[80, 81] have however not been able to predict individual risk above that achieved by the traditional risk factors. Therefore, there is still an urgent need to find true and useful biomarkers that can identify vulnerable patients and guide treatment development[81].

Circulating blood is the most used sample in proteomic atherosclerotic biomarker discovery studies probably because of the ease and convenience of sampling[82]. Other proteomic samples include urine[83], circulating cells extracted from plasma/serum such as monocytes, platelets and leukocytes, plasma extracellular vesicles such as exosomes and microvesicles and tissues like carotid artery[81, 84, 85]. In using the *ApoE*$^{-/-}$ mice in atherosclerosis studies, blood and urine samples collected can be viable source for proteomic work[86]. Proteomics on blood and tissues from these mice has the benefit of providing insights into the molecular mechanisms associated with the disease. The availability of tissues from mice for proteomic work is particularly advantageous since obtaining similar sufficient tissues from humans is difficult, especially in considering control samples for comparative analyses[80].

Although mice can be a good source for proteomic work, their small size can limit the amount of samples collected and this should be considered in the experimental design of such studies. Potential atherosclerotic biomarkers can be determined by comparing the data generated from *ApoE*$^{-/-}$ samples to that from control group of the study. A correlation analysis can also be performed between identified proteins from the proteomic analysis and lesion components, morphology or size.

The *ApoE*$^{-/-}$ mouse model is used in this dissertation to study lesion types and patterns with factors such as age and also make available blood and tissue samples for proteomic analysis for biomarkers of atherosclerosis.

CHAPTER 2

IMMUNODEPLETION OF MULTIPLE HIGH-ABUNDANT PROTEINS FROM BOVINE FLUIDS

2.1 ABSTRACT

Immunodepletion of high-abundant proteins (HAPs) aids in the identification and analysis of low-abundant proteins (LAPs) in complex samples. Currently, immunodepletion methods for bovine samples are very limited whereas greater availability exists for human and murine animals. In this study, we report the simultaneous depletion of HAPs from bovine samples using an immunoaffinity depletion cartridge (the multiple affinity removal system; MARS) designed to target six human HAPs, while such a depletion kit for bovine samples is not available. Sandwich ELISA analysis showed 98.7 to 99.9% depletion of albumin, IgG and IgA from bovine plasma, follicular fluid (FF), ejaculated and epididymis sperm types. A similar percentage is expected of alpha-1-antitrypsin due to the dramatic removal in its SDS PAGE band compared to the crude samples. The method has high reproducibility and can be incorporated into proteomic workflows to increase sensitivity of proteomics analysis of LAPs in bovine biological fluids.

2.2 BACKGROUND AND MOTIVATION

Proteomics is a high-throughput approach to study protein expression, structure, function and post-translational modifications in a cell or tissue. Advancement in proteomic sample preparation technologies, mass spectrometry instrumentation and bioinformatics[87-89] have increased the application of proteomics to understand various biological systems. Bovine proteomics i.e. the application of proteomic strategies to bovine biological samples is an area of increasing interest[90]. Bovine proteomics potential benefits are extensive and include identification of biomarkers (i) predictive of early pregnancy detection, fetus and maternal survival[35, 36]; (ii) for evaluation of quality sperm, oocyte and embryo[37, 38]; (iii) for assessing the quality and safety of meat, milk and dairy products; and (iv) for detection, diagnosis and monitoring of genetic/physiological and environmental causal diseases[90, 91].

As is characteristic of biological samples, the complexity and wide dynamic range in protein concentrations found in bovine samples present a challenging step in their preparation for proteomic analysis[92]. The wide dynamic range in protein concentrations results in high abundant proteins (HAPs; 1-100 mg/mL) masking the identification and characterization of low abundant proteins (LAPs, <100 ng/mL). However, biomarkers of disease and normal states are most probably of the low abundant types, which make the ability to characterize these LAPs imperative in proteomic analysis.

To bridge the wide concentration range and reduce sample complexity, proteomic workflows often incorporate fractionation method(s). Immunodepletion is a popular fractionation method due to its simplicity, specificity and reliability. Immunodepletion

method involves using antibodies to remove target HAPs with subsequent enhanced detection of LAPs. Immunodepletion of HAPs allows for loading of LAPs at higher concentrations for improved visualization by one-dimensional (1-D) or two-dimensional (2-D) gel electrophoresis and liquid chromatography (LC) and increase the sensitivity of proteomics analyses[19]. The reliability of the immunodepletion method has led to advancement in immunodepletion technologies including commercialized kits for humans[19] and murine biological samples[93, 94]. However, a method for immunodepletion of HAPs in samples from other species, including bovine, is very limited.

In the absence of available immunodepletion technology, the majority of proteomic analysis of bovine biological samples have used gel-based 2-D gel electrophoresis and modified forms of 2-DE such as 2-D fluorescence differential gel electrophoresis (2D-DIGE) followed by mass spectrometry analysis[36, 43, 95-97]. However, incorporating immunodepletion of HAPs will enhance the gel-based approach and also decrease the number of fractionation steps often employed in shotgun proteomic analysis. Faulkner *et al*[18] presented separate depletion methods for albumin and IgG, the two top abundant proteins in bovine plasma. However, combinations of depletions each targeting an abundant protein increase analysis time and can result in sample loss and contamination. Sequential depletions can also result in a decrease in the number of uniquely identified peptides[98].

2.3 OBJECTIVE OF STUDY

The objective of this study was to develop an efficient and reproducible immunodepletion method for simultaneous removal of HAPs in bovine fluids. We

employed the high capacity multiple affinity removal system (MARS) originally designed to target six HAPs- albumin, Ig G, IgA, transferrin, alpha-1-antitrypsin, and haptoglobin (hp) in human biological fluids while a similar technology for bovine is not available. The six target HAPs represent 85-90% of the total protein mass in human serum. The MARS technology has been successfully utilized in many proteomic applications of human bio-fluids[99-102].

2.4 MATERIALS AND METHOD

2.4.1 Chemicals and Reagents

All chemicals and water were of LC/MS grade. Bio-Safe™ G-250 stain, Tris/glycine/SDS buffer, 2-mercaptoethanol (β-ME), laemmli sample buffer and 4-20% Criterion™ TGX precast gel were purchased from Bio-Rad Laboratories Inc. (California, USA). Formic acid, acetonitrile (ACN), triethylammonium bicarbonate (TEAB), and water were obtained from Fischer Scientific (New Jersey, USA). Ammonium bicarbonate (ABC) and iodoacetamide were purchased from Acros Organics (New Jersey, USA). Dithiothreitol (DTT) and TPCK treated trypsin was purchased from Promega (Wisconsin, USA).

2.4.2 Cows Experimental Design

All procedures were approved by the South Dakota State University Institutional Animal Care and Use Committee. Samples in the present study were collected from a previous study to characterize changes in steroidogenic enzymes and FF steroid concentrations[103]. Briefly, 32 beef cows were synchronized by injecting with GnRH (100

mg as 2 mL of Factrel, intramuscularly; Pfizer Animal Health (Madison, NJ, USA) on day -7 and prostaglandin F2α ($PGF_{2\alpha}$) (PG; 25 mg as 5 mL of Lutalyse intramuscularly (Zoetis, Florham Park, NJ, USA) on day 0. Estrus was monitored every 3 h from PG on day 0 until hour 33 and at slaughter (hour 36 to 42) with the aid of EstroTect (Western Point, Inc, Apple Valley, MN, USA) estrus detection aids. Ovaries of all cows were examined on day -7, -4, and 0 by transrectal ultrasonography using an Aloka 500V ultrasound with a 7.5-MHz linear probe (Aloka,Wallingford, CT, USA) to assess follicular dynamics and ovulatory response. Ten cows that were determined to initiate a new follicular wave by day -4 were slaughtered on day 2 (hour 36 to 42) for ovary collection.

2.4.3 Follicular Fluid (FF) and Blood Samples Collection

Immediately after ovary collection, follicular fluid (FF) was aspirated from dominant follicles (DF; >10mm diameter) and the GCs were separated from the FF by centrifugation (1,000 x g for 1 min). The FF was place in RNase Free Tubes (USA Scientific), snap frozen in liquid nitrogen and stored at -80^{o}C until ready for analysis. Blood samples were collected at slaughter to provide better comparison to the FF collected at slaughter. To obtain plasma, blood collected at slaughter was placed in EDTA vacutainer tubes (Beckman Dickerson) and centrifuged at 1,200 x g for 30 min at 4°C. The plasma supernatant was snap frozen in liquid nitrogen and stored at -80^{o}C until ready for further analysis.

2.4.4 Bulls Experimental Design and Sperms Collection

All procedures were approved by the South Dakota State University Institutional Animal Care and Use Committee. Ejaculated sperm from bulls (n = 9) were collected by electro-ejaculation weekly for three consecutive weeks. Collected ejaculated sperm on the second week was centrifuged at 700 x g for 10 minutes to separate the spermatozoa from the seminal plasma. The seminal plasma fraction was labeled as 'ejaculated semen plasma'. The remaining spermatozoa fraction was washed with a high ionic solution[104] and vortexed for one minute to remove any proteins attached and then centrifuged at 700 x g for 10 min. The supernatant was labeled as 'ejaculated sperm proteins'. Following third sperm collection, bulls were rested for six weeks to allow epididymal reserves to renormalize. At the end of the resting period, bulls were slaughtered and the testes and epididymides collected. Collected epididymides were dissected and epididymal fluid and sperm collected from the cauda section and processed as described for the ejaculated sperm. The epididymal fluid fraction collected after separation from the epididymal spermatozoa was labeled as 'epididymis semen proteins'. The spermatozoa were than wash as described above and the liquid fraction from washing off proteins on the epididymal spermatozoa was labeled as 'epididymis sperm proteins'. All samples were stored at -80^{o}C.

2.4.5 Depletion of High Abundant Proteins (HAPs)

Depletion of the different bovine fluids (PL, FF, epididymis sperm proteins, epididymis semen proteins, ejaculated sperm proteins, and ejaculated semen plasma) were performed using the High Capacity Multiple Affinity Spin Cartridge (MARS Hu-

6HC) # 5188-5341 (Agilent Technologies, CA, USA). The MARS Hu-6 system contains polyclonal antibodies designed to remove six HAPs- albumin, IgG, IgA, transferrin, α-antitrypsin, and haptoglobin (Hp) in human biological fluids. The depletion was done with vendor provided buffers. Initial depletions investigated 2, 4, 6, 8, 10, and 12 µL of bovine plasma and 4, 5, 7, 10, and 12 µL of bovine FF to determine optimal volume for depletion. Each plasma and FF sample volume was diluted with 1x buffer A, pH 7.4 (# 5185-5987, Agilent Technologies, CA, USA) to achieve a final volume of 200 µL.

Initial quantification of the crude samples showed the sperm samples were markedly of lower concentration compared to that of plasma or FF and upon depletion resulted in very low yield. Therefore, to ensure enough proteins is obtained in depleted samples for downstream analysis depletion volumes were increased to 60 µL for ejaculated semen plasma and 154 µL each for ejaculated sperm proteins, epididymis semen proteins and epididymis sperm proteins. For 154 µL depletion volume, 46 µL of 4x buffer A (# 5188-8283, Agilent Technologies, CA, USA) was added to achieve a total volume of 200 µL. For depletion volume of 60 µL, 94 µL of water was added after addition of 46 µL of the 4x buffer A to obtain a final volume of 200 µL. The 4x dilution buffer A was used for the higher depletion volumes of the sperm to ensure similar neutral pH achieved with the plasma and FF samples using 1x buffer A.

Diluted samples were transferred to 0.22µm spin filters (Corning Incorporated, NY, USA) and centrifuged at 16 000 x g for one minute. Filtered samples were applied to the spin cartridge which was previously equilibrated with 4 mL 1x buffer A. Flow-through (FT) fraction (*i.e.* depleted fraction) was collected by centrifuging at 100 x g for 1.5 minutes. To ensure optimal recovery of FT, the cartridge was washed twice each with

400 µL 1x buffer A. Each wash volume was collected by centrifuging for 2.5 minutes at 100 x g. Collected wash volumes were combined with initial collected FT. Bound fraction were eluted using 2 mL of elution buffer B (#5185-5988, Agilent Technologies, CA, USA) at a flow rate of about 0.15 mL/min. Non-depleted samples, eluates, FT, and buffers were stored on ice throughout the experiment period to ensure protein integrity. Collected FT and eluates were stored at -80^{o}C until ready for analysis.

2.4.6 Coomassie Bradford Assay

Coomassie (Bradford) assay kit, (#23200, Pierce Biotechnology, IL, USA) was used to determine protein concentrations of bound, depleted and non-depleted samples. The quantification was done according to manufacturer's instruction. Bovine serum albumin, 2 mg/mL (#23209, Thermo Scientific, IL, USA) was used as a standard for making a calibration curve which covered a concentration range of 0.00-1500 µg/mL.

2.4.7 Sandwich ELISA Analysis

BSA, IgG and IgA concentrations in non-depleted and depleted (FT) samples were determined using sandwich ELISA assay kits (Bethyl laboratories Inc., TX, USA). IgG was analyzed with bovine IgG ELISA quantitation set (Cat. No. E10-118), IgA with bovine IgA ELISA quantitation set (Cat. No. E10-131) and albumin with bovine albumin ELISA kit (Cat. No. E11-113). Samples were diluted and washed with vendor-provided buffers. Specific dilution factors used for the different samples are shown in Table 2. All quantifications were performed according to manufacturer protocols. Briefly, 100 µL of dilute IgA or IgG Coating Antibody solution was added to each assay well. The wells were incubated at room temperature for an hour and washed with 1x Wash Buffer. 200

µL Blocking Solution was added to each well and incubated at room temperature for 30 minutes to block non-specific binding sites. Wells were then washed with 1x Wash Buffer. Assay wells for determining BSA concentration were obtained pre-coated with anti-bovine albumin antibody. 100 µL of the diluted FT or non-depleted fractions were then added to the assay wells with the coated antibodies. After one hour incubation at room temperature, unbound proteins were washed with 1x Wash Buffer.

In determining IgA or IgG concentrations, 100 µL of horseradish peroxidase (HRP) conjugated anti-bovine IgA or IgG Detection Antibody solution was added to each well and incubated at room temperature for an hour to bind to the captured IgA or IgG. For albumin determination, 100 µL of Albumin Detection Antibody solution and 100 µL of HRP solution were added stepwise with incubations at room temperature for an hour after the Detection Antibody addition and for 30 minutes after the HRP solution addition. Wells were then washed with 1x Wash Buffer. 100 µl of 3,3',5,5'-Tetramethylbenzidine (TMB) Substrate Solution was added to each well and incubated in the dark for 15 minutes in IgA or IgG measurements or 30 minutes in albumin measurement to initiate a calorimetric reaction which was stopped by addition of 100 µL Stop Solution to each well. Absorbance was measured at 450 nm by Synergy H1 Hybrid Multi-Mode Reader (BioTek, VT, USA). BSA, IgA and IgG concentrations were derived from calibration curves of reference standards included in the quantitation kits.

2.4.8 SDS PAGE

Depleted and bound proteins were buffer exchanged into 0.05% TEAB using zeba spin desalting columns, 7k MWCO (# 89891, Pierce Biotechnology, IL, USA) according

to manufacturer protocol. Samples were vacuum dried prior to SDS-PAGE analysis. SDS-PAGE was performed under reducing and non-reducing conditions. Under reducing conditions, β-ME was diluted 1:20 in laemmli buffer and the resulting solution diluted twice with water. 15 µL of the prepared sample buffer was added to each vacuum dried sample. Samples were vortexed, centrifuged and then boiled in a water bath for three minutes. Boiled samples were quickly loaded onto a pre-cast gel. Non-reducing conditions excluded the addition of the β-ME and heating step. Equal amounts of 9 or 20 µg of proteins and 5-8 µL of Precision Plus Protein^{TM} unstained standard, 10-250 kDa (Bio-Rad Laboratories Inc., CA, USA) was used in the gel runs. Gels were electrophoresed in Bio-Rad Power Pac^{TM} unit using 1x Tris/glycine buffer and at constant voltage of 150 for 62 minutes. Gel bands were visualized using Coomassie BioSafe G250 stain according to manufacturer instructions. Images were acquired using Proteineer SPII (Bruker Daltonics) equipped with SP3 Control software.

2.4.9 In-Gel Tryptic Digestion of Coomassie-Stained Gel Bands

Identities of protein-gel bands from bound fractions (HAPs fraction) were determined using in-gel digestion nano-LC-MS/MS. For in-gel digestion, each gel band from the bound protein lane was excised with sanitized cutting blade, transferred onto previously sanitized glass plate and then chopped into pieces. Gel pieces were transferred to a 0.5mL microcentrifuge tube and washed with 100µL LC/MS-grade water with gentle vortexing for five minutes. The water was removed and the gel pieces completely destained by washing with several 100µL portions of 25 mM ammonium bicarbonate (ABC) in ACN/ water (v/v = 50/50) solution. Destained gel pieces were dehydrated with

100 µl ACN for 10 minutes and dried in a speed-vac at 4ºC for 5 minutes. Reduction was done with 100 µl of 10 mM DTT at 55ºC for 30 minutes.

After removal of reduction solution, alkylation was carried out by addition of 100 µL of freshly prepared 55 mM iodoacetamide and incubating in a dark room for 45 minutes. Gel pieces were washed with 100µL 25 mM ABC solution for 10 minutes, dehydrated with 100 µL ACN, and dried in speed-vac at 4ºC for five minutes. 30 µL of freshly prepared cold 20 µg/mL TPCK treated trypsin (P/N 4370282; Ab Sciex Pte Ltd, MA, USA) in 25 mM ABC solution was then added to each sample and incubated on ice until gel pieces became fully rehydrated and clear. Excess trypsin solution was removed and the gel pieces were covered with 30 µL 25 mM ABC solution and incubated for 16 h at 37ºC. To extract tryptic peptides, 25 µL of 25 mM ABC solution was added and the liquid fraction collected. Then 50 µL of ACN was added and incubated for 10 minutes with slight shaking and the liquid fraction also collected. Finally, 30 µL water and 50 µL ACN were added stepwise with 10 minutes incubation with shaking in each step and the liquid fraction also collected. All extracted liquid fractions were combined, frozen for 15 minutes and dried in a speed-vac at 4ºC. Dried peptides were stored at -80ºC.

2.4.10 Nano-LC-MS/MS

Dried peptides were purified and concentrated with either Pierce® C18 spin columns (Pierce Biotechnology, IL, USA) or ZipTip C_{18} tips (Millipore, MA, USA) based respectively on high intensity or low intensity of coomassie blue stained-gel band prior to de-staining. Purification was done according to manufacturer protocols. Purified samples were dried in a speed-vac at 4ºC and stored at -80ºC until analysis. Protein

identification was performed with nano-liquid chromatography tandem mass spectrometry (nanoLC-MS/MS) analysis by using Eksigent nanoLC - Thermo LTQ mass spectrometer. The dried, purified digest from each interested protein band was brought up in water/ACN/formic acid (95%5%/0.1%) and then was loaded on IntegraFrit Sample trap (ProteoPep II^{TM} C18, 300 Å, 5µm , 100 µm × 25 mm New Objective, Inc., Woburn, MA). The retained peptides were washed isocratically with water premixed with 0.1% formic acid pumped from channel 1A to remove any excess reagents. The cleaned peptides were resolved on an analytical column (ProteoPep^{TM} II C18, 300 Å, 5µm, 75 μm ×100 mm, 75 µm tip size, New Objective, Inc., Woburn, MA) with a multistep gradient of solvent 2A (water premixed with 0.1% formic acid) and solvent 2B (ACN premixed with 0.1% formic acid) at a flow rate of 200 nL/min. A 90-min or a 240-min gradient was used for the peptides separation. The 90-min gradient started at 5% solvent B and was held for 5 minutes, then linearly increased to 40% solvent B at 55 min and to 95% solvent B at 65 min and finally held at 95% solvent B for 5 min before allowing to return to initial 5% solvent B at 73 min. Column re-equilibration with initial 5% solvent B was done for 17 min. The 240-min gradient started at 5% solvent B and was held for 5 minutes, then linearly increased to 40% solvent B at 190 min and to 95% solvent B at 205 min and finally held at 95% solvent B for 15 min before allowing to return to initial 5% solvent B at 223 min. Column re-equilibration with initial 5% solvent B was done for 17 min.

The LTQ mass spectrometer was operated in the data-dependent mode. The full MS spectra were acquired in positive mode within a range of 300-1800 m/z. Top three ions with intensities exceeding a preset threshold in full mass scan were chosen for

Table 2.1. Concentrations of crude bovine fluids and data on yield (flow-through proteins) obtained after immunodepletion of abundant proteins

Sample	Concentration of crude (µg/ml)	Load volume (µl)	Load (µg)	Yield (µg)	Yield (%)	Yield concentration (µg/ml)
Plasma	63960.2 ± 6523.0	4	255.8 ± 26.1	71.2 ± 11.4	27.9 ± 3.8	17798. ± 2839.4
Follicular fluid	56445 ± 4196.8	5	287.9 ± 19.9	47.9 ± 11.1	17.3 ± 4.2	9988.6 ± 2119.4
Epididymis sperm proteins	582.8 ± 64.3	154	89.8 ± 9.9	30.5 ± 4.5	34.1 ± 4.6	200.5 ± 30.8
Epididymis semen proteins	1857.6 ± 236.7	154	286.1 ± 36.5	109.7 ± 7.33	38.7 ± 3.82	712.6 ± 47.6
Ejaculated sperm proteins	1744.6 ± 42.35	154	268.7 ± 6.52	134.6 ± 9.4	50.9 ± 3.4	874.2 ± 61.13
Ejaculated semen plasma	19678.9 ± 2866.7	60	1238.2 ± 156.8	552.2 ± 66.4	44.6 ± 1.5	9202.9 ± 1106.9

Table 2.2. Dilution factors used in sandwich ELISA assay for measuring BSA, IgG and IgA concentrations in non-depleted and flow-through (FT) fractions

	Dilution factors					
	Albumin		IgG		IgA	
Sample	Non-depleted	FT	Non-depleted	FT	Non-depleted	FT
Plasma	2.5E+05	4.0E+02	1.0E+05	2.0	7.5E+04	3.0
Follicular fluid	1.5E+05	2.0E+01	9.0E+04	2.0	1.5E+04	2.0
Epididymis sperm proteins	3.0E+03	1.0E+02	1.0E+02	2.0	5.0E+01	1.0
Epididymis semen proteins	1.0E+04	3.0E+02	3.0E+02	8.0	5.0E+01	2.0
Ejaculated sperm proteins	3.0E+03	5.0E+02	2.0E+02	2.0	1.0E+02	5.0
Ejaculated semen plasma	1.0E+04	2.0E+01	3.0E+02	2.0	2.0E+02	1.5

collision- induced dissociation (CID) in LTQ. The Q activation and time was set respectively at 0.25 eV and 30 ms. The maximum ion injection times used were 5.0 $x10^4$ ms for the MS scan and 1.2 $x10^5$ for the MS/MS scan. The automatic gain control target settings were 3.0 $x10^4$ for the MS scan mode and 1.0 x 10^4 for the MS/MS scan mode. The normalized collision energy was 35 eV and the isolation window employed was 2.5 m/z. The dynamic exclusion settings utilized were repeat count 2, exclusion duration 36 s, exclusion list size 500, exclusion mass width low 1.0 and exclusion mass width high 1.5.

2.4.11 Protein Identification

The LC-MS/MS raw data from nanoLC-LTQ were correlated to theoretical fragmentation patterns of tryptic peptide sequences from the Fasta databases (Bovine and human) using SEQUEST™ (Thermo Fisher). The search parameters included (i) fixed cysteine modifications of +57 Da for carbamidomethyl-cysteines, (ii) variable modifications allowing +16 Da with methionines for methionine sulfoxide; (iii) restricted to trypsin-digested peptides and allowed for two missed cleavages; (iv) precursor mass range was 310-5000 Da; (v) precursor mass tolerance of 2.5 Da and fragment mass tolerance of ±0.8 Da; (vi) target false discovery rate (FDR) strict was 0.01 and FDR relaxed was 0.05; (vii) peptide were identified based on top hit(s) with individual cross correlation exceeding a threshold dependent on the precursor charge state. The proteins matched with at least two peptides at minimum 95% confidence (false discovery rate (FDR) of ≤5%) were considered as positive identification.

2.4.12 Reproducibility and Recovery of MARS Hu-6HC on Bovine Fluids

To determine reproducibility of the MARS Hu-6HC cartridge, the bovine fluids were subjected to 3-5 replicate depletions on same day for 2-5 separate days. Reproducibility was assessed by coefficient of variations (CVs) of the percent of total protein depleted (Table 2.3.) and by SDS PAGE separation of crude, bound and depleted fractions (Figure 2.2. and 2.4.). Recovery was determined as protein content in bound plus FT fractions expressed as percent of protein content in non-depleted sample (Table 2.4). Recovery ranged from 73-101%. Recovery of plasma (94%) and FF (101%) were higher than that of the sperm samples (73-82%).

Table 2.3. *Total protein depleted with the MARS Hu-6HC cartridge on bovine fluids

Sample	Volume Depleted (µl)	Total protein depleted on same day (%)		Total protein depleted on separate days (%)	
		Mean ± SD	% CV	Mean ± SD	%CV
Plasma	4	71.9 ± 4.9	6.8	72.1 ± 3.8	5.2
Follicular fluid	5	86.0 ± 3.6	4.2	82.6 ± 3.8	4.6
Epididymis sperm proteins	154	66.2 ± 2.1	3.2	66. 1 ± 4.6	6.9
Epididymis semen proteins	154	58.2 ± 2.9	5	61.3 ± 3.8	6.2
Ejaculated sperm proteins	154	49.7 ± 2.9	5.9	49.8 ± 3.3	6.6
Ejaculated semen plasma	60	53.6 ± 2.4	4.5	53.7 ± 1.9	3.5

*Total protein depleted data were obtained from 2-5 separate days of depletions with n= 3-5 replicates on day depletion.

2.5 RESULTS

2.5.1 Depletion Efficiency of Target Proteins from the Bovine Fluids

Percent depletion of the bovine samples by using the MARS Hu-6HC cartridge in removing the target HAPs was determined by comparing the total protein content in the FT (depleted) fraction to that of the non-depleted samples. Total protein depleted from each bovine fluid is shown in Table 3. Total protein depleted, expressed as percent depletion were comparable for different volumes of plasma or FF investigated: 67.9 ± 3.1 (4.1%) for 2, 4, 6, 8, 10, 12, and 14 µL of plasma and 83.4 ± 6.0 (7.2%) for 4, 5, 7, 10, 12, and 14 µL of FF; mean ± SD (%CV) (Figures 1 and 2). Therefore, 4 µL plasma and 5 µL of FF were used in further investigation to conserve samples. Percent of LAPs (yield) from each bovine fluid is shown in Table 1. From two to five separate days of depletion, total protein depleted was highest for the FF sample (82.6 ± 3.8%) followed by the plasma sample (72.1 ± 3.8%) and then the four sperm- sample types- 66.1 ± 4.6 for epididymis sperm proteins, 61.3 ± 3.8% for epididymis semen proteins, 49.8 ± 3.3% for ejaculated sperm proteins and 53.7 ± 1.9% for ejaculated semen plasma. Similar values were obtained for same day depletions (Table 2.3).

The effectiveness of depletion of abundant proteins was also assessed by SDS PAGE separation of non-depleted, bound and depleted proteins. Figures 2.2, 2.3, and 2.4 reveal the unmasking and highlighting of LAPs after dramatic removal of HAPs from the different bovine fluids. In-gel digestion nano-LC-MS/MS analysis of gel bands from bound fractions identified four out of the six target HAPs namely serum bovine albumin (BSA), IgG, IgA and α-1-antitrypsin. Gel bands containing these proteins are shown in

Figure. 2.2. Transferrin and Hp were not identified in the bound fractions by the nanoLC-MS/MS method.

2.5.2 Specific Depletion Efficiency of BSA, IgG and IgA

Depletion efficiency (i.e. the extent of removal) of BSA, IgG and IgA from the different bovine fluids was individually assessed using sandwich ELISA. Results showed depletion of 98.25 to 99.99% BSA, 98.65 to 99.96% IgG and 98.85 to 99.96% IgA from all the bovine samples studied (Table 2.5). The observed depletion rates are comparable to manufacturer specification of 98.9-99.9% obtained for human biological fluids. Depletion efficiency for α-1-antitrypsin was not measured by the ELISA method. However, the dramatic removal of its protein gel band (Figure. 2.2) indicates similar depletion rate for this protein can be expected.

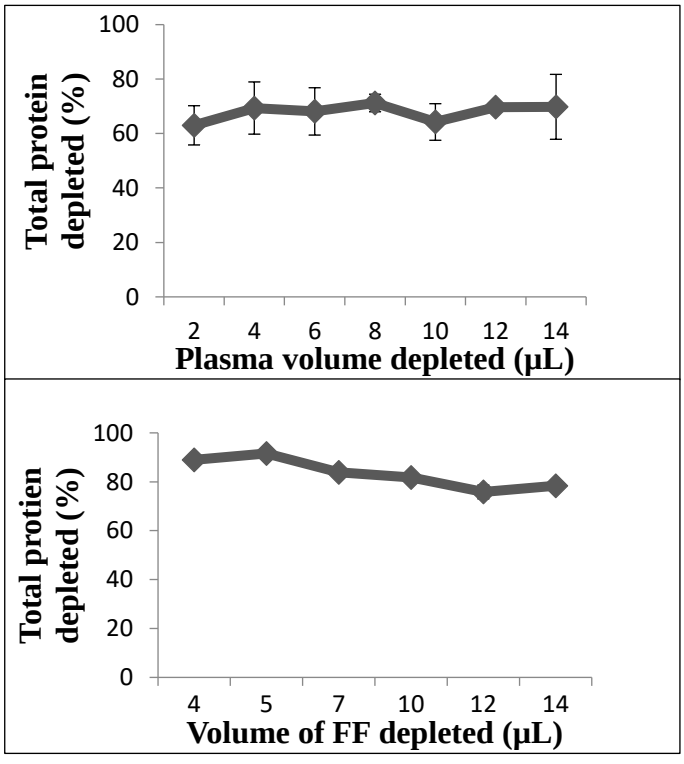

Figure 2.1. Total proteins depleted from different volumes of bovine plasma and follicular fluid (FF) with the MARS Hu-6HC cartridge. Total protein depleted is similar over 2 (n=1), 4 (n=7), 6 (n= 7), 8 (n=2), 10 (n=5), 12 (n=2), and 14 (n=8) µL of plasma and 4 (n=1), 5 (n=1), 7 (n=3), 10 (n=2), 12 (n=2), and 14 (n=2) µL of FF.

2.5.3 Specificity of the Immunodepletion

To assess the specificity of the depletion method for the target proteins in bovine fluids, 1-D SDS PAGE nano-LC-MS/MS analysis was performed on bound fractions. Concomitant removal of non-target proteins were observed from all the bovine samples depleted. These are summarized in Table 2.6. Non-target proteins from bound fraction of the ejaculated sperm types included three major binder of sperm (BSP) proteins namely PDC-109, BSP-A3 and BSP-30kD (Figure 2.3). Among the BSP depleted, the highest depletion rate was observed for PDC-109 which forms 25-47% of total BSP proteins[105].

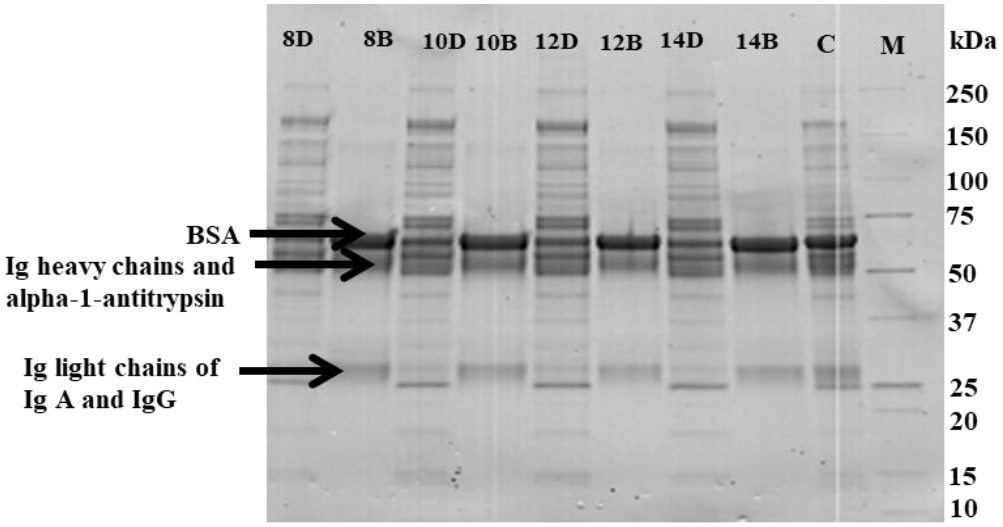

Figure 2.2. Reproducibility of the MARS Hu-6HC cartridge on different depletion volumes of bovine plasma. Lanes: 8D, 10D, 12D and 14D- Depleted fractions respectively from depletion of 8, 10, 12 and 14 µL of bovine plasma; B8, B10, B12 and B14- Bound fractions respectively from depletion of 8, 10, 12 and 14µL of bovine plasma; C-Crude bovine plasma; M- Molecular weight marker. Reproducibility of the separation show similar depletion efficiencies were obtained for the different volumes of plasma depleted. Arrows show gel bands at the respective molecular weights of depleted BSA, IgA, IgG, and alpha-1- antitrypsin. 9µg of proteins were loaded on each lane of 4-20% Criterion™ TGX precast gel and run under reducing conditions using β-ME. Bands were visualized with Coomassie blue staining

2.5.4 Reproducibility

The immunodepletion method had good reproducibility for all the bovine samples studied. The coefficient of variations (%CVs) of depletion efficiencies determined on the same day or separate days ranged 3.2 to 6.8 and 3.5 to 6.9 %, respectively (Table 2.3). The good reproducibility is also supported by the consistent protein band pattern on the SDS PAGE gel as is demonstrated in Figure 2.4.

Table 2.4. Recovery with depletion method

Sample	Volume Depleted (µL)	Recovery (%)	
		Mean ± SD	% CV
Plasma	4	93.96 ± 11.57	12.31
Follicular fluid	5	101.35 ± 10.98	10.83
Epididymis sperm proteins	154	73.65 ± 7.51	10.2
Epididymis semen proteins	154	81.77 ± 7.42	9.08
Ejaculated sperm proteins	154	79.65 ± 3.82	4.8
Ejaculated semen plasma	60	81.45 ± 3.53	4.33

Data obtained from 2-5 separate days of depletions with n= 3-5 replicates on day depletion

Table 2.5. Depletion efficiencies of BSA, IgG and IgA obtained with the MARS Hu-6HC cartridge on Bovine fluids from Sandwich ELISA Analysis

	% Depletion Efficiency (Mean ± SD)		
Sample	Albumin	IgG	IgA
Plasma	98.73 ± 0.29	99.45 ± 0.01	98.85 ± 0.21
Follicular fluid	99.97 ± 0.02	99.96 ± 0.00	98.85 ± 0.60
Epididymis sperm proteins	99.92 ± 0.04	99.61 ± 0.24	98.79 ± 0.45
Epididymis semen plasma	99.98 ± 0.00	99.57 ± 0.21	99.40 ± 0.12
Ejaculated sperm proteins	99.52 ± 0.20	99.52 ± 0.03	99.63 ± 0.04
Ejaculated semen plasma	99.45 ± 0.01	98.65 ± 0.06	99.96 ± 0.02

N= 2 replicates on 1-2 separate day

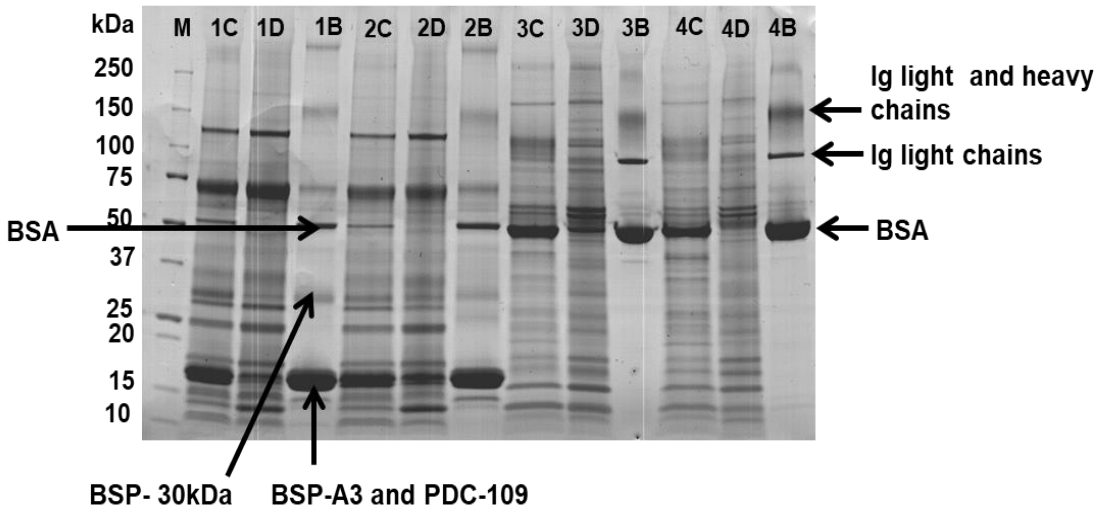

Figure 2.3. Unmasking and highlighting of LAPs after removal of HAPs from bovine ejaculated and epididymis sperm types with MARS Hu-6Hc cartridge. M- Molecular weight marker. C- Crude sperm sample; D- Depleted fraction; B- Bound fraction. 1, 2, 3, and 4 respectively ejaculated sperm proteins, ejaculated semen plasma, epididymis sperm proteins and epididymis semen proteins. BSA, IgG and IgA were targeted proteins depleted. Seminal plasma proteins- PDC-109, BSP-A3 and BSAP-30 kDa were non-specifically depleted from ejaculated sperm sample types. These seminal plasma proteins are HAPs found in ejaculated sperm. 20 µg of proteins were loaded on each lane of 4-20% Criterion™ TGX precast gel and run under non-reducing conditions. Bands were visualized with Coomassie blue staining.

2.6 DISCUSSION

Immunodepletion methods are popular and often the first step fractionation to narrow the wide concentration range in biological samples and reduce sample complexity. To date, available immunodepletion methods for bovine samples are very limited. This study report a method for simultaneous immunodepletion of abundant proteins BSA, IgG, IgA and alpha-1-antitrypsin from bovine plasma, FF, epididymis and ejaculated sperm types with high depletion rates. Depletion rates for BSA, IgG and IgA were confirmed as 98.7 to 99.9% from all the bovine fluids studied using sandwich ELISA. The observed depletion rates are comparable to that stated by manufacturer for

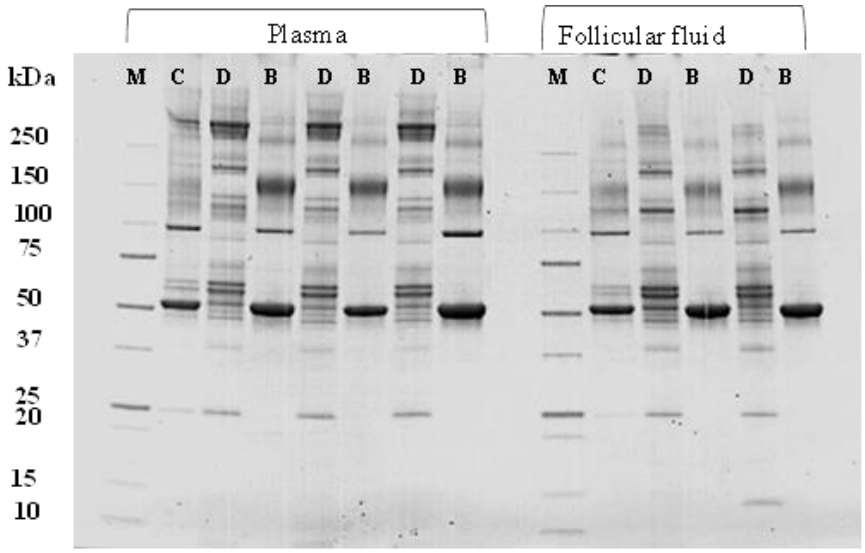

Figure 2.4. Reproducibility of the immunodepletion of bovine plasma and follicular fluid (FF) with the MARS Hu-6HC spin cartridge. Three replicates of plasma and two replicates of FF depletions were carried out with respectively 4µL and 5µL depleted volume in each case. Lanes: M-Molecular weight marker; C-Crude sample; D- Depleted fraction; B-Bound fraction. 6 µg of proteins were loaded on each lane of 4-20% Criterion™ TGX precast gel and run under non-reducing conditions. Bands were visualized with Coomassie blue staining.

these proteins from human fluids which is 98.9-99.9%. The similar depletion rates indicate sample variability did not significantly affect the affinity of the MARS polyclonal antibodies for the target proteins in the bovine fluids. Greater sequence similarities between the target proteins in human and bovine explains the effective application of this immunodepletion technology on bovine fluids. A search in UniprotKB database (http://www.uniprot.org) showed human serum albumin and alpha-1-antitrypsin respectively share greater than 75 and 68% sequence identity with their respective proteins in bovine. Sequence identity between human and bovine immunoglobulins light chains range is 53-76% whiles the heavy chains range is 33-65%. The high depletion rates achieved with the presented method makes it a viable alternative for achieving

immunodepletion of these abundant proteins in bovine biological fluids while similar technology is currently unavailable

Table 2.6. SEQUEST results showing non-target proteins* in bound fractions of bovine plasma, follicular fluid (FF), epididymis, and ejaculated sperms after depletion with MARS Hu-6HC cartridge.

Accession	No of peptides identified	Score	Description	Protein Family[ɪ]
B8Y9S9	38	528.63	Embryo-specific fibronectin 1 transcript variant	
P07589	27	515.40	Fibronectin	
Q7SIH1	33	395.84	Alpha-2-macroglobulin	
P02784[a]	8	323.32	Seminal plasma protein PDC-109	
F1MAV0	19	238.79	Fibrinogen beta chain	
A5PJE3	16	229.46	Fibrinogen alpha chain	
G3X7A5	17	179.49	Complement C3	
P12799	8	173.91	Fibrinogen gamma-B chain	
P81019[a]	3	62.58	Seminal plasma protein BSP-30 kDa	
P01030	2	42.92	Complement C4	
P04557[a]	2	34.56	Seminal plasma protein A3	
F1MBL6	2	32.17	Uncharacterized protein (Fragment)	P13/P14 kinase family
F1MI18	2	24.05	Uncharacterized protein	Alpha-2 macroglobin family
E1BIF6	2	19.75	Uncharacterized protein	Ubiquitin associated domain
P23805	4	16.95	Conglutinin	
Q28085	2	15.71	Complement factor H	
G3N0S9	2	11.42	Uncharacterized protein	Sushi CCP/SCR domain family
F1N5M2	2	8.76	Vitamin D-binding protein	

*List excludes trypsin and keratin related proteins
[ɪ] Identified from UniProt KB search with accession number
[a]Only observed in ejaculated sperm types

Contrary to the lack of effect of sample variability on individual target protein depletion rate, sample variability seems to affect the total proteins depleted in a sample. Total protein depleted was about 50- 83% for the bovine samples investigated. This range

was lower than the manufacturer specifications of 85-90% for human serum. But bovine FF and plasma were closer to the lower end range; respectively 83% and 71%. The total protein depleted is based on the levels of the target proteins in certain samples. Thus, differences in the levels of the target proteins in the different bovine fluids and between human and bovine would affect the total protein depleted. For instance, albumin, the most abundant protein in plasma represents more than 50% of the total protein in human plasma[15] and about 42% in bovine plasma[106]. Plasma and FF are closely related in composition and majority of proteins in FF are viewed to originate from the blood[107-109]. But albumin is higher in FF compared to serum[110, 111] which might explain the highest depletion rate attained with the FF. 2-DE analysis of caudal epididymis fluid found albumin represented ~21% of all proteins spots detected [42]. By contrast, albumin concentration is very minimal in ejaculated sperm[112]. Accordingly, total proteins depleted were lower for the sperm sample types compared to the plasma and FF samples.

The lower total proteins depleted from the bovine fluids are also contributed by the lack of depletion of Hp and transferrin which are both target proteins of the MARS Hu-6HC cartridge, contributing to the manufacture stated 85-90% . Sequence homology could not explain the lack of removal of both proteins as they are highly homologous between human and bovine, respectively 69% and 75% sequence identity. High specificity of the MARS Hu-6HC cartridge for human transferrin and Hp appears to be the primary reason for both proteins not depleted from the bovine fluids. Although Hp and transferrin were not depleted, the simultaneous rapid depletion of albumin, IgG, IgA and alpha-1-antitrypsin from all the bovine fluids show the effectiveness of application of the current immunodepletion method to bovine fluids. Albumin and IgG represents about

60% of the bovine plasma proteome. Depletion of both proteins increased the number of spots and intensities on a 2-DE map[18]. The additional depletion of abundant proteins by this depletion method is expected to provide more desirable probing of low copied proteins in gel-based and gel-free proteomic workflows for bovine fluids analysis. As shown in this study, the depletion of the four major proteins unmasked and highlighted more protein gel bands in SDS PAGE gels presented. Because the HAPs were removed in a single step, sample loss is expected to be minimized. Also, time is reduced.

To determine reproducibility of the immunodepletion, replicate depletions on same day and on separate days were analyzed. The results show the method had high reproducibility on the bovine fluids as revealed by the low % CV values of total proteins depleted from different and same volumes. Because immunodepletion is often a first step fractionation option, a good reproducibility for its application is critical to the accuracy and further reproducibility of downstream protein separation, identification, and quantification. Low loading volumes of plasma and FF (4 and 5 µL) did not affect the reproducibility and this can be beneficial if sample is limiting.

Concomitant removal of non-target proteins in immunodepletion methods is often inevitable[99, 100]. Non-target proteins removal from the bovine fluids included other HAPs, e.g. PDC-109, BSP-A3, BSP-30kD, alpha-2-macroglobulin, complement C3, complement C4, and fibrinogen. Non-target proteins removal could result from non-specific binding to cartridge resin, accidental/specific cross reaction of the antibodies, or interactions with the target proteins. The BSP proteins were consistently removed from the ejaculated sperm samples. Their dramatic removal is considered beneficial since they are major proteins constituting 40-57% of the total protein in the seminal plasma

component of ejaculates. PDC-109 alone forms 25-47% of the BSP proteins mass[105]. Thus, depletion of the BSP proteins can additionally enhance the analysis of LAPs in these ejaculates. However, caution should be taken when applying this depletion method to target these seminal proteins since their removal is non-specific. In such cases, a better approach would be to analyze both the bound and unbound fractions to ensure adequate estimation of their depletions.

2.7 CONCLUSION

Immunodepletion methods for bovine fluids are currently very limited. This study describes an immunodepletion method for simultaneous removal of minimum of four HAPs in different bovine fluids. The high depletion efficiencies (98.7-99.9%) and reproducibility make it practical for its application in bovine proteomic analyses.

2.8 ACKNOWLEDGEMENT

We thank the support of National Science Foundation (NSF) grant number 1446886, and USDA National Institute of Food and Agriculture, Hatch project 1004566. We also thank the Core Campus Mass Spectrometry Facility at South Dakota State University (SDSU) supported in part by the National Science Foundation (NSF)/EPSCoR Grant No. 0091948 and NSF MRI Grant No. SS1000060 and the State of South Dakota and the Functional Genomics Core Facility at SDSU supported in part by NSF/EPSCoR Grant No. 0091948 and by the State of South Dakota.

CHAPTER 3

iTRAQ-BASED QUANTITATIVE ANALYSIS OF BOVINE PLASMA AND FOLLICULAR FLUID

3.1 ABSTRACT

Bovine follicular fluid (FF) creates a unique microenvironment in follicles necessary for follicle growth and oocyte maturation, and preovulatory concentrations of estradiol (E2) have been reported to impact several processes involved with fertility. The objective of this study was to analyze changes in proteins in FF and plasma (PL) from animals with high E2 (HE2) or low E2 (LE2) during the pre-ovulatory period. Beef cows were synchronized with an injection of GnRH on day -7 and an injection of prostaglandin $F_{2\alpha}$ ($PGF_{2\alpha}$) on day 0. Follicular dynamics and ovulatory response were monitored using transrectal ultrasonography. Nine cows were selected and slaughtered, blood samples were collected at slaughter and FF was aspirated from dominant follicles (DF; >10 mm). Abundant proteins (albumin, IgG, IgA, and alpha-1-antitrypsin) were depleted from both PL and FF. Peptides were labeled with iTRAQ reagents and quantified using two-dimentional liquid chromatography ESI-based mass spectrometry. Estradiol was associated with increased protein changes in PL and FF. Protein expression changes between FF HE2 and FF LE2 were higher than PL HE2 and PL LE2. There were 15 up-regulated proteins and 10 down-regulated proteins in FF HE2 compared to FF LE2. Seven proteins were up-regulated and nine proteins down-regulated in PL HE2 compared to PL LE2. Proteins were more predominant in PL than in FF but the extent of protein increase with HE2 was greater in FF than in PL. Several of the differentially expressed

proteins function in follicle development and were mainly categorized under cellular process and metabolic process. Pathway analysis identified the up- and down-regulated proteins were predominantly associated with the complement and coagulation cascades. The data demonstrates E2 regulates a wide range of reproductive associated proteins in bovine PL and FF, and can provide the basis for further investigation of specific processes involved in such regulation.

3.2 BACKGROUND AND MOTIVATION

Follicular fluid (FF) provides a unique microenvironment for developing oocytes. It contains substances that primarily originate from circulating blood and from secretions by granulosa cells (GCs), theca cells, and the oocyte[108]. Proteins are a major proportion of the FF with total concentrations comparable with that in plasma[113]; however, the composition of the proteins in FF changes with follicle development[40, 114] which indicates their involvement in the development of the follicle and competent oocyte. Accordingly, FF proteins have been implicated in oocyte meiosis, ovulation, formation of the corpus luteum, and fertilization[108]. Thus, FF proteins can reflect the physiological condition of the follicle and may serve as biomarkers for follicle growth and maturation.

Estrogens are an important component of FF. During the steroidogenesis process, androgens produced in the theca cells traverse the basement membrane of the neighboring GCs where they are converted by cytochrome P450 aromatase (CYP19A1) under the influence of follicle stimulating hormone (FSH) to estrogens[115], with Estradiol-17β (E2) being the principal form of estrogen present[115, 116]. The pre-ovulatory follicle is reported to have the highest intra-follicular levels of E2 mainly because of the large number of GCs and its capacity for androgen aromatization[115].

In developing follicles, E2 stimulates proliferation and differentiation of GCs[115], and promotes growth, gap-junction formation, antrum formation, and inhibition of atresia[117]. Perry et al[118] reported that among cows exhibiting standing estrus peak concentration of E2 were greater and positively associated with follicle size, but this association was not found in cows not exhibiting standing estrus. Cows with increased

concentration of circulating E2 had an up-regulation of the steroidogenic pathway during the pre-ovulatory period as evidenced by increased concentrations of steroidogenic associated enzymes 3β-hydroxysteroid dehydrogenase (3β-HSD), CYP19A1, and cytochrome P450 side-chain cleavage enzyme (CYP11A1) and steroidogenic products estradiol and androstenedione[103].

An important means by which E2 achieves its regulatory reproductive functions is via regulation of proteins and protein receptors involved in the relevant functions. Such proteins include insulin-like growth factor 1 (IGF-1) which promotes proliferation of GCs and endometrial epithelial cells[119], follicle stimulating hormone (FSH) receptors in GCs, and LH/human chorionic gonadotropin (hCG) receptors in GCs and thecal interstitial tissues when coupled with FSH[120]. Quantitative shot-gun proteomics, incorporating isobaric labeling techniques such as isobaric tags for relative and absolute quantitation (iTRAQ) and tandem mass tags (TMT), allow measuring of protein changes in time-dependent manner with greater precision and accuracy than label-free methods[26]. This can be applied to determine the influence of E2 on the expression of several proteins in a short period. Its application to FF is also beneficial considering the large number and diversity of the FF proteome. Ferrazza et al[40] recently utilized TMT labels and identified 22 differentially expressed proteins in bovine FF between different stages of follicle development. The group also demonstrated a correlation between some of the differentially expressed proteins (includes modified fibrinogen, alpha-2-macroglobulin, plasminogen, immunoglobulin M heavy chain, and spondin-1) and concentration of E2 or progesterone.

3.3 OBJECTIVE OF STUDY

The objective of this study was to use the iTRAQ proteomic approach to quantitatively measure PL and FF proteomes and identify the influence of high and low pre-ovulatory circulating concentrations of E2 on PL and FF proteomes.

3.4 MATERIALS AND METHODS

3.4.1 Materials and Reagents

Ammonium bicarbonate (ABC) and iodoacetamide were purchased from Acros Organics (New Jersey, USA). Formic acid, acetonitrile (ACN), triethylammonium bicarbonate (TEAB) and water were obtained from Fischer Scientific (New Jersey, USA). Dithiothreitol (DTT) was purchased from Promega (Wisconsin, USA). Zeba™ desalting spin columns from Pierce (Rockford, IL,USA). All chemicals and water were of LC/MS grade.

3.4.2 Estradiol Measurement

Estradiol (E2) concentrations in PL and FF (PL and FF collected as described in Chapter Two) were measured by radioimmunoassays (RIA) according to procedures as previously described[121] and animals were then classified as either high E2 (peak estradiol $\geq$ 6.0 pg/mL; PL: n = 4, FF: n = 4) or low E2 (peak estradiol $\leq$ 4.5 pg/mL; PL: n = 5, FF: n = 5) according Jinks et al[122]. Concentrations of E2 and changes in the steroidogenic pathway have previously been reported by Larimore and coworkers[103].

3.4.3 Coomassie Bradford Assay Quantitation

The protein contents in depleted samples were quantified using Coomassie (Bradford) assay kit, #23200 (Pierce Biotechnology, IL, USA) according to manufacturer's instruction. Bovine serum albumin (#23209, Thermo Scientific, IL, USA) was used as a standard for making a calibration curve. The standard (2 mg/mL) was diluted with 50 mM TEAB and the calibration curve covered a concentration range of 0.00-1500 µg/mL.

3.4.4 Reduction, Alkylation, Digestion, and iTRAQ Labeling of Proteins

Fifty µg of each of the four depleted bovine samples (PL and FF) containing high or low E2 (i.e. PL HE2, PL LE2, FF HE2 and FF LE2) were pooled and vacuum dried (Labconco, Kansas, MO, USA) at 4 ^{o}C. The dried proteins were prepared with 4-plex iTRAQ reagents according to manufacturer protocol (Applied Biosystems, Foster City, CA, USA). Briefly, the dried proteins were re-suspended in 25µL 1M TEAB solution. The proteins were denatured with 1µL 2% SDS solution, reduced with 2µL 50 mM tris-(2-carboxy) ethylphosphine hydrochloride (TCEP), and alkylated with 1 µL of freshly prepared 84 mM iodoacetamide solution and incubated in dark room temperature for 30 minutes. Each sample (50 µg) was digested overnight at 37 ^{o}C with 10 µL of freshly prepared 1µg/µL TPCK treated trypsin solution, P/N 4370282 (Ab Sciex Pte Ltd, MA, USA). iTRAQ reagents 114, 115, 116 and 117 were each resuspended in 70µL ethanol and added individually to the four digested PL and FF protein samples. The samples were incubated at room temperature for 1h and the reaction quenched by adding 100 µL of HPLC-grade water and incubating at room temperature for 30 minutes. Each labeled

peptide was vacuum dried at 4ºC, cleaned with Zeba™ desalting spin columns according to vendor instructions (Pierce, Rockford, IL,USA) and then vacuum dried at 4ºC. Samples were stored at -80ºC until ready for analysis.

3.4.5 Off-line Strong Cation Exchange (SCX) Separation

The iTRAQ-labeled peptides were separated using ICAT® Cartridge–Cation Exchange, # 4326752 (POROS® 50 HS, 50-µm, 4.0 mm × 15 mm), Opti-Lynx Quick Connect Hardware, # 4326688, and ICAT® Cation Exchange Buffer Pack, # 4326747 (Applied Biosystems, Foster City, CA, USA). The iTRAQ-labeled dried peptides were each diluted 10-fold with Load Buffer (10mM KH_2PO_4 in 25% ACN; pH 3) and the four samples combined in one new vial. Equilibration of the SCX cartridge was done with 1mL of Clean Buffer (10 mM KH_2PO_4 in 25% ACN / 1M KCl; pH 3) followed by 2mL Load Buffer. The mixed iTRAQ labeled peptides were then loaded onto the SCX cartridge. Excess iTRAQ reagents and salts in the cartridge were removed by washing the cartridge with 1mL of Load Buffer. The bound peptides on the cartridge were eluted by sequential injection of 500 µL of a series of salt solutions: 0, 30, 40, 50, 60, 70, 85, 100, 130, 160, 350, 500, and 1000 mM KCl in Load Buffer. The flow rate of elution was ~1 drop/second. Each eluted fraction and wash solution was cleaned with Zeba™ desalting spin columns according to vendor instructions (Pierce, Rockford, IL,USA). Purified peptides were vacuum dried at at 4ºC (Labconco, Kansas, MO, USA) and stored at -80ºC until further analysis.

3.4.6 Nano-LC-MS/MS Analysis

Aliquots of the dried SCX peptide fractions were analyzed using the Thermo-Fisher Finnigan™ LTQ™ mass spectrometer equipped with a nano-electrospray source (New Objective, Woburn, MA, USA) and coupled with a nano-LC separation system (Eksigent nanoLC 1D-plus). The LC system is equipped with an autosampler (Spark Holland 920 Endurance Autosampler). Each peptide fraction was re-suspended in 10 µL of water/ACN/formic acid (95%/5%/0.1%) and then 3 µL loaded onto IntegraFrit Sample trap (ProteoPep II™ C18, 300 Å, 5µm , 100 µm × 25 mm New Objective, Inc., Woburn, MA). The retained peptides were washed isocratically with water premixed with 0.1% formic acid pumped from channel 1A to remove any excess reagents. Peptide separation was performed on an IntegraFrit Analytical Column (ProteoPep™ II C18, 300 Å, 5µm, 75 μm ×100 mm, 75µm tip, New Objective, Inc., Woburn, MA) with a multistep 4-h gradient using solvent A (water premixed with 0.1% formic acid) and solvent B (acetonitrile premixed with 0.1% formic acid) at a flow rate of 200 nL/min. The gradient started at 5% solvent B and was held for 5 minutes, then linearly increased to 50% solvent B at 205 min and to 95% solvent B at 213 min and finally held at 95% solvent B for 5 min before allowing to return to initial 5% solvent B at 223 min. Column re-equilibration with initial 5% solvent B was done for 17 min.

The LTQ mass spectrometer was operated in a data-dependent mode. The full MS spectra were acquired in positive mode within a range of 400-1800 m/z. The top four most intense ions in the acquired full mass scan were selected for followed pulsed Q dissociation (PQD) in LTQ. The Q activation and time was set respectively at 0.7 and 0.1 ms. The maximum ion injection times used were 50 ms for the MS scan and 120 ms for

the MS/MS scans. The automatic gain control target settings were 3.0 $x10^4$ for the MS scan mode and 1.0 x 10^4 for the MS/MS scan mode. One microscan of full MS was performed. The normalized collision energy was 29.5% and the isolation window employed was 2 m/z. The dynamic exclusion settings utilized were repeat count 2, exclusion duration 25 s, exclusion list size 500, exclusion mass width low 0.5 and exclusion mass width high 1.5.

3.4.7 Protein Identification and Quantification

The LC-MS/MS raw data from nanoLC-LTQ were correlated to theoretical fragmentation patterns of tryptic peptide sequences in bovine protein fasta database using SEQUEST^{TM} search engine embedded in Proteome Discoverer (version 2.1; Thermo Fisher Scientific). The search parameters included were as follows: fixed cysteine modifications of +57 Da for carbamidomethyl-cysteines, +144 Da for lysine-iTRAQ labeling and N-terminal peptides; dynamic modifications allowing +16 with methionines for methionine sulfoxide and + 144 Da for Y-iTRAQ labeling; restricted to trypsin digested peptides and allowed for two missed cleavages; precursor mass range was 350-5000 Da; peptide mass tolerance of 2.5 Da and fragment mass tolerance of ±0.8 Da; target FDR strict was 0.01 and FDR relaxed was 0.05; most confident centroid was selected for peak integration method and a 0.25 Da integration window tolerance was allowed. The proteins matched with at least one unique peptide at minimum 95% confidence (FDR < 5%) were considered positive identifications.

The relative quantification of proteins in the samples was performed with the Proteome Discover (1.2). The quantification utilized the relative peak intensities of the

iTRAQ reporter ions derived from MS/MS spectra of all unique peptides that represented each protein. iTRAQ ratios of the reporter ions were calculated using reporter ions representing any two samples. The final ratios obtained from the relative protein quantifications were normalized according to the median protein quantification ratio to reduce experimental bias. The protein ratios were the median ratio of the corresponding peptide ratios. To determine protein expression levels, a fold change of >2.0 or <0.5 between any two samples were respectively set for up- and down-regulated proteins. Functional analysis was performed for all identified proteins and for up- and down-regulated proteins.

3.4.8 Bioinformatic Analysis of Identified Proteins

The PANTHER (Protein Analysis Through Evolutionary Relationships) classification system[123] was used to categorize the up- and down regulated proteins based on their molecular function (MF), biological process (BP), and cellular component (CC)/localization. Similar PANTHER analysis of all identified proteins in PL and FF are shown in Appendix 3. Pathway analysis was performed using the Database for Annotation, Visualization, and Integrated Discovery (DAVID)[124]. Pathway plot was derived using Kyoto Encyclopedia of Genes and Genomes (KEGG)[125]. Protein-protein intereactiosn were annotated using Search Tool for the Retrieval of Interacting Genes/Proteins (STRING)[126] database.

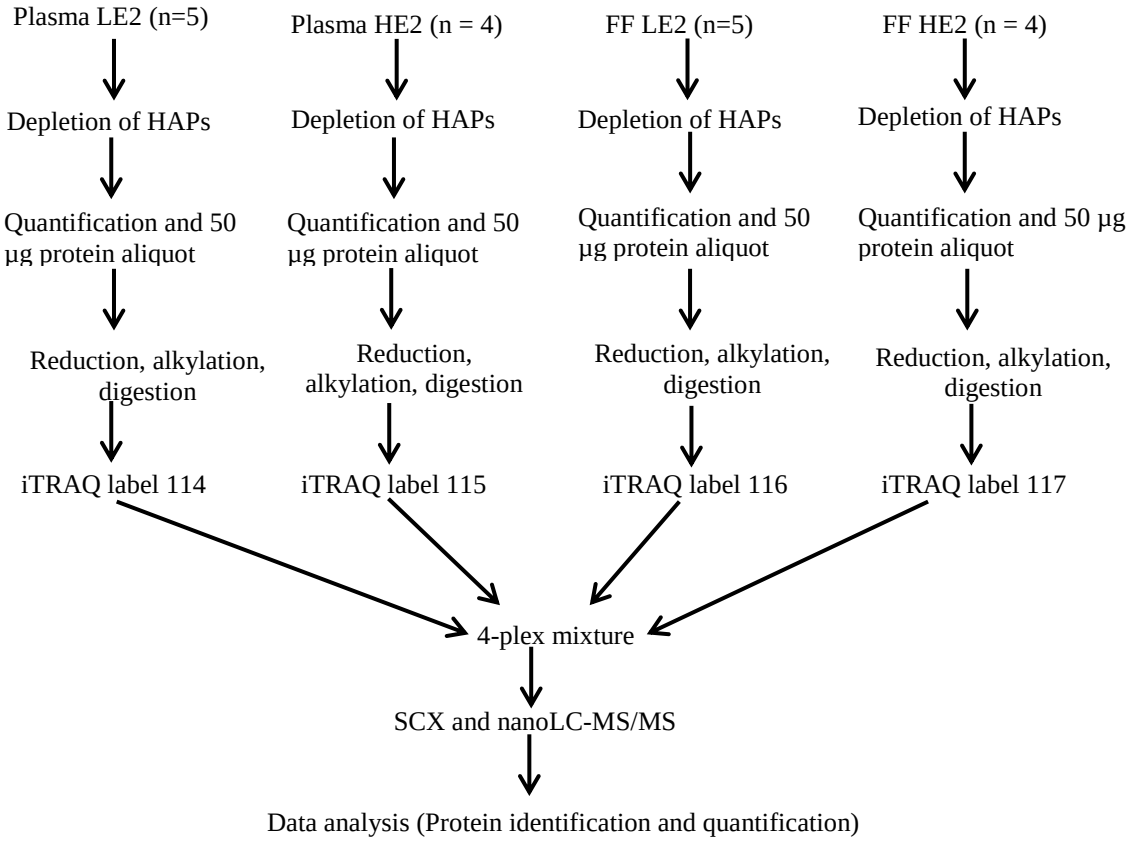

Figure 3.1. Overview of workflow for identification and relative quantification of proteins in bovine plasma and follicular fluid containing high and low pre-ovulatory levels of E2.

3.5 RESULTS

3.5.1 General information on iTRAQ Analysis

The overview of our iTRAQ-based SCX nano-LC/MS/MS ESI PQD method for analyzing the proteomes in bovine PL and FF is show in Figure 1. A total of 231 proteins matched to 793 unique peptides were identified with high confidence (FDR of 5% or less) and were subsequently included in further analysis. Details of all 231 identified proteins are shown in Appendix Table 1. Approximately 61% (140/231) of proteins were

identified by one unique peptide and ~39% by at least 2 up to 47 unique peptides (Figure 3.2.A). About a third of proteins identified by one unique peptide were identified at 99% confidence. Analysis of the distribution of the sequence coverage (Figure 3.2.B) of the detected peptides of the proteins found ~53% (123/231) of identified proteins had greater than 5% coverage. Protein pI values ranged from 4.41 to 11.05 (Figure 3.2.C). The molecular mass of the identified proteins ranged from 10.3 to 3811.5 kDa with majority of the proteins (~60%) between 20 to 80 kDa (Figure 3.2.D). Several of the proteins identified herein have been previously reported as components of bovine PL and/or FF[40, 127].

3.5.2 Comparative Analysis of Protein Expression in Plasma and Follicular Fluid

Paired comparisons were made to determine differences in protein expression between any two samples. Figure 3.3 depicts the different paired comparisons and the number of up- and down-regulated proteins obtained in each analysis. Up- and down-regulated proteins were determined using a ratio fold-change of >2.0 or <0.5 between any two samples. Comparison between same fluid type (i.e. high and low of PL or FF) revealed nine down-regulated and seven up-regulated proteins in PL HE2 compared to PL LE2 and 10 down-regulated and 15 up regulated proteins in FF HE2 compared to FF LE2. Comparison between PL and FF showed more proteins up-regulated in PL compared to FF. Each PL and FF pair, (i.e. PL LE2 and FF LE2; PL HE2 and FF HE2) revealed 51 up-regulated proteins in PL. 21 proteins were down-regulated in PL LE2 compared to FF LE2 whereas 27 proteins were down-regulated in the PL HE2 compared to the FF HE2. 39 up-regulated proteins and 11 down-regulated proteins were commonly

identified from both PL and FF paired analyses. Overlaps of numbers of proteins from the different paired comparisons are depicted in Figure 3.4 and the protein details in each pair are reported in Table 3.1.

The fold change, i.e. iTRAQ ratio value of a protein, is indicative of the extent of up- or down-regulation of the protein in a sample. iTRAQ ratios of up- and down-regulated proteins in PL compared to FF ranged from 2.017 to 27.247 and 0.036 and 0.499 respectively. NADH dehydrogenase (ubiquinone) 1 beta subcomplex subunit 11 mitochondrial (NDUFB11), dpy-19 like 4 (DPY19L4), apolipoprotein B (APOB), cytohesin 1 (CYTH1), delta-like protein (JAG1), and gametocyte-specific factor 1-like (GTSF1L) were among the top up-regulated proteins whereas versican core protein (VCAN), inhibin alpha chain (INHA), serglycin (SRGN), protein tyrosine phosphatase receptor type R protein (PTPRR), and dynein heavy chain domain 1 (DNHD1) were among the top down-regulated proteins in PL compared to FF.

Protein predominance in the HE2 sample was higher after FF HE2/FF LE2 comparison than the PL HE2/PL LE2 (respectively 2.08-6.21 and 2.00-3.71 fold change). Comparison of FF HE2 to FF LE2 identified keratin type II cytoskeletal 7 (KRT7), serum albumin (ALB), and cytokine receptor-like factor 3 (CRLF3) as the top three up-regulated proteins and hemoglobin subunit alpha (HBA), hemoglobin subunit beta (HBB), and ubiquitin protein ligase E3 component n-recognin 4 (UBR4) as the top three down-regulated proteins in the FF HE2. Suppressor of G2 allele of SKP1 homolog(SUGT1), C8G protein (C8G), and SRGN were the top three up-regulated proteins and DDB1 and CUL4 associated factor 5 (DCAF5), transmembrane protein 186

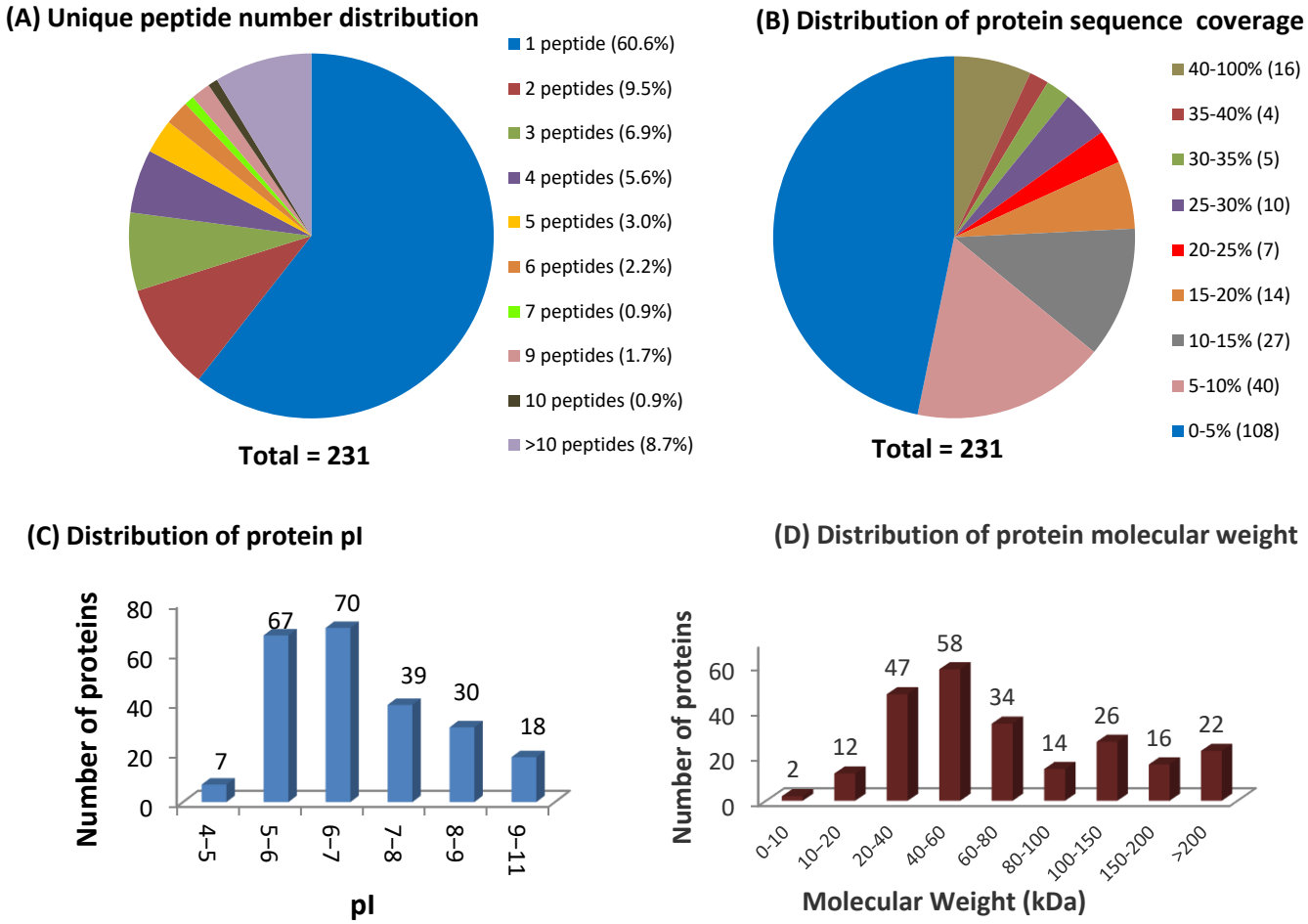

Figure 3.2. General information on 231 proteins identified by the itraq-based scx nano-LC-MS/MS ESI PQD method with high confidence. (A) Number of unique peptides of the identified proteins; (B) Distribution of protein sequence coverage; (C) Distribution of protein pI values. (D) Distribution of protein molecular weights.

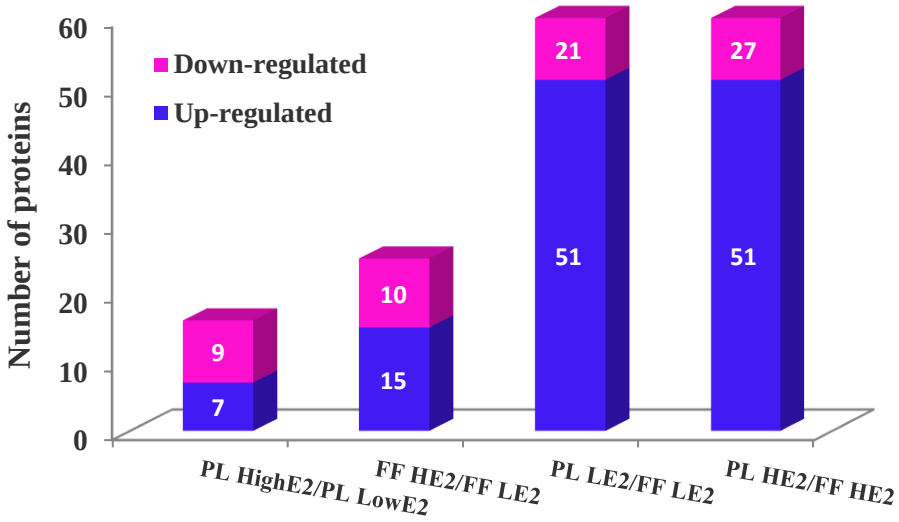

Figure 3.3. The number of up- and down regulated proteins (y-axis) after comparisons between any two samples (x-axis). The number of proteins in each category is shown on the bar. PL HE2: Plasma high E2; PL LE2: Plasma low E2; FF HE2: Follicular fluid high E2; FF LE2: Follicular fluid low E2.

(TMEM186), and HP the top three down-regulated proteins in PL HE2 compared to PL LE2. Seven proteins were commonly found from PL HE2/ PL LE2 and FF HE2/FF LE2 analyses: SUGT1, engulfment and cell motility 1 (ELMO1) and family with sequence similarity 81 member A (FAM81A) had opposite expressions in either fluid; KRT7 was up-regulated and immunoglobulin lambda-like polypeptide 1 (LOC100297192), HP and TMEM186 were down-regulated in the HE2 samples compared to the respective LE2 samples of either fluid type.

3.5.3 Functions of Identified Proteins

To determine the functions of all proteins showing expression changes, the up- and down-regulated proteins derived from all paired analyses were compiled (103 in total) and functional analysis performed using PANTHER classification system. The up-

and down-regulated proteins were categorized into 4 MF, 11 BP, and 7 CC (Figure 3.5). The major MF were binding (52%) and catalytic activity (40.0%). The BP categorized were cellular component organization or biogenesis (6.8%), cellular process (33.3%), localization (6.8%), biological regulation (6.8%), response to stimulus (5.1%), developmental process (6.8%), multicellular organismal process (6.0%), biological adhesion (4.3%), locomotion (0.9%), metabolic process (20.5%), and immune system process (2.6%). The CC analysis revealed majority of the up- and down-regulated proteins were localized in the cell (31.8%), the extracellular region (22.7%), and organelle (21.2%). Panther classification for all identified proteins is shown in Appendix 3.

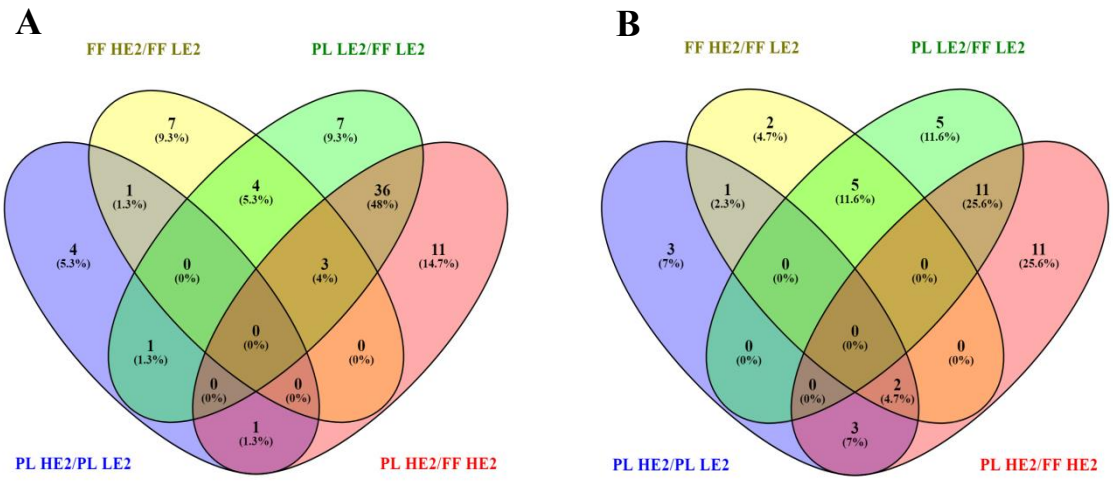

Figure 3.4. Overlap of number of up-regulated (a) and down- regulated (b) proteins in Pl and FF after paired analyses. PL HE2: Plasma high E2; PL LE2: Plasma low E2; FF HE2: Follicular fluid high E2; FF LE2: Follicular fluid low E2. Details of proteins from each paired analysis are shown in **Table 3.1**.

3.5.4 Enriched Pathways

DAVID was used to determine the pathways associated with the up- and down-regulated proteins in PL and FF. The databases within the DAVID platform searched were KEGG and Reactome [128] databases. Results from KEGG showed the complement and coagulation cascades were enriched ($p = 3.5 \times 10^{-14}$); Figure 3.6. The search in Reactome supported these enriched pathways by identifying platelet degranulation ($p = 8.2 \times 10^{-9}$), intrinsic pathway of fibrin clot formation ($p = 1.4 \times 10^{-5}$), common pathway of fibrin clot formation ($p = 2.4 \times 10^{-4}$), scavenging of heme from plasma ($p = 6.0 \times 10^{-3}$), and terminal pathway of complement ($p = 5.7 \times 10^{-2}$) as the main pathways.

3.6 DISCUSSION

Proteomic workflows utilizing iTRAQ labeling allows for the simultaneous high-throughput identification and quantification of proteins. In this study, 4plex iTRAQ reagents were used to label PL and FF samples containing high or low concentrations of E2 (HE2 or LE2). Ovaries of all cows were examined by transrectal ultrasonography and FF was subsequently aspirated from the DF. Blood was collected at slaughter. To reduce the masking effect of HAPs and matrix effect due to sample complexity, the samples were first subjected to an immunodepletion method which dramatically depleted targeted HAPs ALB, IgG, IgA, and alpha-1-antitrypsin. Subsequent steps in the workflow for the analysis included reduction, alkylation, and digestion of the plasma and FF proteins prior to labelling with the iTRAQ reagents. The iTRAQ-labeled peptides from each of the four samples were mixed at an equal mass ratio. The samples were then analyzed with off-line SCX and nanoLC-ESI-LTQ (PQD) method. Our approach enabled us to quantitatively

Table 3.1 Identified Up- and Down- regulated proteins in plasma and follicular fluid containing high or low pre-ovulatory E2

Protein Description	Uniprot Accession	Gene ID	PL HE2/ PL LE2	FF HE2/ FF LE2	PL LE2/ FF LE2	PL HE2/ FF HE2
			iTRAQ Ratio			
(A) Up-regulated proteins						
2-acylglycerol O-acyltransferase 3 (Fragment)	E1BN30	LOC618076			5.370	3.971
Alpha-2-macroglobulin	Q7SIH1	A2M			6.965	7.617
Ankyrin repeat and KH domain containing 1	G3MZJ0	ANKHD1			5.482	7.516
AP complex subunit beta	F6PZ41	AP4B1				2.144
Apolipoprotein B	E1BNR0	APOB		2.340	11.669	7.312
Apolipoprotein R	G3N0S9	LOC515150			5.234	4.912
ApoN protein	Q2KIH2	ApoN				2.809
Asparagine-linked glycosylation 5, dolichyl-phosphate beta-glucosyltransferase homolog (S. cerevisiae)	Q2KIM7	ALG5			2.103	3.265
ATP binding cassette subfamily B member 9	E1BKR0	ABCB9		2.075	7.448	3.384
B double prime 1, subunit of RNA polymerase III transcription initiation factor IIIB	F1MEB1	BDP1			5.131	2.928
C8G protein	A8YXZ2	C8G	3.000			
CAD protein	F1MVC0	CAD	2.359			
CCDC80 protein	A5PKA3	CCDC80	2.007		6.742	
Cell adhesion molecule 1	Q2TBL2	CADM1			2.680	2.187
Coagulation factor V	F1N0I3	F5			2.323	
Coagulation factor XII	F1MTT3	F12		2.418		
Coagulation factor XIII A chain	F1MW44	F13A1			3.170	2.328

Table 1. Continued

Protein Description	Uniprot Accession	Gene ID	PL HE2/ PL LE2	FF HE2/ FF LE2	PL LE2/ FF LE2	PL HE2/ FF HE2
			iTRAQ Ratio			
Cohesin subunit SA-3	E1B9B0	STAG3			3.175	5.194
Complement C1s subcomponent	Q0VCX1	C1S			3.884	6.060
Conglutinin	P23805	CGN1			3.279	3.521
Cumulus cell-specific fibronectin 1 transcript variant	B8Y9T0	FN1			2.620	2.334
Cytochrome P450 20A1	Q5E980	CYP20A1		2.484	8.593	4.068
Cytohesin 1 (Fragment)	F1MCV3	CYTH1			5.453	15.900
Cytokine receptor like factor 3	E1BCF2	CRLF3		3.048		
Delta-like protein	E1BDN7	JAG1				13.738
Dolichyl-diphosphooligosaccharide--protein glycosyltransferase subunit 1	F1MJ36	LOC539818				2.280
Dpy-19 like 4 (Fragment)	F1MJJ1	DPY19L4			16.517	12.811
DUOXA1 protein	A6H723	DUOXA1		2.751	5.914	
Dynein heavy chain domain 1	F1MEF7	DNHD1		2.972		
E3 ubiquitin-protein ligase CHIP	F1MUH4	STUB1			2.322	2.360
Engulfment and cell motility 1	F1MQH0	ELMO1	2.133			2.514
EPS8 like 1	E1BKS0	EPS8L1			2.727	2.352
Family with sequence similarity 81 member A	F1N4N5	FAM81A		2.279	2.035	
Fas activated serine/threonine kinase	F1N4L0	FASTK			2.724	
FGG protein	Q3SZZ9	FGG			6.258	4.117
Fibrinogen alpha chain	A5PJE3	FGA			9.225	5.720
Fibrinogen beta chain	F1MAV0	FGB			7.909	4.895

Table 1. Continued

Protein Description	Uniprot Accession	Gene ID	PL HE2/ PL LE2	FF HE2/ FF LE2	PL LE2/ FF LE2	PL HE2/ FF HE2
			iTRAQ Ratio			
Fibulin-1	F1MYN5	FBLN1			2.488	2.276
Gametocyte-specific factor 1-like	Q3T026	GTSF1L			8.291	10.840
HEAT repeat containing 5B	E1BB26	HEATR5B				3.123
HECT domain E3 ubiquitin protein ligase 2	F1N7A0	HECTD2			2.196	2.908
Homeobox D3	E1B856	HOXD3			2.453	
Keratin, type II cytoskeletal 7	Q29S21	KRT7	2.271	6.209		
KRAS proto-oncogene, GTPase	E1BMX0	KRAS				2.192
Kruppel like factor 17 (Fragment)	G3N1K6	KLF17				2.915
Lumican	Q05443	LUM		2.904		
Lysine methyltransferase 2C (Fragment)	F1MYZ3	KMT2C			3.774	3.229
NADH dehydrogenase [ubiquinone] 1 alpha subcomplex assembly factor 4	A4FUH5	NDUFAF4			5.033	4.573
NADH dehydrogenase [ubiquinone] 1 beta subcomplex subunit 11, mitochondrial	Q8HXG5	NDUFB11			27.247	23.059
NIMA (Never in mitosis gene a)-related kinase 2	Q2KIQ0	NEK2		2.215		
Ornithine decarboxylase 1	E1BG69	ODC1			4.726	4.681
Pantothenate kinase 3	Q08DA5	PANK3			5.058	4.976
Phosphoglycolate phosphatase	Q2T9S4	PGP				2.091
Protocadherin Fat 2 precursor (Fragment)	F1MPF3	-		2.807		
Regulating synaptic membrane exocytosis 2 (Fragment)	E1B7V2	RIMS2		2.480	2.125	

Table 1. Continued

Protein Description	Uniprot Accession	Gene ID	PL HE2/ PL LE2	FF HE2/ FF LE2	PL LE2/ FF LE2	PL HE2/ FF HE2
			iTRAQ Ratio			
Serglycin (Fragment)	G5E5K5	SRGN	2.929			
Serum albumin	P02769	ALB		5.960		
SH3 domain and tetratricopeptide repeats 1	G3MZW4	SH3TC1			2.137	
Sodium/glucose cotransporter 1-like (Fragment)	G3MXJ0	LOC531152				3.779
Sphingomyelin phosphodiesterase 5 (Fragment)	F1N6X9	SMPD5			2.017	
Suppressor of G2 allele of SKP1 homolog	Q2KIK0	SUGT1	3.741			
Synaptonemal complex protein 1	E1BLN1	SYCP1			5.469	5.407
Synaptotagmin 12	E1BEH9	SYT12			4.194	
Titin	F1N757	TTN				2.320
Trans-2-enoyl-CoA reductase, mitochondrial	Q7YS70	MECR			10.791	4.597
Transcription factor 7-like 2	G3N0T7	-			2.519	
Transcription initiation factor TFIID subunit (Fragment)	F1MF62	TAF1			3.579	2.963
Transthyretin	O46375	TTR		2.403	3.208	
Uncharacterized protein	E1BPG1	-				2.677
Uncharacterized protein	F1MI18	-			2.848	2.311
Uncharacterized protein (Fragment)	G3X6V5	-			5.022	12.917
Vacuolar protein sorting-associated protein 28 homolog	E1BIB3	VPS28			6.898	8.348
Von Willebrand factor A domain containing 5B1	E1BB39	VWA5B1			2.316	2.377
Zinc finger SWIM-type containing 3 (Fragment)	F1MTI1	ZSWIM3			3.527	2.750

Table 1. Continued

Protein Description	Uniprot Accession	Gene ID	PL HE2/ PL LE2	FF HE2/ FF LE2	PL LE2/ FF LE2	PL HE2/ FF HE2
			iTRAQ Ratio			
Zona pellucida binding protein 2	Q0VCG8	ZPBP2			5.962	5.099
(B) Down-regulated proteins						
Alpha-1-antiproteinase	P34955	SERPINA1			0.392	0.201
C8G protein	A8YXZ2	C8G			0.289	
CAD protein	F1MVC0	CAD			0.332	
Chromosome 14 open reading frame 166 ortholog	Q3T0S7	RTRAF				0.467
Complement component C6	F1MM86	C6				0.496
Cytohesin 1 (Fragment)	F1MCV3	CYTH1		0.341		
DDB1 and CUL4 associated factor 5	F1N0J7	DCAF5	0.043			
Dynein axonemal heavy chain 11	F1N724	DNAH11	0.263			0.492
Dynein heavy chain domain 1	F1MEF7	DNHD1			0.493	0.036
Endophilin-A2	Q2KJA1	SH3GL1			0.384	0.478
Engulfment and cell motility 1	F1MQH0	ELMO1		0.372	0.453	
Factor XIIa inhibitor precursor	E1BMJ0	SERPING1			0.434	0.472
Family with sequence similarity 81 member A	F1N4N5	FAM81A	0.283			0.245
Fas activated serine/threonine kinase	F1N4L0	FASTK	0.396			
Filamin B	E1BKX7	FLNB			0.471	
Gasdermin B	F1MCQ4	GSDMB			0.479	0.439
Haptoglobin	G3X6K8	HP	0.211	0.351		

Table 1. Continued

Protein Description	Uniprot Accession	Gene ID	PL HE2/ PL LE2	FF HE2/ FF LE2	PL LE2/ FF LE2	PL HE2/ FF HE2
			iTRAQ Ratio			
HECT, UBA and WWE domain containing 1, E3 ubiquitin protein ligase	E1BNY9	HUWE1				0.305
Hemoglobin subunit alpha	P01966	HBA		0.115	0.200	
Hemoglobin subunit beta	P02070	HBB		0.177	0.261	
Immunoglobulin lambda-like polypeptide 1	F1MLW7	LOC100297 192	0.242	0.433		0.499
Immunoglobulin lambda-like polypeptide 1 (Fragment)	G3N2D7	LOC100297 192	0.401			
Inhibin alpha chain	P07994	INHA			0.079	0.062
Keratin, type II cytoskeletal 7	Q29S21	KRT7				0.491
Leucine rich repeat kinase 2	E1BPU0	LRRK2				0.422
Lumican	Q05443	LUM				0.469
NIMA (Never in mitosis gene a)-related kinase 2	Q2KIQ0	NEK2				0.453
Plasma serine protease inhibitor	Q9N2I2	SERPINA5			0.353	
Protocadherin Fat 2 precursor (Fragment)	F1MPF3	-				0.360
PTPRR protein	A5PKF8	PTPRR			0.102	
Serglycin (Fragment)	G5E5K5	SRGN			0.036	0.177
Serpin family E member 2	F1MZX2	SERPINE2				0.140
Serpin peptidase inhibitor, clade A (alpha-1 antiproteinase, antitrypsin), member 3	G8JKW7	SERPINA3	0.446			0.422
Serum albumin	P02769	ALB			0.302	0.073

Table 1. Continued

Protein Description	Uniprot Accession	Gene ID	PL HE2/ PL LE2	FF HE2/ FF LE2	PL LE2/ FF LE2	PL HE2/ FF HE2
			iTRAQ Ratio			
SPHK1 interactor, AKAP domain containing (Fragment)	F1MZL5	SPHKAP				0.475
Suppressor of G2 allele of SKP1	Q2KIK0	SUGT1		0.476	0.200	
TBC1 domain family member 4	E1BPA1	TBC1D4			0.315	0.334
Transmembrane protein 186	Q5EA03	TMEM186	0.193	0.435		0.394
Transthyretin	O46375	TTR				0.257
Ubiquitin protein ligase E3 component n-recognin 4	G3N0A8	UBR4		0.328		
Versican core protein	F1N6I7	VCAN			0.129	0.331
Vitamin D-binding protein	F1N5M2	GC		0.393	0.330	
Zinc finger protein 618	E1BJV7	ZNF618			0.309	0.201

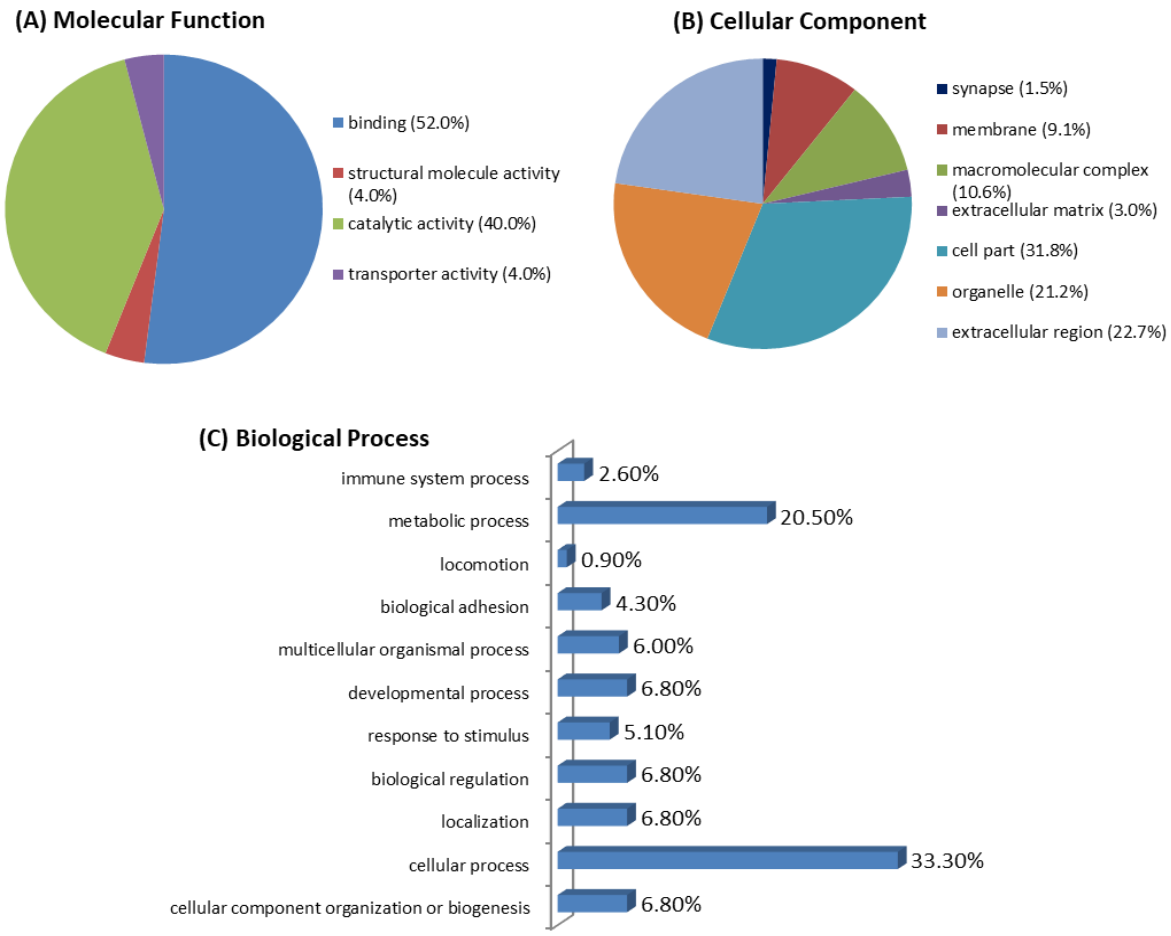

Figure 3.5. Panther analysis of up- and down-regulated proteins identified in bovine plasma (Pl) and follicular fluid (FF) containing low and high pre-ovulatory E2. The up- and down- regulated proteins were compiled from PL HE2/PL LE2, FF HE2/FF LE2, PL LE2/FF LE2 and PL HE2/FF HE2 analyses. Proteins were classified according to (A) Molecular function (B), Cellular localization, and (C) Biological processes.

measure and compare the proteomes in PL and FF containing high- and low-circulating levels of E2 during the pre-ovulatory period. Quantitative measurement of protein changes can confirm and/or provide better understanding of the protein's functions.

E2 is critical to the development and maturation of ovarian follicles[115, 117]. Concentration of E2 in PL and/or FF has been positively correlated to increased oocyte

quality, fertilization and subsequent embryo quality[129], increased follicle size[118], and improved pregnancy success[130]. Considering the vital role of proteins in cell function and regulation, this study thus examined the associations between E2 and protein expressions in FF and PL, because of the significant similarities between PL and FF proteins which results from the number of PL proteins capable of crossing the blood-follicular barrier during folliculogenesis[131, 132].

A total of 103 proteins significantly changed expression in the presence of E2 as defined by fold change. To determine a more direct influence of concentration of E2 on PL or FF proteome, high and low E2 in PL or FF were compared. The number and degree of fold change of proteins from the comparison between high and low E2 in FF was higher than the corresponding PL comparison. This suggests pre-ovulatory circulating concentration of E2 has a greater impact on FF proteome than on PL proteome. This is not surprising as E2 is produced by the GCs of ovarian follicles[116, 133] and FF is the immediate environment of the developing follicle and oocyte. The only predominant protein in PL HE2 which was also predominant in the FF HE2 when compared to the respective LE2 samples was KRT7 (keratin, type II cytoskeletal 7), a member of the keratin gene family. E2 seems to have a higher influence on KRT7 expression in FF than in PL evidenced by the higher fold change in FF (6.21 vs 2.27). The greater effect of E2 on KRT7 in FF is further supported when PL and FF were compared. There was no observable fold change in KRT7 from PL LE2 and FF LE2 comparison but KRT7 was down-regulated in PL HE2 compared to FF HE2. The function of KRT7 is reported to be building structure integrity within complexes. Keratin genes are usually expressed in pairs consisting of one type I and one type II as both are necessary to for an intermediate

filament[134, 135]. The presented data supports KRT7 involvement in developing follicles and possibly eliciting similar structural functions modulated by E2 in FF.

Successful folliculogenesis requires adequate regulation of cellular apoptosis. ELMO1 promotes cellular apoptosis[136]. Specifically, ELMO1 is involved in cytoskeletal rearrangements required for phagocytosis of apoptotic cells and cell motility[137]. Very few apoptotic cells were found in primordial, primary, secondary and vital tertiary follicles. In contrast, apoptosis in atretic tertiary follicles was much more frequent[138]. Our observation of down-regulation of ELMO1 in FF HE2 compared to FF LE2 is therefore in support of decreased apoptosis in the pre-ovulatory follicle. The suppression of ELMO1 in the presence of E2 at the pre-ovulatory stage seems more localized in FF since it was more predominant in PL HE2 when compared to PL LE2.

Proteins were more predominant in PL compared to FF which supports the hypothesis that several FF proteins originate from PL[113]. It should be noted that proteins down-regulated in PL compared to FF indicate their predominance in FF and possibly a more localized role in FF. A greater number of proteins showed expression change in the comparisons between PL and FF than between high and low E2 PL or FF comparisons. This is likely due to the inherent differences between PL and FF. The majority (50 out of 72 or 78) of these proteins was common to the different comparisons between PL and FF and maintained their expressions (i.e. being up- or down-regulated) regardless of the E2 level. Although the expressions for these common proteins did not change, individual iTRAQ ratios were generally lower for up-regulated proteins and higher for down-regulated proteins after PL HE2 and FF HE2 paired comparison than PL LE2 and FF LE2

paired comparison. This further suggests a greater stimulating effect of high E2 on FF proteins such that the concentration difference of these proteins in PL and FF is lower resulting in lower up-regulated iTRAQ ratios and higher down-regulated iTRAQ ratios for the HE2 pair. Twenty-six out of 39 up-regulated proteins and 5 out of 11 down-regulated proteins which were common to the different PL and FF paired comparisons showed this trend. Common up-regulated proteins showing this trend included FGA, FGB, FGG, cumulus cell-specific fibronectin 1 transcript variant (FN1), apolipoprotein B (APOB), A2M, complement C1s subcomponent (C1S), and fibulin-1 (FBLN1). Common down-regulated proteins with this trend were F13A1, VCAN, endophilin-A2 (SH3GL1), SRGN, and TBC1 domain family member 4 (TBC1D4).

PANTHER analysis revealed the up- and down-regulated proteins had multifunctional roles but cellular process and metabolic process were the major functions. Developing ovarian follicles undergo a series of coordinated cellular processes that induce morphological and functional changes within the follicle, leading to cell differentiation and oocyte development[139]**.** Further analysis in PANTHER showed the proteins under cellular function were involved in cell communication (52.4 %), cellular component movement (23.8%), cell growth (4.8%), cell cycle (14.3%), and chromosome segregation (4.8%). Coordinated communications between the granulosa, cumulus and thecal cells, and as well as the oocytes are critical for successful folliculogenesis and the development of an oocyte capable for ovulation and fertilization[140]. Of these communication between the oocyte and GCs is considered the most significant for growth regulation and maturation of the oocyte and follicular luteinization. The proteins linked to cell communication included INHA, FN1, FGG, FGB, lumican (LUM),

synaptotagmin-12 (SYT12), regulating synaptic membrane exocytosis 2 (RIMS2), and KRAS proto-oncogene, GTPase (KRAS). These proteins play vital roles in follicle growth and maturation.

Folliculogenesis is highly regulated by gonadotropins and sex hormones. The secretions of these hormones are in turn regulated by a number of proteins. INHA is one such protein involved in the regulation of FSH secretion. Specifically, INHA selectively inhibits FSH secretion from the pituitary in a negative-feedback mechanism[141]. The decline in FSH continues to a level that is only able to be utilized by the largest follicle thereby enhancing its growth to become the DF. The inability of smaller follicles to utilize the low levels of FSH results in regression of their growth to become subordinate follicles[142, 143]. INHA was found highly down-regulated in PL compared to FF with lower expression in the high E2 pair (PL HE2/FF HE2; iTRAQ ratio 0.062) than the low E2 pair (PL LE2/FF LE2; iTRAQ ratio 0.079). The high INHA concentration in FF from DF and with high E2 is consistent to the vital roles of INHA and E2 in the decline of FSH observed during follicular deviation[142, 143]. Apart from its role in regulating FSH secretion, INHA is also a critical regulator of different cellular processes including differentiation, cell migration, proliferation, and apoptosis[144].

SYT12 is another protein involved in regulation of hormonal secretion during follicular growth. It belongs to synaptotagmin family that serve as Ca^{2+} sensors for Ca^{2+} triggered release of hormones, including FSH from the pituitary gland[145]. RIMS2 is also involved in synaptic membrane exocytosis that results in the release of neurotransmitters. It functions by binding to pre-synaptic proteins including synaptotagmin 1 (SYT1), an

isoform of SYT12[146, 147]. SYT12 and RIMS2 were up-regulated in PL LE2 compared to FF LE2. RIMS2 was also up-regulated in FF HE2 compared to FF LE2. The expression changes in both proteins indicate their involvement in follicle development.

The proteins FN1, FGB, FGG, and apolipoprotein R were up-regulated in PL compared to FF but iTRAQ ratios indicate concentration increases in these proteins in FF with high E2 compared to low E2, signifying an influence of E2 on these proteins. These proteins promote cellular processes by binding to a variety of cells and molecules. Indeed all five proteins were classified under biological adhesion by PANTHER. Cell adhesion leads to alterations in cell shape and motility that are required for different cellular functions during folliculogenesis and the development of a competent oocyte[148, 149]. Cell shape was reported to regulate cell proliferation in mouse GCs[150] and steroidogenesis in rat GCs[151]. FN1 and fibrinogen have been reported to increase proliferation in a number of cells. Specifically, FN1 has been reported to stimulate proliferation of ovarian GCs[152]. Fibrin matrix composed of fibrinogen and thrombin has also been reported in the survival and proliferation of ovarian cells[153] and promoted growth in primordial-primary follicles and secondary follicles. The growth to secondary follicles was greater compared to primordial-primary follicle growth[154]. Successful ovulation and capture of the oocyte by the oviduct and subsequent transport through the oviduct necessitates formation and expansion of the cumulus cell-oocyte (COC) matrix[155]. Stabilization and expansion of the COC matrix involves binding of several proteins including FN1, VCAN, and laminin [156].

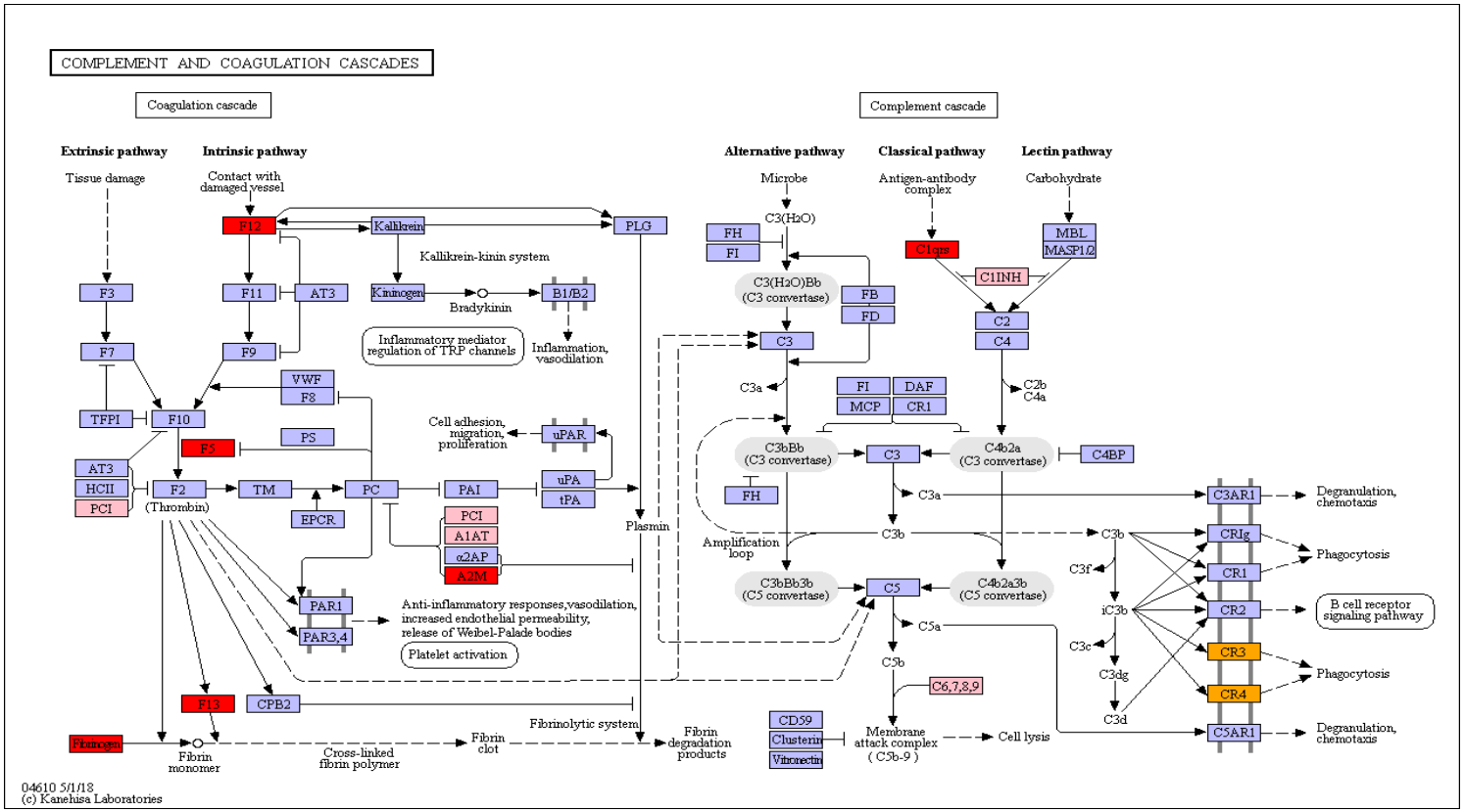

Figure 3.6. Up-regulated (red) and down-regulated (pink) proteins involved in the complement and coagulation cascades identified in this study. Up- and down-regulated in plasma (PL) compared to follicular fluid (FF): Alpha-2-macroglobulin (A2M), coagulation factor V (F5), coagulation factor XIII A chain (F13), complement C1s (C1S), complement C6 (C6), alpha-1-antiproteinase (A1AT or SERPINA1), plasma serine protease inhibitor (PCI or SERPINA5), factor XIIa inhibitor precursor (C1INH or SERPING1), complement C8 gamma chain (C8G; this was also up-regulated in PL HE2 compared to PL LE2), and fibrinogen (fibrinogen alpha chain (FGA), fibrinogen beta chain (FGB), and fibrinogen gamma chain (FGG)). Fibrinogen is a ligand of complement receptor types 3 and 4 (CR3 and CR4; orange). Up-regulated in FF HE2 compared to FF LE2: Coagulation factor XII (F12).

Follicle development involves independent movements of cells and cellular components to sites of action and to enable interaction with other relevant molecules. Proteins with this function were categorized under cellular component movement, a sub-set of cellular process. The proteins were AKAP domain containing SPHKAP (SPHKAP), dynein axonemal heavy chain 11 (DNAH11), DNHD1, ELMO1, and LUM. LUM is a widely distributed protein involved in different biological functions. Accordingly, LUM was categorized in 7 out of the 12 BP hererin: cellular process, biological regulation, cellular component organization or biogenesis, developmental process, locomotion, multicellular organismal process, and response to stimulus. LUM was up-regulated in FF HE2 compared to FF LE2, indicating a positive association with E2 in FF. This positive association is further supported by the PL and FF comparisons where LUM was down-regulated in PL HE2 compared to FF HE2 but showed no significant expression change from the low E2 comparison.

Metabolic process was the second most associated BP. Primary metabolic process formed 46.7% of the metabolic processes which in turn was comprised of protein metabolism (48%) and nucleobase-containing compound metabolic process (28%). Protein metabolism is integral to the growth and maturation of follicles, occurring in cells including granulosa, cumulus, and thecal cells and the developing oocyte[157]. Protein synthesis competence, patterns, and rate in somatic cells and oocytes can be used as a measure of maturation of the follicles[158, 159]. Proteins associated with protein metabolism in the current study were A2M, dpy-19 like 4 (DPY19L4), vacuolar protein sorting-associated protein 28 homolog (VPS28), HP, E3 ubiquitin protein ligase HUWE1 (HUWE1), F13A1, Asparagine-linked glycosylation 5 (ALG5), dolichyl-

diphosphooligosaccharide-protein glycosyltransferase subunit 1 (RPN1), INHA, phosphoglycolate phosphatase (PGP), and transcription initiation factor TFIID subunit (TAF1).

The protein A2M was predominant in PL compared to FF irrespective of high or low E2 levels. The lower concentration in FF than in PL is consistent to previous report[160]. However, concentration of A2M increases with follicle growth, promoted by its secretion by GCs and thecal cells[160]. A2M is involved in metabolic processes as well as regulating E2 production and follicular development via binding to a wide range of reproductive related targets including inhibin, activin, transforming growth factor β and α (TGFβ, TGFα), and insulin-like growth factors to regulate their functions[161-163]. Another important metabolic protein is ALG5, which is involved in the formation of the COC matrix. The predominant component of the COC matrix is glycosaminoglycan hyaluronan (HA)[140]. Glycosylation of amino acids is therefore an important metabolic process in follicle maturation. ALG5 participates in the synthesis of oligosaccharides for asparagine-linked glycosylation. Concentration of ALG5 increased in FF and decreased in PL with high E2 than with low E2 but the expression changes were not significant (iTRAQ ratios 1.519 and 0.836 respectively). However, ALG5 significantly increased in PL when compared to FF (iTRAQ ratios 2.103-3.265). This observation shows a modulation of ALG5 by E2 in follicle growth.

The immune system in the reproductive tract plays a critical role in simultaneously providing a protective microenvironment to support successful reproduction processes and conferring protection against potential pathogens. In fact,

folliculogenesis and ovulation are viewed as a hormone-induced inflammatory process[164]. Sex hormones, E2 and progesterone, significantly regulate the reproductive immune system cells, tissues, and molecules[165]. This is supported by the results of this study by expression changes of immune-related proteins in the presence of high and low E2. Proteins relating to the immune system were categorized under response to stimulus- A2M, INHA, ankyrin repeat and KH domain containing 1 (ANKHD1), SPHK1 interactor, AKAP domain containing (SPHKAP), LUM, and Gasdermin-B (GSDMB); and immune system process- ANKHD1, immunoglobulin lambda-like polypeptide 1 (LOC100297192) and apolipoprotein R (LOC515150).

Follicuclogenesis is a developmental process that results in growth of primordial follicles into primary, secondary, and tertiary follicles. The proteins JAG1, VCAN, INHA, FBLN1, LUM, GSDMB, protocadherin Fat 2 precursor (FAT2), and titin (TTN) functions were classified under developmental process by PANTHER. Cell proliferation is key to the increase in size and transformation of follicles from one stage to the other. INHA and LUM promote cell proliferation. VCAN is a component of the extracellular matrix (ECM) of a variety of tissues. It forms large complexes with HA[166] and in the ovary, binding to the HA of the COC matrix results in stabilization and expansion of the COC matrix[156]. VCAN also promotes cross-linking of the COC matrix by binding to several proteins including FBLN1 and FBLN2[167]. VCAN was up-regulated in FF compared to PL in the presence of low or high E2.

A number of proteins were categorized under biological regulation. These proteins were identified mainly predominant in PL compared to FF. An example of such

proteins is ornithine decarboxylase (ODC1). ODC1 is the initial and rate-limiting step in the biosynthesis of polyamines required for growth, differentiation, and transformation of cells[168]. Inhibition of ODC1 with α-difluoromethylornithine (DFMO) was demonstrated to inhibit ovarian growth, the formation of graafian follicles, and the secretion of progesterone and E2 in immature mice. Administering of DFMO to adult cycling females on evening/night of proestrus markedly decreased plasma progesterone levels at diestrus which was linked to down-regulation of cytochrome cholesterol side-chain cleavage enzyme, steroidogenic factor 1, and steroidogenic acute regulatory protein in the ovary and to a reduced vascularization of the corpora lutea[169]. Other proteins in the biological regulation category were SUGT1, SPHKAP, RIMS2, SYT12, LUM, CGN1, and epidermal growth factor receptor kinase substrate 8-like protein 1 (EPS8L1).

Folliculogenesis involves proteins that transport and/or maintain substances including cells, cell components, metabolites, and proteins in specific locations of action. Proteins involved in this process were categorized under localization. Such proteins included GC and ALB. GC is the main protein involved in the transport of 25-hydroxyvitamin D (25(OH)D), the precursor of the active form of vitamin D, and the recognized optimal indicator of vitamin D status. Vitamin D level is therefore predominantly contributed by GC level[170, 171]. Based on the free hormone hypothesis that protein-bound hormones are not biologically available and that unbound hormones are biologically active, down-regulation of GC as found in this study can indicate more bioavailable 25(OH)D[170]. Apart from its well-known role in bone morphology, vitamin D is increasing being viewed as vital for regulation of reproduction physiology. It has been positively associated with pregnancy, embryo implantation rate and IVF outcomes[172] and

to reproductive steroid hormones[173, 174]. Our data asserts to a regulation of vitamin D by E2.

ALB is a major component of PL and FF. Due to its abundance it was prior depleted to enable detection of lower abundant proteins. ALB transports a wide variety of substances including proteins, steroids, drugs, fatty acids, metabolites, hormones, and cations, facilitated by its multiple binding sites and longer circulatory half-life. ALB's strong attraction to cations, its low molecular weight and its abundance enable it to play a central role in maintaining colloidal osmotic pressure (COP) that regulates the distribution of extracellular fluids between the vascular and extravascular compartments[175, 176]. STRING analysis of the up- and down-regulated proteins showed ALB had the highest interactions with other proteins (Figure 3.7) supporting ALB versatile role. Identified proteins in this study that bind to ALB include GC, F13, HBA, C1S, apolipoprotein C-III (APOC3), and kininogen-2 (KNG2)[177].

Pathway analysis showed the complement and coagulation cascades were the predominant pathways, consistent with previous studies on FF[40, 178]. The stage of follicle development seems to regulate the proteins involved in coagulation pathway. Proteins involved in coagulation were found down-regulated in the pre-deviation, early deviation and pre-ovulatory stages and up-regulated in later deviation to post deviation stages[40]. Here, the coagulation and complement pathway involved 13 proteins showing different levels of expression changes, supporting a dependence on individual protein roles in the pathway. The predominance of the complement and coagulation cascades supports the view that the follicle development and ovulation are hemorrhagic and inflammatory-induced events.

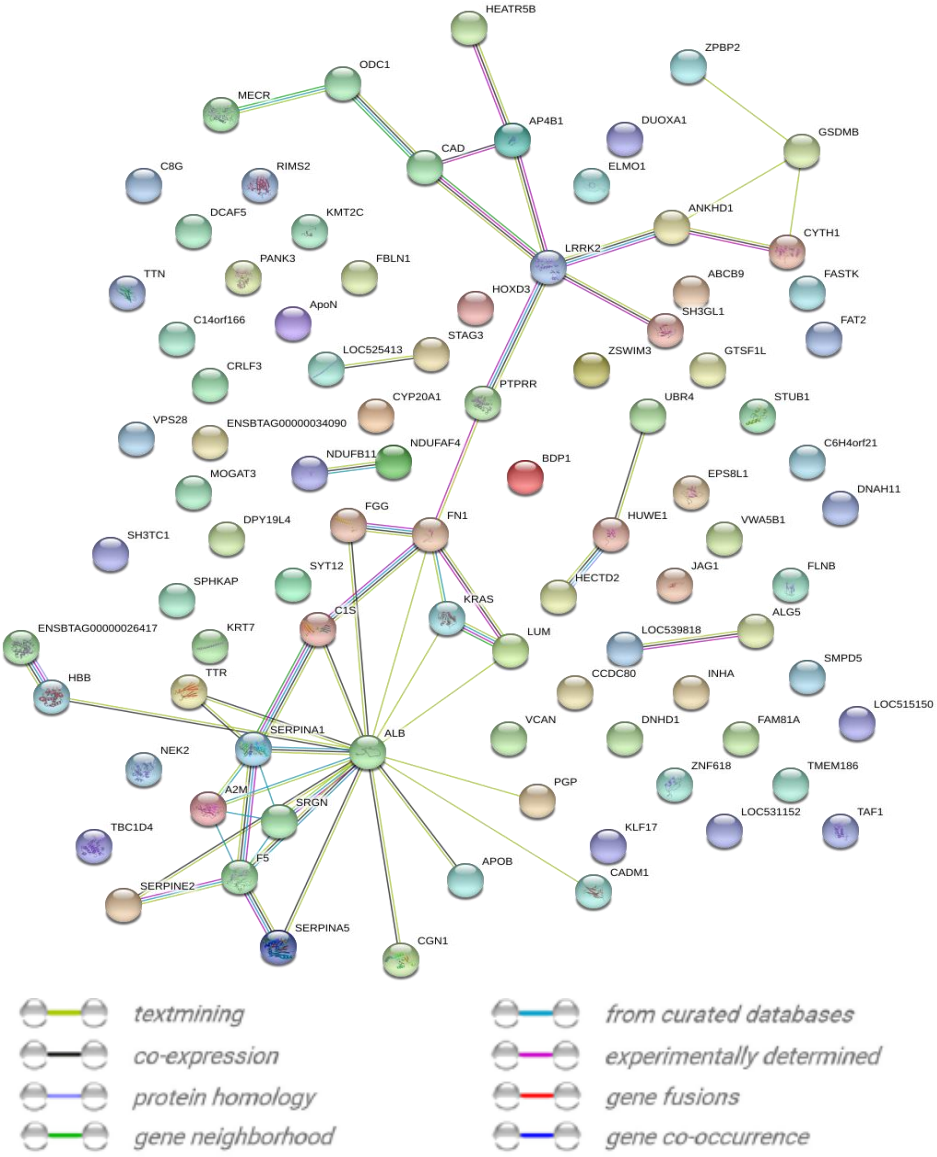

Figure 3.7. Network of identified up- and down-regulated proteins in bovine PL and FF containing low and high concentration of estradiol during the pre-ovulatory stage. A total of 89 proteins are connected with 52 paired interactions annotated by STRING database. The highest number of interaction is seen with ALB, signifying the versatility of its function. There are no interaction among majority of the proteins which can suggest the independence and critical role each play in follicle growth and maturation. The relationships among proteins were derived from evidence from known interactions (from curated databases and experimentally determined), from predicted interaction (gene fusions, gene neighborhood and gene co-occurrence) and from other sources (textmining, co-expression and protein homology). These are shown in the legend with different colors. Details of the proteins are shown in **Table 3.1**.

The complement cascade and coagulation cascade are closely related and each activates the other in a reciprocal way. For instance, activated platelets can activate the classical and alternative complement pathways. Thrombin, coagulation factors FIXa, FXa, FXIa, and plasmin can activate C3 and C5. F12a can activate C1qrs complex to activate the classical complement pathway. Conversely, mannan-binding lectin associated serine protease 2 (MASP-2) and the final stage complement complex C5b–9 are able to generate thrombin through direct cleavage of prothrombin. Thrombin is a vital coagulation component that converts fibrinogen to fibrin. C5a promotes procoagulant activity by several actions on cells including inducing mast cell and basophil to switch from profibrinolytic to prothrombotic activities through the upregulation of the coagulation component plasminogen activator inhibitor-1 (PAI-1)[179].

F12 is the first component of the coagulation pathway and its activation triggers the intrinsic pathway of the coagulation system[179]. F12 was up-regulated in FF HE2 compared to FF LE2, indicating a greater influence of E2 on F12 in FF. Five other proteins were down-regulated in PL compared to FF namely A1AT, PCI, C1INH, C6, and C8G. A1AT expression in FF HE2 was about double that in FF LE2 when compared to the corresponding PL samples. A1AT, C1INH, and PCI are protease inhibitors belonging to the SERPIN superfamily. The SERPINs regulate a wide range of proteins including those involved in the coagulation, fibrinolysis, and complement pathways[180, 181]. Proteins in the coagulation and fibrinolytic system inhibited by A1AT include neutrophil elastase, activated protein C (APC), cathepsin G, thrombin, plasmin, coagulation factor X (F10), and coagulation factor XI (F11)[182-186]. PCI inhibits the down-

regulation of coagulation system by inhibiting the activation of protein C by thrombin in the presence of thrombomodulin and by inhibiting APC[186]. APC down-regulates the coagulation system by degrading the coagulation factors Va and VIIIa by limited proteolysis and by eliciting anti-inflammatory response and cytoprotective signaling in endothelial cells by activating protease-activated receptor 1 (PAR-1)[186]. PCI also down-regulates coagulation by inhibiting proteolytic cleavage of fibrinogen by thrombin in the presence of heparin[187].

C1INH is a vital regulator of complement cascade and functions by inactivating C1r and C1s, components of C1q, and mannan-binding lectin associated serine proteases MASP-1 and MASP-2[188]. C1q is the first component in the classical pathway and MASP-1 and MASP-2 are first components in the lectin pathway. C1INH is also a major regulator of the coagulation cascade. It inhibits inflammation by blocking the activities of activated F12 and plasma kallikrein, two proteins that participate in the production of bradykinin which promotes inflammation by increasing vascular permeability[188, 189]. C6 and C8G are part of the later stage of complement activation and function as membrane attack proteins. They interact to form membrane attack complexes that are able to associate with the lipid bilayer of target molecules, leading to eventual disruption of the lipid bilayer[188]. The up-regulation of the six proteins in FF indicates their vital roles in regulation of coagulation and complement cascades during bovine follicular development.

Other identified proteins in the coagulation and complement system were A2M, F5, F13, C1S, FGA, FGB, and FGG (up-regulated in PL compared to FF) and C8G (up-

regulated in PL HE2 compared to PL LE2). The functions and associations of these proteins in the coagulation and complement pathway are shown in Figure 5. The up-regulation of C8G in PL containing high E2 than low E2 suggests greater influence of E2 on this protein in PL.

3.7 CONCLUSION

In conclusion, iTRAQ proteomic enabled probing of protein changes in PL and FF containing high and low concentrations of E2 during the pre-ovulatory period. E2 influence the expression changes of several proteins in PL and FF. Protein expression changes is greater with high E2 in FF than in PL when compared to their respective low E2. But protein expression change with high and low E2 is similar when PL and FF are compared and this is possibly due to the inherent difference in protein concentrations in PL and FF. The expression changes of several of the proteins are associated to their function in follicle growth and maturation. The coagulation and complement cascades are enriched during bovine follicle development and support the view that folliculogenesis and ovulation are hemorrhagic events.

CHAPTER 4

ATHEROSCLEROSIS DEVELOPMENT IN THREE REGIONS OF THE AORTIC ROOTS OF APOLIPOPROTEIN E KNOCKOUT ($APOE^{-/-}$) MICE

4.1 ABSTRACT

The aortic root is a predilection site for atherosclerosis development in mice. We report a investigation of atherosclerotic progression in three specific regions of the aortic roots, namely the ascending aorta region (AAR), region showing the orifices of the coronary arteries marking the start of the ascending arch (OCAR) and aortic sinus region (ASR) in a large population of *ApoE*$^{-/-}$ male and female mice at different ages. In this study, 67 *ApoE*$^{-/-}$ and 27 wild-type C57BL/6J mice (controls) were fed with a high fat diet (HFD) until age 8, 12, 18, or 24 weeks. Through systematic classification and quantification of lesions in each region and statistical data analysis, we found that the complexity and total atherosclerotic lesion areas in *ApoE*$^{-/-}$ mice was location and age dependent. It was slowest in the AAR with lesions progressing from dominant type I at 8 weeks, type II at 12 weeks, types III at 18 and types III and IV at 24 weeks of age. Lesion development was comparable in the OCAR and ASR regions; types II and III lesions dominated in mice at 8 and 12 weeks of age, respectively, while types IV and types IV and V dominated at 18 and 24 weeks of age, respectively. Average percentage of atherosclerotic lesions typically increased from the AAR to the OCAR to the ASR at a specific age, and from 8 to 24 weeks of *ApoE*$^{-/-}$ mice at each region, correlating with the histological data. Aatherosclerosis development was found to be slightly faster in female than male *ApoE*$^{-/-}$ mice. As expected, no lesions were observed in wild-type mice. These findings would be

beneficial in experimental design and targeting of lesion types in aortic roots of the popular *ApoE*$^{-/-}$ murine atherosclerosis model.

4.2 BACKGROUND AND MOTIVATION

The aortic root is a predilection site for lesion development[67] in mice and is often investigated to determine the overall extent of atherosclerosis[71] in mice. The aortic root has three identifiable regions: the ascending aorta region (AAR), the region showing the orifices of the coronary arteries marking the start of the ascending arch (OCAR), and the aortic sinus region (ASR) characterized by the appearance of the aortic cusps[190]. The apolipoprotein E knock-out (*ApoE*$^{-/-}$) mouse model[65, 66] is efficient for demonstrating the progressive atherosclerotic events and lesion-morphological features found in humans[191]. *ApoE*$^{-/-}$ mice spontaneously develop atherosclerotic lesions when fed a normal mouse chow diet. These conditions are accelerated with a high saturated fat and cholesterol diet[65]. The C57BL/6 mouse strain is more susceptible in developing atherosclerosis[70] and is therefore often the background for *ApoE*$^{-/-}$ mice[71]. In this study, 67 *ApoE*$^{-/-}$ female and male mice on C57BL/6 background were fed a HFD for different periods of time corresponding to four age groups: 8, 12, 18 and 24 weeks. Serial cross-sectioning method[190] with subsequent staining and calculation of lesion areas with image analysis software were then used to carefully identify, and quantify atherosclerotic lesions.

4.3 OBJECTIVES

Although different atherosclerosis studies have examined the aortic root, none have characterized and quantified the three regions simultaneously in a large population. Our primary objective is to meet this limitation. Data from a large population size will be beneficial in experimental design of atherosclerotic studies with this mouse model. Other objectives are to identify atherosclerosis progression trends in the regions and to

investigate gender-specific differences in the disease development. This study provides photomicrographs of the different types of atherosclerotic lesions which could be beneficial, when used in conjunction with related images derived from nuclear and non-nuclear imaging techniques[55] for disease diagnosis and target interventions. Future work is to perform proteomic analysis on blood samples from mice in this study to identify potential phosphoprotein biomarkers of atherosclerosis.

4.4 MATERIALS AND METHODS

4.4.1 Mice Housing

ApoE$^{-/-}$ on C57BL/6 background and wild-type C57BL/6 mice were bought at three weeks of age from Jackson Laboratory (Maine). Both *ApoE*$^{-/-}$ and wild-type C57BL/6 mice were fed standard chow diet (contained 20% protein by weight, 4.5% fat by weight, 0.02% cholesterol by weight, no sodium cholate and casein) for one week upon arrival and then transferred onto a high fat diet (HFD) until they reached 8, 12, 18, or 24 weeks of age. These feeding periods have been shown to induce different degrees of atherosclerotic lesions in *ApoE*$^{-/-}$ mice[67]. The HFD (Harlan Laboratories, Madison, WI) contained 21% fat by weight, 0.15% cholesterol and 19.5% by weight casein without sodium cholate. There were 36 male *ApoE*$^{-/-}$ mice, with nine mice in each of the four groups. Female *ApoE*$^{-/-}$ mice totaled 32 with six mice in the 8 week group, eight mice in the 12 week group, nine mice in the 18 week group and nine mice in the 24 week group. One mouse from the 24 weeks female group died after the feeding period and was excluded from further analysis. For wild-type C57BL/6 male mice, there were four in the 8-week group and three in each of the 12, 18 and 24 week groups (13 in total). There

were 14 female wild-type mice in total with three mice each in the 8- and 12-week groups and four mice in each of the 18 and 24 week groups. Mice were given diet and tap water *ad libitum*. The mice were housed in pathogen free 12 h dark cycles. All research protocols in this mouse study were approved by Institutional Animal Care and Use Committee (IACUC) in South Dakota State University.

4.4.2 Histological Analysis of Aortic Roots

All mice were sacrificed at the end of their designed feeding period and then dissected and sectioned according to the method previously described[190]. During dissection, the heart was separated from the aorta and placed in phosphate-buffered saline solution. At the time of sectioning, the lower ventricular portion of the heart was cut away such that the remaining upper cardiac portion was about 30% of the total heart tissue size. The upper cardiac portion was placed in a tissue mold and then completely covered with optimal cutting temperature (OCT) compound. Each OCT-embedded tissue was manipulated to ensure that it was placed center and perpendicular to the tissue mold and free of any bubbles. The mold was then quickly frozen on dry ice and sectioned immediately or wrapped in parafilm and frozen at -20^{o}C for later sectioning.

Tissues were sectioned with the upper ventricular portion facing outwards in the tissue mold. During sectioning, the frozen tissue was mounted on a cryostat (Leica CM3050 S) and cross-sectioned at 8 μm intervals until all three regions of the aortic root (i.e. AAR, OCAR, AAR, ASR) are collected, identified by the region spanning the appearance of the aortic cusps to the region of the disappearance of the circular shape of the ascending aorta. About 140 sections per mouse were collected spanning the three

regions. Frozen sections were collected in sequence on histological slides (8 to10 tissue sections per slide) and frozen at -80 °C until ready for staining.

4.4.3 Oil Red Staining and Imaging

Oil red O is commonly used to assist in quantification of atherosclerotic lesions in mice. Oil red O stains neutral lipids, enabling determination of lesions areas with image analysis softwares[190]. Oil red O stock solution was prepared by dissolving 0.5 g Oil red O (CI 26125; Sigma Aldrich, Saint Louis, MO, USA) in isopropanol (Fisher Scientific, Hampton, NH, USA) using a gentle heat of a water bath. Oil red O working solution was prepared by diluting 30 mL of stock solution with 20 mL of distilled water and filtering. Working solution was prepared fresh for use at each staining time. For Oil red O staining, frozen sections were first dried under room temperature for about 15 minutes to reduce tissue loss resulting from a weak bond with the histological slide. Tissue sections were fixed in formalin (paraformaldehyde in PBS; 4% w/v, pH = 6.9) and then washed under running tab water for about 10 minutes and rinsed with 60% isopropanol. Tissues were then stained with freshly prepared Oil red O working solution, rinsed with 60% isopropanol and then counter stained with Harris hematoxylin solution (Sigma Aldrich, St. Louis, MO, USA). Stained tissues were cover slipped with glycerin jelly mounting medium (Electron Microscopy Sciences, Hatfield, PA) and imaged immediately or refrigerated overnight or stored at -20 ºC until ready for imaging. All tissue sections collected from each *ApoE*$^{-/-}$ mouse were stained. For C57BL/6 controls, alternating histological slides from the serial cross-sectioning were selected for staining. Images of Oil Red O stained aortic root tissues on histological slides were captured at 35

magnification using a Leica EZ4HD light microscope (0.057 nA) equipped with Leica Acquiring Service, V.4.0 software. 200 (0.4 nA) and 600 (oil immersion nA 1.4-0.6) magnifications were obtained using Leica DM14000B inverted light microscope connected to a Cool Snap Pro color video camera (Media Cybernetics) equipped with QCapture-Pro 5.1 software. Other magnifications (50 µm) were obtained with Olympus AX70 Upright Compound Microscope equipped with Olympus DP70 Digital Camera.

4.4.4 Classification of Lesions

Lesions were classified based on their size and morphology as previously described[58-60] for atherosclerotic lesions. Lesion classification was done by individuals not involved in mice experimental design and feeding to prevent classification errors and bias. Lesion types observed in this study are shown in Figures 4.2 to 4.4. Type I lesions were characterized by the presence of scattered macrophages containing lipid droplets (foam cells) (Figure 4.2). Multilayer macrophage foam cells and lipid-laden smooth muscle cells were characterized as type II lesions (fatty streaks) (Figure 4.2, Panel C and D). Lesions that had pools of extracellular lipids in addition to features of type II lesions but lack the lipid rich core (necrotic core) were labeled type III (intermediate) lesions (Figure 4.3). The necrotic core is a key feature of types IV and V lesions. Type V lesion (Figure 4.4, Panels C and D) was differentiated from type IV (Figure 4.4, Panel A and B) by the additional presence of a substantial amount of spindle-shaped fibrous tissues mixed with the necrotic core lipids (sometimes occurred as multilayers of fibrous tissues in the lipid core) and/or a fibrous cap covering the top of the lipid core.

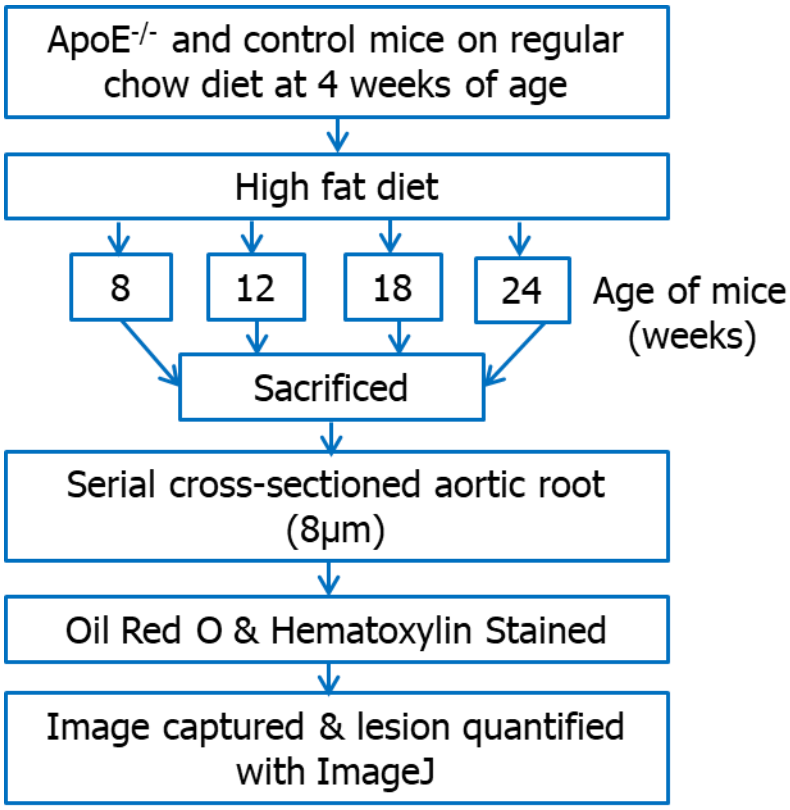

Figure 4.1. Workflow of the experimental design for the characterization and quantification of atherosclerotic lesions from aortic root regions of *ApoE*$^{-/-}$ mice.

Type VI lesion, the complicated lesion, is characterized by the presence of fissure, hematoma, and thrombus, sometimes in addition to features of type IV or V. Type VI lesion was not observed in aortic roots from mice in this study. The overall disease state in a region was defined by the highest lesion type observed in tissues from that region.

4.4.5 Quantification of Lesions

Lesion areas and aortic luminal boundaries were manually measured using ImageJ analysis software developed by NIH. Lesion-area calculation with imageJ was achieved by tracing along a lesion outer boundary. Measurement of lesion areas was carried out on

alternating tissue sections on all histological slides collected from the serial cross-sectioning of an *ApoE*$^{-/-}$ mouse. About 70 tissue sections per mouse were quantified. A total of 15 mice, seven male and eight female *ApoE*$^{-/-}$ mice, were excluded from the quantification due to tissue loss from at least one of the regions during sectioning and/or staining. Thus a total of 29 male and 23 female *ApoE*$^{-/-}$ mice were quantified. To determine the percent of lesions in each stained tissue, the sum of all lesion areas (obtained from ImageJ analysis) in the tissue was expressed as the percent of the area corresponding to aortic luminal boundary. Average percent lesion for an aortic root region per mouse was calculated by taking the average of all the percent lesions calculated for tissues from that region. The average percent for a region per mouse was used to calculate the average percent of a region for a group, standard deviations and perform one-way analysis of variance (ANOVA).

ANOVA performed included comparisons between the aortic root regions from mice within a group, the aortic root regions between the different groups and the aortic root regions between genders. The comparisons were made to determine whether the differences in lesion development were purely random or significant. Significant difference was established at $p<0.05$.

4.5 RESULTS

4.5.1 Atherosclerotic Lesions Progression and Characteristics in *ApoE*$^{-/-}$ Mice

Atherosclerosis lesions were observed in all three regions of the aortic root of *ApoE*$^{-/-}$ mice but as expected, not in C57BL/6 control mice fed with the same HFD for the same time periods. Lesion size, distribution, and complexity increased from the AAR to

the OCAR and to the ASR. The size and severity of lesions also increased in all three regions with increasing age of mice (Figure 4.6). Lesion types I to V were observed and the progression occurred faster in female than in male mice. Type I lesions were dominant in the AAR while type II lesions were dominant in the OCAR and the ASR in 8 week *ApoE*$^{-/-}$ male and female mice. By 12 weeks of age, type II lesions were dominant in the AAR. The dominant lesion was type III which were in some cases undergoing progression to type IV in the OCAR and ASR regions for both genders. At 18 weeks, lesion progression in the AAR was dominantly type III in females and type II in males. Both genders showed mainly type IV lesions in the other two regions. The 24-week group developed dominant type IV lesions and type III lesions in AAR of females and males respectively. Types IV and V lesions were dominant in the other two regions. The degree of fibrous tissues, identified at 200 and 630 magnification as spindle- shaped fibrous tissues in lesions were higher in 24 weeks mice than in 18 weeks mice. In both the 18- and 24-week groups, fibrous tissues were higher in the ASR compared to the OCAR. However, fibrous tissues were not quantified. Although advanced lesions (types IV to V) were dominant feature in older mice (18 to 24 weeks), early lesions (types I to III) were also observed, often at the shoulder regions of advanced lesions.

The overall disease state in a region was defined by the highest lesion type observed in tissues from that region. The disease state in the AAR was type I at 8 weeks, types II at 12 weeks, type III at 18 weeks, and type V at 24 weeks. The disease state in the OCAR and ASR regions were type II at 8 weeks, type III (in some cases undergoing progression to type IV) at 12 weeks, and type V at 18 and 24 weeks.

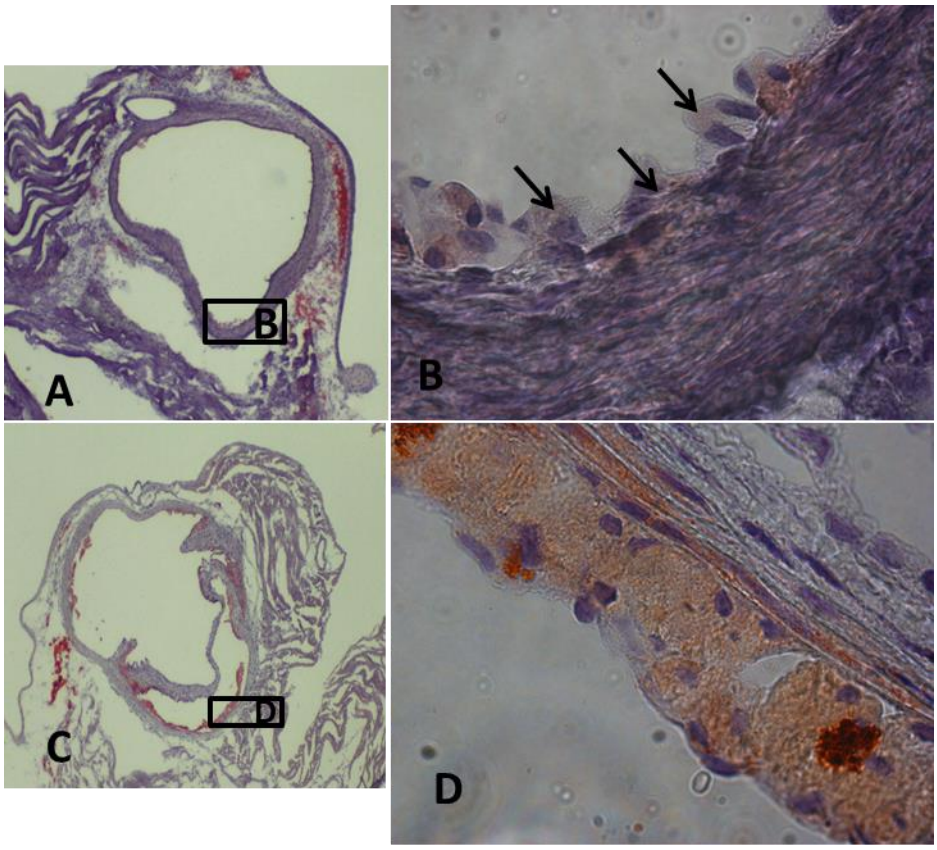

Figure 4.2. Photomicrographs of type I and type II lesions in tissue from the region showing the orifice of the coronary artery (OCAR) and from the arotic sinus region (ASR) respectively in 8 weeks female *ApoE*$^{-/-}$ mice fed a HFD. Insert in panel A and C (original magnification x35) are areas shown in Panel B and D (original magnification x630). Type I lesion consists of scattered macrophage foam cells (arrows). Type II consists of multilayer of foam cells and lipid-laden smooth muscle cells. Type I and II lesions are clinically benign. Tissues were embedded in formalin and then stained with oil red O to detect neutral lipids. Hematoxylin was used as the counter-stain.

4.5.2 Magnitude of Atherosclerotic Lesions in *ApoE*$^{-/-}$ Mice

Average percent lesion values (**Table 4.1**) for the *ApoE*$^{-/-}$ mice correlated well with histological observation of oil red-stained tissue sections from the regions of the different age groups. Average percent lesion values increased from the AAR to the OCAR to the ASR. This trend (Table 4.1, Figure 4.7) was observed in all age groups except in 24-

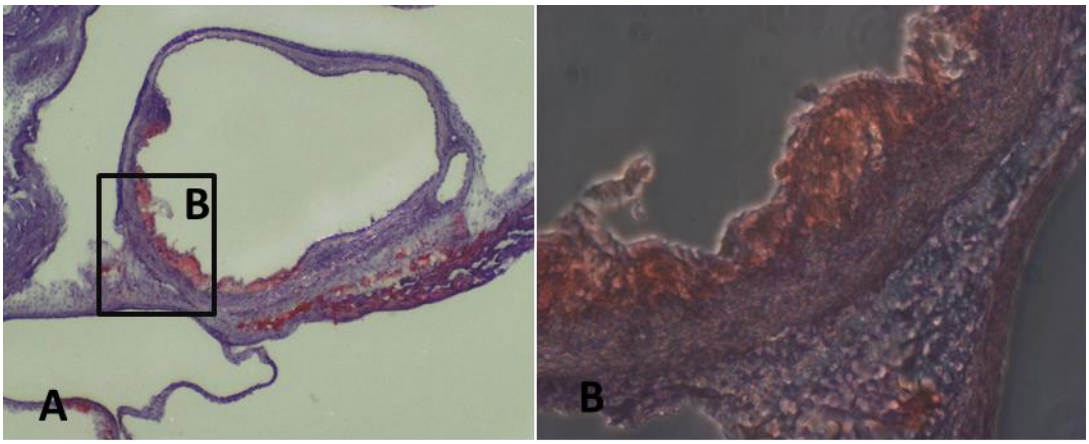

Figure 4.3. Photomicrograph of type III (intermediate) lesion from the region showing the orifice of the coronary arteries (OCAR) from 12 week male *ApoE*$^{-/-}$ mouse. Insert on panels A (original magnifications, x35) is area shown on panel B (original magnification, x200). Type III is an intermediate between the advanced types of lesions that can cause symptoms of atherosclerosis and the clinically benign lesions of type I and II. Type III is distinguished from the advanced types by the lack of the presence of necrotic lipid cores. Mouse was fed with high-fat diet. Tissue was stained with oil red O to visualize neutral lipids and counter-stained with hematoxylin.

week female mice, whose average percent lesion value was slightly higher for the OCAR (47.96 ± 5.75) than the ASR (44.51 ± 6.07) but not statistically significant based on result ($p = 0.263$) from ANOVA analysis. Results from comparison between aortic root regions from mice within an age group showed that the average percent lesion value increased significantly ($p<0.05$; Table 2) from OCAR to ASR in 8 weeks mice. Comparison was not made between AAR and OCAR or AAR and ASR due to limited data obtained for the AAR in this age group. In the 12-week group, the percent lesion difference was significant between any two of the three regions. Among 18- and 24-week mice groups, lesion percentage differences were significant between any two regions except between the OCAR and the ASR of the 18/24- week male mice and of the 24-week female mice.

Average percent lesion values for the three regions also increased in an age-dependent manner as showed in Figure 4.6. Average percentage lesions increased faster in older mice (18-week to 24-weeks) than younger mice (8 to 12 weeks) in the AAR. By contrast, it increased slower in older mice in the OCAR and the ASR. The similar changing trend observed in the OCAR and the ASR suggests that atherosclerotic development became more similar in these two regions as mice grew.

To determine the significant level of lesion increase between the ages for each region, an ANOVA statistical analysis was performed. P-values obtained after comparison between the different ages for each region of the aortic root are listed in Table 4.3. In the AAR, a significant change ($p< 0.05$) of average percentage of atherosclerotic lesions was only observed from 18 to 24 weeks. In the OCAR and ASR, significant changes were observed from 8 to 12 to 18 weeks for both female and male *ApoE*$^{-/-}$ mice. Only female mice showed significantly lesion increase in OCAR from week 18 to 24. No significant changes were observed in the ASR from week 18 to 24 for both genders.

As observed in the histological data, the percent values were generally higher in females than in males (Table 4.1). However, ANOVA comparisons between males and females for the regions and different ages only found significant differences in the OCAR of 12-week ($p = 0.0005$) and 24-week ($p=0.0049$) male and female mice.

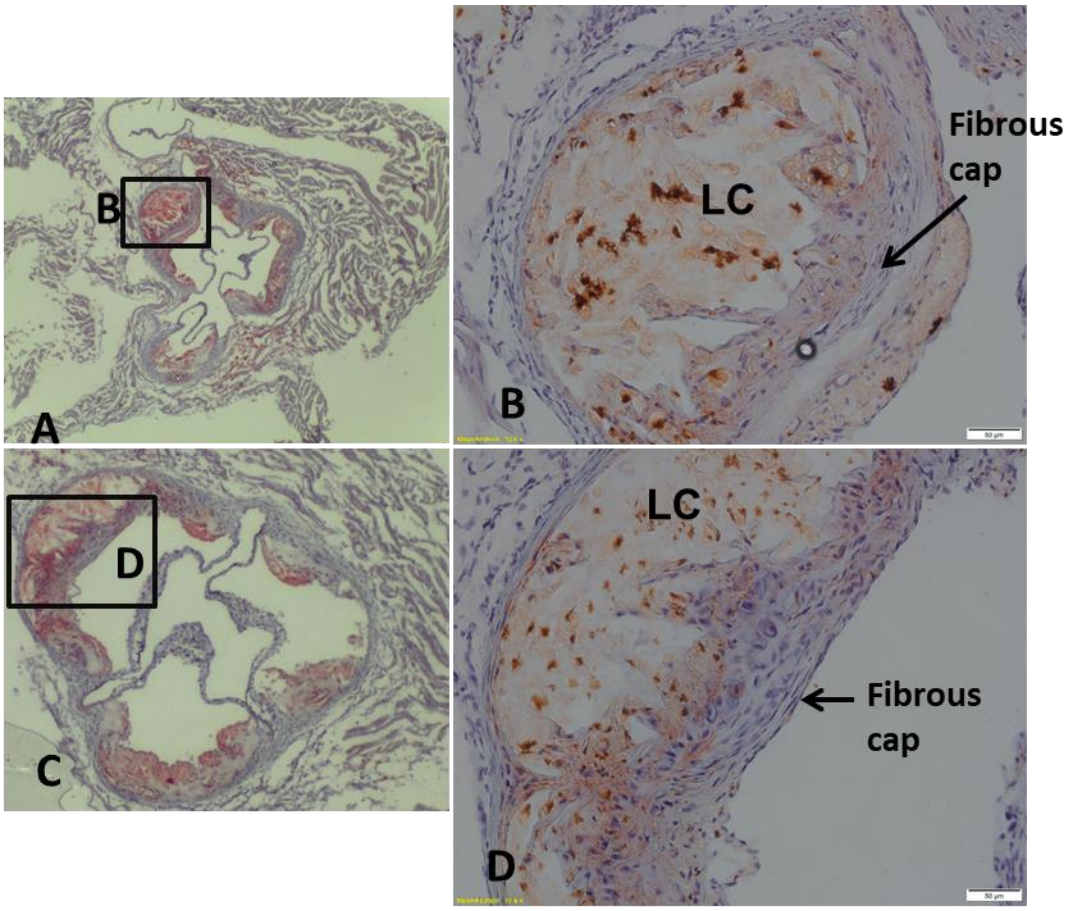

Figure 4.4. Photomicrographs of types IV and V lesions from the aortic sinus region (ASR) from 18 weeks respectively male and female *ApoE*$^{-/-}$ mice. Insert on panels A and C (original magnifications, x35) are areas shown on panel B and D (50 µm). The necrotic lipid core (LC) is a distinguishable feature of advanced lesions (types IV and V). A fibrous cap (arrows) covers the LC. A distinguishing feature of type IV form type V is substantial amount of fibrous tissues in type V. Both types of lesions can cause complications of atherosclerosis. Mice were fed with a high fat diet. Tissues were stained with oil red O to visualize neutral lipids and counter-stained with hematoxylin.

4.6 DISCUSSION

4.6.1 Atherosclerosis in Aortic Root Regions of *ApoE*$^{-/-}$ Mice

The atherogenic process is progressive in nature[68]. In this study, increases in lesion

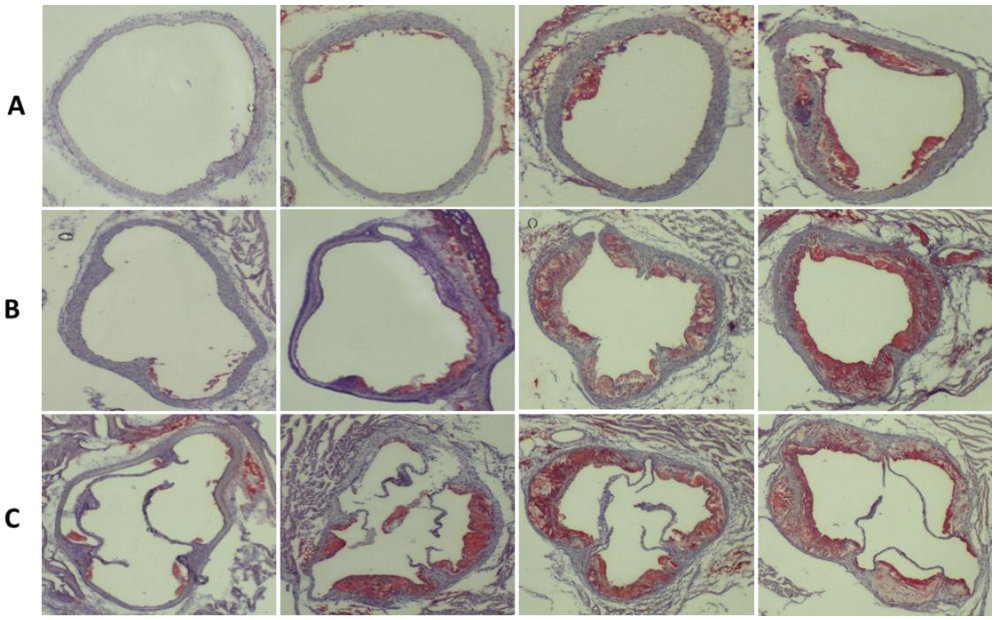

Figure 4.5. Atherosclerosis in three regions of *ApoE*$^{-/-}$ mice at ages (from left to right) 8, 12, 18 and 24 weeks. A. AAR. B. OCAR. C. ASR. Lesion distribution and complexity increase from the AAR to the OCAR to the ASR. Lesions also increased with age of mice. Mice were fed a high fat diet. Tissues were embedded in formalin and stained with oil red O and hematoxylin. Original magnification, x35.

Table 4.1. Average % lesions in three regions of the aortic root of *ApoE*$^{-/-}$ mice.

Age of Mice (Weeks)	AAR	OCAR	ASR
	Average %Lesion ± SD (*# of mice quantified)		
Males			
8	0.90 (1)	1.02 ± 0.78 (3)	3.65 ± 0.77 (5)
12	2.70 ± 1.47 (5)	6.78 ± 2.90 (7)	14.61 ± 6.99 (7)
18	4.22 ± 2.84 (5)	33.83 ± 9.75 (7)	37.67 ± 7.66 (8)
24	21.16 ± 7.65 (6)	37.88 ± 6.33 (8)	41.30 ± 7.04 (9)
Females			
8	0.45 ± 0.12 (2)	0.78 ± 0.16 (3)	4.57 ± 0.36 (3)
12	1.80 ± 1.70 (3)	16.14 ± 2.60 (4)	22.30 ± 2.72 (4)
18	8.97 ± 2.54 (4)	35.20 ± 6.39 (8)	43.29 ± 7.39 (7)
24	30.20 ± 1.85 (3)	47.96± 5.75 (8)	44.51± 6.07 (8)

* Total number quantified. This is less than the total number of mice in each age category used in the overall study.

Table 4.2. p-values obtained from comparison between aortic root regions from mice within an age group.

Age of Mice (Weeks)	*AAR *vs.* OCAR	*AAR *vs.* ASR	OCAR vs. ASR
Males			
8	N/A	N/A	3.47E-03
12	1.66E-02	4.10E-03	1.81E-02
18	6.77E-05	1.60E-06	4.08E-01
24	7.50E-04	1.57E-04	3.11E-01
Females			
8	N/A	N/A	7.74E-05
12	2.33E-03	6.98E-04	1.70E-02
18	1.54E-05	1.01E-05	4.05E-02
24	6.47E-04	3.63E-03	2.63E-01

*Comparisons was not done between AAR and OCAR and AAR and ASR of 8 weeks *ApoE*$^{-/-}$ mice due to limited quantification data for the AAR.

severity and percentage from 8 weeks to 24 weeks in different *ApoE*$^{-/-}$ mice demonstrated this progressiveness. *ApoE*$^{-/-}$ mice on C57BL/6 background provided an effective model for studying disease progression in the aortic root. The aortic root is commonly examined in murine-atherosclerotic studies due to its predisposition to develop atherosclerosis. Majority of studies in the mouse aortic root have been focused on the ASR[68] because complicated lesions develops in this region[72, 192] and the appearance of the aortic cusps of the ASR allows for easy comparison between different mice. Accordingly, lesion types and progression in the ASR has been broadly characterized whiles similar descriptions for the AAR and OCAR are rare. This study presents simultaneous characterization and quantification of all three regions of the aortic root in a large population of *ApoE*$^{-/-}$ mice on C57BL/6 background.

Table 4.3. p-values obtained after comparison between the different ages for each region of the aortic root.

Age of Mice (Weeks)	*AAR	OCAR	ASR
Males			
8 to 12	N/A	1.11E-02	6.32E-03
12 to 18	3.19E-01	1.36E-05	4.06E-05
18 to 24	1.19E-03	3.51E-01	3.25E-01
Females			
8 to 12	N/A	1.73E-04	1.10E-04
12 to 18	2.46E-02	2.19E-04	4.50E-04
18 to 24	6.67E-05	8.94E-04	9.87E-01

*Comparison was not done between 8 and 12 weeks *ApoE*$^{-/-}$ mice for AAR due to limited quantification data for the AAR.

Lesion distribution, size, and complexity increased from the AAR to the OCAR to the ASR. Differences in the extent of atherosclerotic lesions in these three regions of the aortic root are linked to hemodynamic factors in each region. The AAR is circular and straight, which enables uniform laminar blood flow and the generation of high shear stress on the region's endothelium lining. Straight arterial segments with high shear stress have been correlated to minimal/no development of atherosclerotic lesions. Conversely, areas where shear stress is low, such as the inner curve of the aortic arch, or where flow is oscillatory, such as near bifurcations, have turbulent blood flow and are associated with increased or extensive development of atherosclerotic lesions[193, 194]. Low and/or oscillatory shear stress (OSS) increases atherosclerosis risk by primarily inducing dysfunction of the local endothelium[57, 195]. Endothelial dysfunction is an established condition that triggers initial atherosclerosis events including increasing the expression of cellular adhesion molecules ICAMs (e.g. ICAM-1), vascular cell adhesion molecules (VCAMs) (e.g. VCAM-1), chemokines, and platelets[55-57]. Progression of atherosclerotic

lesions can then rapidly occur when risk factors such as hyperlipidemia, diabetes, and hypertension are present[195]. The high susceptibility of mouse ASR to develop lesions is a result of OSS[196] caused by the aortic cusps. The extent of lesion formation in the OCAR is also associated with OSS and/or low shear stress in this region, predisposed by the branching of the coronary arteries. Also, closer proximity to the ASR potentially encourages easy spreading of the disease to this region. The generally higher lesion prevalence in the ASR compared to OCAR suggests higher OSS in the ASR.

The morphology of atherosclerotic lesions is an indication of the severity of the disease. Accordingly, lesion types in a region corresponded to the severity of the disease in that region. The observation of complex lesions in the ASR in this study supports the common use of this region for probing advanced types of lesions However, the AAR can be of use if early forms of lesion are the target of interest, such as in drug intervention studies aimed at preventing advancement of early atherosclerotic lesions. This would be particularly useful as the early types of lesion in OCAR and ASR in the *ApoE*$^{-/-}$ mice fed HFD rapidly progresses to advanced forms which could make early lesions difficult to target or enough time for expected effect of a target drug. In using the AAR for comparative studies, the, circular shape of this region could be a guide for accurate identification. The statistical differences or similarities in the average percent lesion values between regions and ages as shown above can provide a guide for designing future atherosclerotic studies.

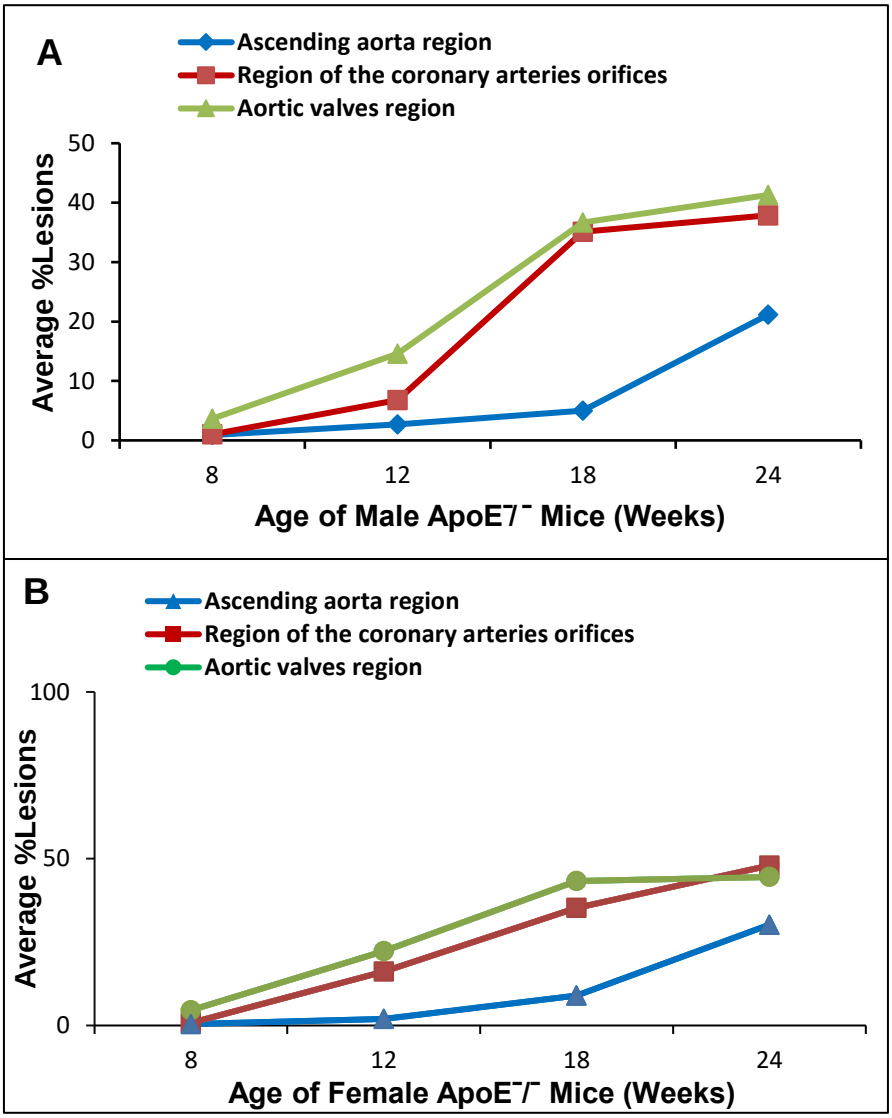

Figure 4.6. Average percent lesions in three regions (i.e., AAR, OCAR and ASR) of the aortic root of 8- to 24-week male (a) and female (b) *ApoE*$^{-/-}$ mice.

4.6.2 Lesion Progression with Age of *ApoE*$^{-/-}$ Mice

The progression of lesion severity in the three aortic root regions from 8 to 24 weeks observed in our study confirms age as a risk factor of atherosclerosis[197]. The risk with age is validated by the types of lesions formed at different ages in a specific region.

8-week *ApoE*$^{-/-}$ mice developed type I or II lesions (known to be clinically benign). By contrast, clinical important types IV and V lesions (necrotic core lesions) developed in older mice.

4.6.3 Influence of Gender on Lesion Formation in Aortic Root Regions

Histological data from this study revealed that lesion development were generally faster in female than in males *ApoE*$^{-/-}$ mice. However, statistical significant difference in average percentage of lesions between genders was only observed in the OCAR of 12- and 24-week mice. Higher disease proliferation in female mice is consistent with previous report[198]. However, the opposite is observed in humans. Premenopausal women are viewed to have lower risk of atherosclerosis and related heart diseases than age matched males, but the risk become similar in postmenopausal women and men of comparable age[199]. The decreased risk with younger women has been linked to protective effects of estrogen which decrease in women with age. The cardioprotective mechanisms of estrogen include decreased low-density lipoprotein (LDL), increased high-density lipoprotein (HDL), and release of vasodilators such as nitric oxide (NO) and prostacyclin (PGI2) from vessel walls, which results in inhibition of vascular constriction and lowering of blood pressure, as well as decreased platelet aggregation[199]. Similar disease proliferation in both genders with increased age was observed in mice from this study demonstrated by comparable lesions (in size and type) in higher prevalent regions.

4.7 CONCLUSIONS

This study showed a simultaneous comparison of atherosclerosis progression in three regions of the aortic root of *ApoE*$^{-/-}$ mice fed HFD. The ASR is a predilection site for lesion development in mice. Lesions in this region progress rapidly to advanced types of lesions by 18 weeks of age, which implies that this region is better suited for the study of advanced types of atherosclerotic lesions using the *ApoE*$^{-/-}$ mouse model. By contrast, the slowest lesion formation is in the AAR, with lesions progressing to the advanced forms in this region only in the 24-week mice. Therefore, AAR is suitable for the study of drug targeted at early types of lesions. Lesion types in the OCAR are mainly of types I and III in younger mice (8 and 12 weeks) and types IV-V in older mice (18 and 24 weeks). This region is thus best suited for investigating all lesion types guided by the presented age limits for various lesion developments. The progressiveness and age dependency of the atherogenic process is also confirmed in this study. The data presented serve well as a guide in designing future murine atherosclerotic studies.

4.8 ACKNOWLEDGEMENT

We acknowledge using the Animal Resource Wing (ARW), the Functional Genomics Core Facility, and the High Magnification Microscope Laboratory and Dr. Adam Hoppe Microscope Laboratory at South Dakota State University (SDSU) for housing mice, cross-sectioning aortic roots, and high magnifications imaging of stained aortic root tissue slides, respectively. This work was supported by American Heart Association Award #11GRNT7800009.

CHAPTER FIVE

5.0 SUMMARY AND FUTURE WORK

5.1 Summary

The objectives of this work were (i) develop an immunodepletion method for bovine fluids, (ii) to analyze changes in proteins in FF and plasma (PL) from cattle with high E2 (HE2) or low E2 (LE2) during the pre-ovulatory period, and (iii) characterize and quantify atherosclerotic lesion development in three regions of the aortic root of *ApoE*$^{-/-}$ mice.

A proteomic-shotgun (bottom down) approach was selected to achieve our second objective. This approach is suitable for analyzing complex matrices. An important and often required step in the shotgun approach is to employ a protein fractionation step. The protein fractionation method of choice was immunodepletion due to the high selectivity, sensitivity, and reproducibility reported for this method. However, because immunodepletion methods for bovine fluids are currently very limited, development of an immunodepletion method became necessary and this formed our first objective. Therefore an immmunodepletion method utilizing MARS Hu6-HC was developed for bovine PL, FF, epididymis sperm types, and ejaculated sperm types. High depletion rates for targeted HAPs albumin, IgG, IgA, and alpha-1-antitrypsin (or alpha-1-antiproteinase) was achieved. The depletion rates confirmed by sandwich ELISA for albumin, IgG, and IgA ranged from 98.7 to 99.9% in all the bovine samples investigated. A similar depletion rate was expected for alpha-1-anti-trypsin based on dramatic depletion of its gel band. The observed high depletion rates were primarily attributed to the high structural

similarity of these proteins between human and bovine. There was also dramatic depletion of binder of sperm proteins (BSP) - PDC-109, BSP-A3, and BSP-30kDa, which are HAPs in seminal plasma component of ejaculated sperm, forming 40-57% of the total protein component. The depletion of the BSP proteins was therefore considered beneficial if both bound and depleted fractions are analyzed.

Protein quantification in proteomics enables detection of expression changes between treatments. iTRAQ reagents were successfully used for the quantification. 4-plex iTRAQ reagents were used to individually label PL HE2, PL LE2, FF HE2, and FF LE2 and subsequent nanoLC-ESI-LTQ (PQD) analysis identified a total of 231 proteins with high confidence (FDR $\leq$0.05). 103 of the identified proteins showed expression changes (up-regulated or down-regulated) after comparisons between samples. Important information was drawn from our proteomic approach: higher number of proteins showed expression change between different fluid types (i.e. PL and FF) than between HE2 and LE2 of a fluid; E2 has a greater effect on FF proteins than PL proteins; the up- and down-regulated proteins were mainly localized in the cell, the extracellular region and organelle and were mainly associated to cellular process and metabolic process. Binding and catalytic activity were the most associated molecular processes; E2 is critical to the development and maturation of ovarian follicles. Several of the proteins showing expression changes play important roles in folliculogenesis and are modulated by E2; and complement and coagulation pathways were the main pathways associated with the proteins, supporting the view that folliculogenesis and ovulation are hemorrhagic events. This work therefore demonstrates the ability of proteomic to provide insights into reproduction in bovine. The presented data specifically provides the basis for further

investigation of specific processes involved in E2 regulation of reproductive associated proteins.

Atherosclerosis is the underlining cause for heart attack and stroke, the two leading cause of cardiovascular death worldwide. The *ApoE*$^{-/-}$ -mouse model is popular for atherosclerosis research. This work characterized and quantified atherosclerosis development in three regions of the aortic root of *ApoE*$^{-/-}$ mice. The examined three regions of the aortic root were ascending aorta region (AAR), region showing the orifices of the coronary arteries marking the start of the ascending arch (OCAR), and aortic sinus region (ASR). Lesion development in the three regions was location and age dependent. It was slowest in the AAR and formed types I-III lesions in this region from 8-18 weeks of age and type IV at 24 weeks of age. Lesion development was faster in OCAR and ASR and developed to types IV and V by 18 weeks. Average percent lesion values increased from the AAR to the OCAR to the ASR, correlating to the histological data. These findings would be beneficial in experimental design and targeting certain lesion types in aortic roots of the popular *ApoE*$^{-/-}$ murine atherosclerosis model.

5.2 Future Work

5.2.1 Identification of phosphoproteins biomarker candidates for atherosclerosis

Protein phosphorylation entails the reversible incorporation of phosphate group to amino acid side chains of proteins and it is the most studied post-translational modification (PTM). Phosphoproteins are important biomarker targets for atherosclerosis because of the crucial regulatory role of protein phosphorylation in most cellular processes. Cellular processes such as metabolism, contraction and relaxation of muscles,

transcription and genetic information, hormonal and nerve signaling, proliferation, apoptosis, differentiation, cell growth, aging, and inflammation are directly or indirectly regulated by protein phosphorylation[200, 201]. Because casual factors for atherosclerosis development are widely recognized to be multiple, it is expected that alteration in associated phosphorylation/dephosphorylation regulatory processes could create disease conditions with the associated phosphoproteins being up- or down-regulated. For example, the most studied potential phosphoprotein biomarker is VSMC heat shock protein 27 (HSP27)[81, 202]. HSP27 expression is reported to increase in normal appearing vessels adjacent to atherosclerotic lesion whereas levels in the atherosclerotic lesion itself are significantly decreased. Both lesion and adjacent artery show decreased HSP27 phosphorylation compared with reference vessel[81, 203].

The future work would be to use proteomic approach to identify and quantify the expression levels of phosphoproteins in the plasma samples from the *ApoE*$^{-/-}$ and control mice of all the ages from this study. Comparison between the plasma proteome of the *ApoE*$^{-/-}$ and control mice, and between the different ages groups could provide more insights into the differentially expressed phosphoproteins in the development of atherosclerosis. Possible biomarker candidates could then be sought for and further investigated.

The experimental approach could employ proteomic bottom-up methods which could include enrichment of phosphoproteins in the plasma sample, trypsin digestion of proteins into peptides, iTRAQ labeling of peptides, SCX separation of peptides, and analysis of samples using nanoLC-MS/MS with subsequent protein identification and quantification with the SEQUEST and Proteome Discoverer softwares. Enrichment of

phosphoproteins is particularly important for three main reasons: 1. Phosphoproteins are PTMs and therefore are low abundance in nature. 2. Phosphorylation is a transient modification, so the target protein could present in both the native and phosphorylated form and 3. Phosphopeptides ionize poorly in MS strategies particularly in the presence of non-phosphorylated molecules resulting in lower signal intensities[204]. Phosphoproteins enrichment can be achieved using metal oxide affinity chromatography (MOAC), immobilized metal affinity chromatography (IMAC), and titanium dioxide (TiO2)[204, 205].

Because the *ApoE*$^{-/-}$ group developed atherosclerosis as shown in this dissertation, it is expected the phosphoproteome in this group to differ, with phosphoproteins levels either up- or down-regulated compared to the control group. Our study shows that *ApoE*$^{-/-}$ mice fed with a HFD developed atherosclerosis as early as 8 weeks, with lesions mainly in the early-staged form. By 24 weeks, the disease had reached its advanced stage as visualized by the presence of features like the necrotic lipid core (LC) and greater degree of fibrous tissues. Therefore, identified phosphoprotein candidates showing expression changes in plasma samples from younger *ApoE*$^{-/-}$ mice (8 or 12 weeks) would be better markers for early stages of the disease whereas those from older *ApoE*$^{-/-}$ mice (18 and 24 weeks) would be better biomarkers for advanced stage of the disease. Accordingly, special attention would be given to such proteins. Also, protein candidates that would be consistently present throughout all the stages of the disease would be sought for as these would be more robust in predicting risk of the disease.

5.2.2 Profiling and iTRAQ quantification of Epididymis and Ejaculated Sperm Proteins

A focus of this dissertation was to profile proteins relevant to productivity of the cow, specifically at the folliculogenesis stage. Future work will be to profile sperm proteins relevant to bull productivity. During ejaculation, stored sperms from the cauda epididymis transit through the vas deferens and secretions from the accessory sex glands (prostate gland, cowper's gland, and seminal vesicles) called seminal plasma is added and is released together with sperm as semen. With the contact with the seminal fluid, sperm undergoes series of biochemical and structural changes associated with sperm capacitation. Capacitation is required to make sperm competent to fertilize an oocyte[206]. Therefore, the protein composition of epididymis and ejaculated sperms are different. The future work would use proteomic shotgun approach to investigate these differences. Proteins of the sperm membranes and in the fluids surrounding either sperm type (herein labeled as ejaculated sperm proteins, ejaculated semen plasma, epididymis sperm proteins, and epididymis semen proteins) would be quantitatively measured using iTRAQ reagents. The immunodepletion method discussed in this work showed high depletion rates for abundant proteins in either sperm type and would be incorporated in the analysis.

REFERENCE

1. Graves, P. R.; Haystead, T. A. J., Molecular biologist's guide to proteomics. *Microbiology and molecular biology reviews : MMBR* **2002,** *66* (1), 39-63.
2. Aebersold, R.; Mann, M., Mass spectrometry-based proteomics. *Nature* **2003,** *422* (6928), 198-207.
3. Banerjee, S.; Mazumdar, S., Electrospray Ionization Mass Spectrometry: A Technique to Access the Information beyond the Molecular Weight of the Analyte. *International Journal of Analytical Chemistry* **2012,** *2012*, 1-40.
4. Bantscheff, M.; Lemeer, S.; Savitski, M. M.; Kuster, B., Quantitative mass spectrometry in proteomics: critical review update from 2007 to the present. *Analytical and Bioanalytical Chemistry* **2012,** *404* (4), 939-965.
5. Savaryn, J. P.; Toby, T. K.; Kelleher, N. L., A Researcher's Guide to Mass Spectrometry-Based Proteomics. *Proteomics* **2016,** *16* (18), 2435-2443.
6. Schwartz, J. C.; Senko, M. W.; Syka, J. E. P., A two-dimensional quadrupole ion trap mass spectrometer. *Journal of the American Society for Mass Spectrometry* **2002,** *13* (6), 659-669.
7. Wu, W. W.; Wang, G.; Insel, P. A.; Hsiao, C.-T.; Zou, S.; Maudsley, S.; Martin, B.; Shen, R.-F., Identification of proteins and phosphoproteins using pulsed Q collision induced dissociation (PQD). *Journal of the American Society for Mass Spectrometry* **2011,** *22* (10), 1753-1762.
8. Schwartz, J. C., Syka, J.E.P., Quarmby, S.T., Improving the Fundamentals of MSn on 2D Linear Ion Traps: New Ion Activation and Isolation Techniques. The 53rd ASMS Conference on Mass Spectrometry and Allied Topic. *San Antonio, TX*, **2005**, June 5–9.
9. Rauniyar, N.; Yates, J. R., Isobaric Labeling-Based Relative Quantification in Shotgun Proteomics. *Journal of Proteome Research* **2014,** *13* (12), 5293-5309.
10. Hu, A.; Noble, W. S.; Wolf-Yadlin, A., Technical advances in proteomics: new developments in data-independent acquisition. *F1000Research* **2016,** *5*, F1000 Faculty Rev-419.
11. Abdallah, C.; Dumas-Gaudot, E.; Renaut, J.; Sergeant, K., Gel-Based and Gel-Free Quantitative Proteomics Approaches at a Glance. *International Journal of Plant Genomics* **2012,** *2012*, 17.
12. Kalli, A.; Smith, G. T.; Sweredoski, M. J.; Hess, S., Evaluation and optimization of mass spectrometric settings during data-dependent acquisition mode: focus on LTQ-Orbitrap mass analyzers. *Journal of proteome research* **2013,** *12* (7), 3071-3086.
13. Baldwin, M. A., Protein Identification by Mass Spectrometry. *Molecular & Cellular Proteomics* **2004,** *3* (1), 1-9.
14. Zhang, Y.; Fonslow, B. R.; Shan, B.; Baek, M.-C.; Yates, J. R., Protein Analysis by Shotgun/Bottom-up Proteomics. *Chemical reviews* **2013,** *113* (4), 2343-2394.
15. Anderson, N. L.; Anderson, N. G., The human plasma proteome: history, character, and diagnostic prospects. *Mol Cell Proteomics* **2002,** *1*, 845-867.
16. Hortin, G. L.; Jortani, S. A.; Ritchie, J. C.; Valdes, R.; Chan, D. W., Proteomics: A New Diagnostic Frontier. *Clinical Chemistry* **2006,** *52* (7), 1218-1222.

17. Tirumalai, R. S.; Chan, K. C.; Prieto, D. A.; Issaq, H. J.; Conrads, T. P.; Veenstra, T. D., Characterization of the Low Molecular Weight Human Serum Proteome. *Molecular & Cellular Proteomics* **2003,** *2* (10), 1096-1103.
18. Faulkner, S.; Elia, G.; Hillard, M.; O'Boyle, P.; Dunn, M.; Morris, D., Immunodepletion of albumin and immunoglobulin G from bovine plasma. *Proteomics* **2011,** *11* (11), 2329-2335.
19. Wu, C. C.; Duan, J. C.; Liu, T.; Smith, R. D.; Qian, W. J., Contributions of immunoaffinity chromatography to deep proteome profiling of human biofluids. *J. Chromatogr. B* **2016,** *1021*, 57-68.
20. Laemmli, U. K., Cleavage of Structural Proteins during the Assembly of the Head of Bacteriophage T4. *Nature* **1970,** *227*, 680.
21. Shevchenko, A.; Tomas, H.; Havlis, J.; Olsen, J. V.; Mann, M., In-gel digestion for mass spectrometric characterization of proteins and proteomes. *Nat Protoc* **2006,** *1* (6), 2856-60.
22. Zhang, X.; Fang, A.; Riley, C. P.; Wang, M.; Regnier, F. E.; Buck, C., Multi-dimensional liquid chromatography in proteomics--a review. *Analytica chimica acta* **2010,** *664* (2), 101-113.
23. Washburn, M. P.; Wolters, D.; Yates Iii, J. R., Large-scale analysis of the yeast proteome by multidimensional protein identification technology. *Nature Biotechnology* **2001,** *19*, 242-247.
24. Yates, J. R.; Ruse, C. I.; Nakorchevsky, A., Proteomics by Mass Spectrometry: Approaches, Advances, and Applications. In *Annual Review of Biomedical Engineering*, 2009; Vol. 11, pp 49-79.
25. Thiede, B.; Höhenwarter, W.; Krah, A.; Mattow, J.; Schmid, M.; Schmidt, F.; Jungblut, P. R., Peptide mass fingerprinting. *Methods* **2005,** *35* (3), 237-247.
26. Aggarwal, S.; Yadav, A. K., Dissecting the iTRAQ Data Analysis. In *Statistical Analysis in Proteomics*, Jung, K., Ed. Springer New York: New York, NY, 2016; pp 277-291.
27. Zhang, G.; Ueberheide, B. M.; Waldemarson, S.; Myung, S.; Molloy, K.; Eriksson, J.; Chait, B. T.; Neubert, T. A.; Fenyö, D., Protein Quantitation Using Mass Spectrometry. *Methods in molecular biology (Clifton, N.J.)* **2010,** *673*, 211-222.
28. Casey, T. M.; Khan, J. M.; Bringans, S. D.; Koudelka, T.; Takle, P. S.; Downs, R. A.; Livk, A.; Syme, R. A.; Tan, K.-C.; Lipscombe, R. J., Analysis of Reproducibility of Proteome Coverage and Quantitation Using Isobaric Mass Tags (iTRAQ and TMT). *Journal of Proteome Research* **2017,** *16* (2), 384-392.
29. Pichler, P.; Köcher, T.; Holzmann, J.; Mazanek, M.; Taus, T.; Ammerer, G.; Mechtler, K., Peptide Labeling with Isobaric Tags Yields Higher Identification Rates Using iTRAQ 4-Plex Compared to TMT 6-Plex and iTRAQ 8-Plex on LTQ Orbitrap. *Anal. Chem.* **2010,** *82* (15), 6549-6558.
30. Ross, P. L.; Huang, Y. N.; Marchese, J. N.; Williamson, B.; Parker, K.; Hattan, S.; Khainovski, N.; Pillai, S.; Dey, S.; Daniels, S.; Purkayastha, S.; Juhasz, P.; Martin, S.; Bartlet-Jones, M.; He, F.; Jacobson, A.; Pappin, D. J., Multiplexed Protein Quantitation in Saccharomyces cerevisiae Using Amine-reactive Isobaric Tagging Reagents. *Molecular & Cellular Proteomics* **2004,** *3* (12), 1154-1169.
31. Ross, P. L.; Huang, Y. N.; Marchese, J. N.; Williamson, B.; Parker, K.; Hattan, S.; Khainovski, N.; Pillai, S.; Dey, S.; Daniels, S., Multiplexed protein quantitation in

Saccharomyces cerevisiae using amine-reactive isobaric tagging reagents. *Mol Cell Proteomics* **2004,** *3*, 1154-1169.
32. Brewis, I. A., Proteomics in reproductive research: The potential importance of proteomics to research in reproduction. *Human Reproduction* **1999,** *14* (12), 2927-2929.
33. KOSTERIA, I.; ANAGNOSTOPOULOS, A. K.; KANAKA-GANTENBEIN, C.; CHROUSOS, G. P.; TSANGARIS, G. T., The Use of Proteomics in Assisted Reproduction. *In Vivo* **2017,** *31* (3), 267-283.
34. Mukasa-Mugerwa, E., A review of reproductive performance of female Bos Indicus (Zebu) cattle. **1989**.
35. Balhara, A. K.; Gupta, M.; Singh, S.; Mohanty, A. K.; Singh, I., Early Pregnancy Diagnosis in Bovines: Current Status and Future Directions. *The Scientific World Journal* **2013,** *2013*, 958540.
36. Lee, J. E.; Lee, J. Y.; Kim, H. R.; Shin, H. Y.; Lin, T.; Jin, D. I., Proteomic Analysis of Bovine Pregnancy-specific Serum Proteins by 2D Fluorescence Difference Gel Electrophoresis. *Asian-Australasian Journal of Animal Sciences* **2015,** *28* (6), 788-795.
37. Orozco Lucero, E., Molecular markers of fertility in cattle oocytes and embryos: progress and challenges. *Anim. Reprod.* **2014,** *11* (3), 183-194.
38. Park, Y.-J.; Kim, J.; You, Y.-A.; Pang, M.-G., Proteomic Revolution to Improve Tools for Evaluating Male Fertility in Animals. *Journal of Proteome Research* **2013,** *12* (11), 4738-4747.
39. Faulkner, S.; Elia, G.; Mullen, M. P.; O'Boyle, P.; Dunn, M. J.; Morris, D., A comparison of the bovine uterine and plasma proteome using iTRAQ proteomics. *Proteomics* **2012,** *12* (12), 2014-2023.
40. Ferrazza, R. d. A.; Garcia, H. D. M.; Schmidt, E. M. d. S.; Mihm Carmichael, M.; de Souza, F. F.; Burchmore, R.; Sartori, R.; Eckersall, P. D.; Ferreira, J. C. P., Quantitative proteomic profiling of bovine follicular fluid during follicle development. *Biology of Reproduction* **2017,** *0* (0), 1-15.
41. Moura, A. A.; Chapman, D. A.; Killian, G. J., Proteins of the accessory sex glands associated with the oocyte-penetrating capacity of cauda epididymal sperm from Holstein bulls of documented fertility. *Mol. Reprod. Dev.* **2007,** *74* (2), 214-222.
42. Moura, A. A.; Souza, C. E.; Stanley, B. A.; Chapman, D. A.; Killian, G. J., Proteomics of cauda epididymal fluid from mature Holstein bulls. *Journal of Proteomics* **2010,** *73* (10), 2006-2020.
43. Park, Y. J.; Kwon, W. S.; Oh, S. A.; Pang, M. G., Fertility-Related Proteomic Profiling Bull Spermatozoa Separated by Percoll. *Journal of Proteome Research* **2012,** *11* (8), 4162-4168.
44. Aerts, J.; Bols, P., Ovarian Follicular Dynamics: A Review with Emphasis on the Bovine Species. Part I: Folliculogenesis and Pre-antral Follicle Development. *Reproduction in Domestic Animals* **2010,** *45* (1), 171-179.
45. Roberts, R. M., Interferon-tau, a Type 1 interferon involved in maternal recognition of pregnancy. *Cytokine & growth factor reviews* **2007,** *18* (5-6), 403-408.
46. Harris, L. K.; Crocker, I. P.; Baker, P. N.; Aplin, J. D.; Westwood, M., IGF2 actions on trophoblast in human placenta are regulated by the insulin-like growth factor 2 receptor, which can function as both a signaling and clearance receptor. *Biology of reproduction* **2011,** *84* (3), 440-446.

47. Ko, Y.; Lee, C. Y.; Ott, T. L.; Davis, M. A.; Simmen, R. C.; Bazer, F. W.; Simmen, F. A., Insulin-like growth factors in sheep uterine fluids: concentrations and relationship to ovine trophoblast protein-1 production during early pregnancy. *Biol Reprod* **1991,** *45* (1), 135-42.
48. Zachut, M.; Sood, P.; Livshitz, L.; Kra, G.; Levin, Y.; Moallem, U., Proteome dataset of pre-ovulatory follicular fluids from less fertile dairy cows. *Data in Brief* **2016,** *7*, 1515-1518.
49. Fahiminiya, S.; Labas, V.; Roche, S.; Dacheux, J.-L.; Gérard, N., Proteomic analysis of mare follicular fluid during late follicle development. *Proteome Science* **2011,** *9*, 54-54.
50. Mendis, S. P., P.; Norrving, B.;World Health Organization; World Heart Federation; et al., Global Atlas on cardiovascular disease prevention and control. **2011**.
51. Hadi, N. R.; Mohammad, B. I.; Ajeena, I. M.; Sahib, H. H., Antiatherosclerotic Potential of Clopidogrel: Antioxidant and Anti-Inflammatory Approaches. *BioMed research international* **2013,** *2013*, 10.
52. Upadhyay, R. K., Emerging Risk Biomarkers in Cardiovascular Diseases and Disorders. *Journal of Lipids* **2015,** *2015*, 50.
53. Ross , R., Atherosclerosis — An Inflammatory Disease. *New England Journal of Medicine* **1999,** *340* (2), 115-126.
54. Soeki, T.; Sata, M., Inflammatory Biomarkers and Atherosclerosis. *International Heart Journal* **2016,** *57* (2), 134-139.
55. Glaudemans, A. W. J. M.; Slart, R. H. J. A.; Bozzao, A.; Bonanno, E.; Arca, M.; Dierckx, R. A. J. O.; Signore, A., Molecular imaging in atherosclerosis. *European journal of nuclear medicine and molecular imaging* **2010,** *37* (12), 2381-2397.
56. Libby, P.; Ridker, P. M.; Maseri, A., Inflammation and Atherosclerosis. *Circulation* **2002,** *105* (9), 1135-1143.
57. Chappell, D. C.; Varner, S. E.; Nerem, R. M.; Medford, R. M.; Alexander, R. W., Oscillatory Shear Stress Stimulates Adhesion Molecule Expression in Cultured Human Endothelium. *Circulation research* **1998,** *82* (5), 532-539.
58. Stary, H. C.; Chandler, A. B.; Dinsmore, R. E.; Fuster, V.; Glagov, S.; Insull, W.; Rosenfeld, M. E.; Schwartz, C. J.; Wagner, W. D.; Wissler, R. W., A Definition of Advanced Types of Atherosclerotic Lesions and a Histological Classification of Atherosclerosis: A Report From the Committee on Vascular Lesions of the Council on Arteriosclerosis, American Heart Association. *Circulation* **1995,** *92* (5), 1355-1374.
59. Stary, H. C.; Chandler, A. B.; Glagov, S.; Guyton, J. R.; Insull, W.; Rosenfeld, M. E.; Schaffer, S. A.; Schwartz, C. J.; Wagner, W. D.; Wissler, R. W., A definition of initial, fatty streak, and intermediate lesions of atherosclerosis. A report from the Committee on Vascular Lesions of the Council on Arteriosclerosis, American Heart Association. *Circulation* **1994,** *89* (5), 2462-78.
60. Whitman, S. C., A Practical Approach to Using Mice in Atherosclerosis Research. *The Clinical Biochemist Reviews* **2004,** *25* (1), 81-93.
61. Stary, H. C., Natural History and Histological Classification of Atherosclerotic Lesions : An Update. *Arteriosclerosis, Thrombosis, and Vascular Biology* **2000,** *20* (5), 1177-1178.
62. Getz, G. S.; Reardon, C. A., Animal Models of Atherosclerosis. *Arteriosclerosis, Thrombosis, and Vascular Biology* **2012,** *32* (5), 1104-1115.

63. Lee, Y. T.; Lin, H. Y.; Chan, Y. W. F.; Li, K. H. C.; To, O. T. L.; Yan, B. P.; Liu, T.; Li, G.; Wong, W. T.; Keung, W.; Tse, G., Mouse models of atherosclerosis: a historical perspective and recent advances. *Lipids in health and disease* **2017,** *16* (1), 1-11.
64. Schreyer, S. A.; Wilson, D. L.; LeBoeuf, R. C., C57BL/6 mice fed high fat diets as models for diabetes-accelerated atherosclerosis. *Atherosclerosis* **1998,** *136* (1), 17-24.
65. Plump, A. S.; Smith, J. D.; Hayek, T.; Aalto-Setälä, K.; Walsh, A.; Verstuyft, J. G.; Rubin, E. M.; Breslow, J. L., Severe hypercholesterolemia and atherosclerosis in apolipoprotein E-deficient mice created by homologous recombination in ES cells. *Cell* **1992,** *71* (2), 343-353.
66. Zhang, S. H.; Reddick, R. L.; Piedrahita, J. A.; Maeda, N., Spontaneous hypercholesterolemia and arterial lesions in mice lacking apolipoprotein E. *Science* **1992,** *258* (5081), 468-71.
67. Nakashima, Y.; Plump, A. S.; Raines, E. W.; Breslow, J. L.; Ross, R., ApoE-deficient mice develop lesions of all phases of atherosclerosis throughout the arterial tree. *Arteriosclerosis, Thrombosis, and Vascular Biology* **1994,** *14* (1), 133-140.
68. Meir, K. S.; Leitersdorf, E., Atherosclerosis in the apolipoprotein-E-deficient mouse: a decade of progress. *Arterioscler Thromb Vasc Biol* **2004,** *24* (6), 1006-14.
69. O'Neill, T. P., Apolipoprotein E-Deficient Mouse Model of Human Atherosclerosis. *Toxicologic Pathology* **1997,** *25* (1), 20-21.
70. Paigen, B.; Morrow, A.; Brandon, C.; Mitchell, D.; Holmes, P., Variation in susceptibility to atherosclerosis among inbred strains of mice. *Atherosclerosis* **1985,** *57* (1), 65-73.
71. Daugherty, A.; Rateri, D. L., Development of experimental designs for atherosclerosis studies in mice. *Methods* **2005,** *36* (2), 129-38.
72. Tangirala, R. K.; Rubin, E. M.; Palinski, W., Quantitation of atherosclerosis in murine models: correlation between lesions in the aortic origin and in the entire aorta, and differences in the extent of lesions between sexes in LDL receptor-deficient and apolipoprotein E-deficient mice. *Journal of Lipid Research* **1995,** *36* (11), 2320-8.
73. Paigen, B. M., A.;Holmes,P. A.;Mitchell,D.;and Williams,R. A., Quantitative assessment of atherosclerotic lesions in mice. *Atherosclerosis* **1987,** *68*, 231–240.
74. Julie Baglione; Smith, J. D., Quantitative Assay for Mouse Atherosclerosis in the Aortic Root. *Methods in Molecular Medicine* **2006,** *129*, 83-95.
75. VanderLaan, P. A.; Reardon, C. A.; Getz, G. S., Site specificity of atherosclerosis: site-selective responses to atherosclerotic modulators. *Arterioscler Thromb Vasc Biol* **2004,** *24* (1), 12-22.
76. Baglione, J.; Smith, J. D., Quantitative Assay for Mouse Atherosclerosis in the Aortic Root. *Methods in Molecular Medicine* **2006,** *129*, 83-95.
77. Chopra, V.; Eagle, K. A., Cardiac Biomarkers In The Diagnosis, Prognosis And Management Of Coronary Artery Disease: A Primer For Internists. *Indian Journal of Medical Sciences* **2010,** *64* (12), 564-576.
78. Biomarkers Definitions Working, G., Biomarkers and surrogate endpoints: Preferred definitions and conceptual framework. *Clinical Pharmacology & Therapeutics* **2001,** *69* (3), 89-95.

79. Vasan, R. S., Biomarkers of cardiovascular disease - Molecular basis and practical considerations. *Circulation* **2006,** *113* (19), 2335-2362.
80. de la Cuesta, F.; Mourino-Alvarez, L.; Baldan-Martin, M.; Moreno-Luna, R.; Barderas, M. G., Contribution of proteomics to the management of vascular disorders. *Translational Proteomics* **2015,** *7* (Supplement C), 3-14.
81. Bleijerveld, O. B.; Zhang, Y.-N.; Beldar, S.; Hoefer, I. E.; Sze, S. K.; Pasterkamp, G.; de Kleijn, D. P. V., Proteomics of plaques and novel sources of potential biomarkers for atherosclerosis. *Proteomics – Clinical Applications* **2013,** *7* (7-8), 490-503.
82. Beck, H. C.; Overgaard, M.; Melholt Rasmussen, L., Plasma proteomics to identify biomarkers – application to cardiovascular diseases. *Translational Proteomics* **2015,** *7*, 40-48.
83. von zur Muhlen, C.; Schiffer, E.; Zuerbig, P.; Kellmann, M.; Brasse, M.; Meert, N.; Vanholder, R. C.; Dominiczak, A. F.; Chen, Y. C.; Mischak, H.; Bode, C.; Peter, K., Evaluation of Urine Proteome Pattern Analysis for Its Potential To Reflect Coronary Artery Atherosclerosis in Symptomatic Patients. *J. Proteome Res.* **2009,** *8* (1), 335-345.
84. Lepedda, A. J.; Cigliano, A.; Cherchi, G. M.; Spirito, R.; Maggioni, M.; Carta, F.; Turrini, F.; Edelstein, C.; Scanu, A. M.; Formato, M., A proteomic approach to differentiate histologically classified stable and unstable plaques from human carotid arteries. *Atherosclerosis 203* (1), 112-118.
85. Ucciferri, N.; Rocchiccioli, S.; Comelli, L.; Marconi, M.; Ferrari, M.; Pelosi, G.; Cecchettini, A., Extracellular matrix characterization in plaques from carotid endarterectomy by a proteomics approach. *Talanta* **2017,** *174*, 341-346.
86. von zur Muhlen, C.; Schiffer, E.; Sackmann, C.; Zürbig, P.; Neudorfer, I.; Zirlik, A.; Htun, N.; Iphöfer, A.; Jänsch, L.; Mischak, H.; Bode, C.; Chen, Y. C.; Peter, K., Urine Proteome Analysis Reflects Atherosclerotic Disease in an ApoE−/− Mouse Model and Allows the Discovery of New Candidate Biomarkers in Mouse and Human Atherosclerosis. *Molecular & Cellular Proteomics* **2012,** *11* (7), 1-13.
87. Mayne, J.; Starr, A. E.; Ning, Z.; Chen, R.; Chiang, C.-K.; Figeys, D., Fine Tuning of Proteomic Technologies to Improve Biological Findings: Advancements in 2011–2013. *Anal. Chem.* **2014,** *86* (1), 176-195.
88. Kumar, C.; Mann, M., Bioinformatics analysis of mass spectrometry-based proteomics data sets. *FEBS Letters* **2009,** *583* (11), 1703-1712.
89. Larance, M.; Lamond, A. I., Multidimensional proteomics for cell biology. *Nat Rev Mol Cell Biol* **2015,** *16* (5), 269-280.
90. Almeida, A. M.; Bassols, A.; Bendixen, E.; Bhide, M.; Ceciliani, F.; Cristobal, S.; Eckersall, P. D.; Hollung, K.; Lisacek, F.; Mazzucchelli, G.; McLaughlin, M.; Miller, I.; Nally, J. E.; Plowman, J.; Renaut, J.; Rodrigues, P.; Roncada, P.; Staric, J.; Turk, R., Animal board invited review: advances in proteomics for animal and food sciences. *Animal* **2015,** *9* (1), 1-17.
91. Gašo-Sokač, D.; Kovač, S.; Josić, D., Use of Proteomic Methodology in Optimization of Processing and Quality Control of Food of Animal Origin. *Proteomics for Quality Control of Animal-Origin Food, Food Technol. Biotechnol.* **2011,** *49* (4), 397–412.

92. Chandramouli, K.; Qian, P.-Y., Proteomics: Challenges, Techniques and Possibilities to Overcome Biological Sample Complexity. *Human Genomics and Proteomics : HGP* **2009,** *2009*, 239204.
93. Linke, T.; Doraiswamy, S.; Harrison, E. H., Rat plasma proteomics: Effects of abundant protein depletion on proteomic analysis. *Journal of Chromatography B* **2007,** *849* (1–2), 273-281.
94. Zhou, J.-Y.; Petritis, B. O.; Petritis, K.; Norbeck, A. D.; Weitz, K. K.; Moore, R. J.; Camp, D. G.; Kulkarni, R. N.; Smith, R. D.; Qian, W.-J., Mouse-Specific Tandem IgY7-SuperMix Immunoaffinity Separations for Improved LC-MS/MS Coverage of the Plasma Proteome. *Journal of proteome research* **2009,** *8* (11), 5387-5395.
95. Rego, J. P. A.; Moura, A. A.; Nouwens, A. S.; McGowan, M. R.; Boe-Hansen, G. B., Seminal plasma protein profiles of ejaculates obtained by internal artificial vagina and electroejaculation in Brahman bulls. *Animal Reproduction Science* **2015,** *160*, 126-137.
96. Sarsaifi, K.; Vejayan, J.; Haron, A.; Yusoff, R.; Hani, H.; Rasoli, M.; Omar, M. A.; Othman, A. M., Protein profile and functionality of spermatozoa from two semen collection methods in Bali bulls. *Livest. Sci.* **2015,** *172*, 96-105.
97. Yang, Y. X.; Wang, J. Q.; Bu, D. P.; Li, S. S.; Yuan, T. J.; Zhou, L. Y.; Yang, J. H.; Sun, P., Comparative proteomics analysis of plasma proteins during the transition period in dairy cows with or without subclinical mastitis after calving. *Czech J. Anim. Sci.* **2012,** *57* (10), 481–489.
98. Dayon, L.; Kussmann, M., Proteomics of human plasma: A critical comparison of analytical workflows in terms of effort, throughput and outcome. *EuPA Open Proteomics* **2013,** *1*, 8-16.
99. Björhall, K.; Miliotis, T.; Davidsson, P., Comparison of different depletion strategies for improved resolution in proteomic analysis of human serum samples. *Proteomics* **2005,** *5* (1), 307-317.
100. Tu, C.; Rudnick, P. A.; Martinez, M. Y.; Cheek, K. L.; Stein, S. E.; Slebos, R. J. C.; Liebler, D. C., Depletion of Abundant Plasma Proteins and Limitations of Plasma Proteomics. *Journal of proteome research* **2010,** *9* (10), 4982-4991.
101. Smith, M. P. W.; Wood, S. L.; Zougman, A.; Ho, J. T. C.; Peng, J.; Jackson, D.; Cairns, D. A.; Lewington, A. J. P.; Selby, P. J.; Banks, R. E., A systematic analysis of the effects of increasing degrees of serum immunodepletion in terms of depth of coverage and other key aspects in top-down and bottom-up proteomic analyses. *Proteomics* **2011,** *11* (11), 2222-2235.
102. Liu, B.; Qiu, F.-h.; Voss, C.; Xu, Y.; Zhao, M.-z.; Wu, Y.-x.; Nie, J.; Wang, Z.-l., Evaluation of three high abundance protein depletion kits for umbilical cord serum proteomics. *Proteome Science* **2011,** *9*, 24-24.
103. Larimore, E. L.; Amundson, O. L.; Bridges, G. A.; McNeel, A. K.; Cushman, R. A.; Perry, G. A., Changes in ovarian function associated with circulating concentrations of estradiol before a GnRH-induced ovulation in beef cows. *Domestic Animal Endocrinology* **2016,** *57*, 71-79.
104. Rifkin, J. M.; Olson, G. E., Characterization of maturation-dependent extrinsic proteins of the rat sperm surface. *The Journal of cell biology* **1985,** *100* (5), 1582-1591.

105. Nauc, V.; Manjunath, P., Radioimmunoassays for Bull Seminal Plasma Proteins (BSP-A1/-A2, BSP-A3, and BSP-30-Kilodaltons), and Their Quantification in Seminal Plasma and Sperm. *Biology of Reproduction* **2000,** *63* (4), 1058-1066.
106. Duarte, R. T.; Carvalho Simões, M. C.; Sgarbieri, V. C., Bovine Blood Components: Fractionation, Composition, and Nutritive Value. *Journal of Agricultural and Food Chemistry* **1999,** *47* (1), 231-236.
107. Hanrieder, J.; Nyakas, A.; Naessén, T.; Bergquist, J., Proteomic Analysis of Human Follicular Fluid Using an Alternative Bottom-Up Approach. *Journal of Proteome Research* **2008,** *7* (1), 443-449.
108. Schweigert, F. J.; Gericke, B.; Wolfram, W.; Kaisers, U.; Dudenhausen, J. W., Peptide and protein profiles in serum and follicular fluid of women undergoing IVF. *Human Reproduction* **2006,** *21* (11), 2960-2968.
109. Andersen, M. M.; Kroøll, J.; Byskov, A. G.; Faber, M., Protein composition in the fluid of individual bovine follicles. *J. Reprod. Fert.* **1976,** *48*, 109-118.
110. Alberghina, D.; Giannetto, C.; Vazzana, I.; Ferrantelli, V.; Piccione, G., Reference Intervals for Total Protein Concentration, Serum Protein Fractions, and Albumin/Globulin Ratios in Clinically Healthy Dairy Cows. *Journal of Veterinary Diagnostic Investigation* **2011,** *23* (1), 111-114.
111. Kor, N. M.; Khanghah, K. M.; Veisi, A., Follicular Fluid Concentrations of Biochemical Metabolites and Trace Minerals in Relation to Ovarian Follicle Size in Dairy Cows. *Annual Review & Research in Biology* **2013,** *3* (4), 397-404.
112. Larson, B. L.; Salisbury, G. W., The Proteins of Bovine Seminal Plasma: I. Priliminary and Electrophoretic Studies. *J. Biol. Chem.* **1954,** *206*, 741-749.
113. Shalgi, R.; Kraicer, P.; Rimon, A.; Pinto, M.; Soferman, N., Proteins of Human Follicular Fluid: The Blood-Follicle Barrier. Presented at the Annual Conference of the Society for the Study of Fertility, Reading, England, July 18–22, 1972. *Fertility and Sterility* **1973,** *24* (6), 429-434.
114. Spitzer, D.; Murach, K. F.; Lottspeich, F.; Staudach, A.; Illmensee, K., Different protein patterns derived from follicular fluid of mature and immature human follicles. *Human Reproduction* **1996,** *11*, 798-807.
115. Drummond, A. E.; Findlay, J. K., The role of estrogen in folliculogenesis. *Molecular and Cellular Endocrinology* **1999,** *151* (1), 57-64.
116. Bentov, Y.; Jurisicova, A.; Kenigsberg, S.; Casper, R. F., What maintains the high intra-follicular estradiol concentration in pre-ovulatory follicles? *Journal of Assisted Reproduction and Genetics* **2016,** *33* (1), 85-94.
117. Emmen, J. M. A.; Couse, J. F.; Elmore, S. A.; Yates, M. M.; Kissling, G. E.; Korach, K. S., In Vitro Growth and Ovulation of Follicles from Ovaries of Estrogen Receptor (ER)α and ERβ Null Mice Indicate a Role for ERβ in Follicular Maturation. *Endocrinology* **2005,** *146* (6), 2817-2826.
118. Perry, G. A.; Swanson, O. L.; Larimore, E. L.; Perry, B. L.; Djira, G. D.; Cushman, R. A., Relationship of follicle size and concentrations of estradiol among cows exhibiting or not exhibiting estrus during a fixed-time AI protocol. *Domestic Animal Endocrinology* **2014,** *48*, 15-20.
119. Ogo, Y.; Taniuchi, S.; Ojima, F.; Hayashi, S.; Murakami, I.; Saito, Y.; Takeuchi, S.; Kudo, T.; Takahashi, S., IGF-1 Gene Expression Is Differentially Regulated by Estrogen Receptors α and β in Mouse Endometrial Stromal Cells and

Ovarian Granulosa Cells. *The Journal of Reproduction and Development* **2014,** *60* (3), 216-223.
120. Wang, X. N.; Greenwald, G. S., Synergistic effects of steroids with FSH on folliculogenesis, steroidogenesis and FSH- and hCG-receptors in hypophysectomized mice. *Journal of Reproduction and Fertility* **1993,** *99* (2), 403-413.
121. Perry, G. A.; Perry, B. L., Effect of preovulatory concentrations of estradiol and initiation of standing estrus on uterine pH in beef cows. *Domestic Animal Endocrinology* **2008,** *34* (3), 333-338.
122. Jinks, E. M.; Smith, M. F.; Atkins, J. A.; Pohler, K. G.; Perry, G. A.; MacNeil, M. D.; Roberts, A. J.; Waterman, R. C.; Alexander, L. J.; Geary, T. W., Preovulatory estradiol and the establishment and maintenance of pregnancy in suckled beef cows1. *Journal of Animal Science* **2013,** *91* (3), 1176-1185.
123. Mi, H.; Muruganujan, A.; Casagrande, J. T.; Thomas, P. D., Large-scale gene function analysis with the PANTHER classification system. *Nature Protocols* **2013,** *8*, 1551.
124. Huang, D. W.; Sherman, B. T.; Lempicki, R. A., Systematic and integrative analysis of large gene lists using DAVID bioinformatics resources. *Nat. Protocols* **2008,** *4* (1), 44-57.
125. Kanehisa, M.; Furumichi, M.; Tanabe, M.; Sato, Y.; Morishima, K., KEGG: new perspectives on genomes, pathways, diseases and drugs. *Nucleic Acids Research* **2017,** *45* (Database issue), D353-D361.
126. Szklarczyk, D.; Morris, J. H.; Cook, H.; Kuhn, M.; Wyder, S.; Simonovic, M.; Santos, A.; Doncheva, N. T.; Roth, A.; Bork, P.; Jensen, L. J.; von Mering, C., The STRING database in 2017: quality-controlled protein–protein association networks, made broadly accessible. *Nucleic Acids Research* **2017,** *45* (Database issue), D362-D368.
127. Sun, D.; Zhang, H.; Guo, D.; Sun, A.; Wang, H., Shotgun Proteomic Analysis of Plasma from Dairy Cattle Suffering from Footrot: Characterization of Potential Disease-Associated Factors. *PloS one* **2013,** *8* (2), e55973.
128. Fabregat, A.; Jupe, S.; Matthews, L.; Sidiropoulos, K.; Gillespie, M.; Garapati, P.; Haw, R.; Jassal, B.; Korninger, F.; May, B.; Milacic, M.; Roca, C. D.; Rothfels, K.; Sevilla, C.; Shamovsky, V.; Shorser, S.; Varusai, T.; Viteri, G.; Weiser, J.; Wu, G.; Stein, L.; Hermjakob, H.; D'Eustachio, P., The Reactome Pathway Knowledgebase. *Nucleic Acids Research* **2018,** *46* (D1), D649-D655.
129. Sarhan, D.; El Mazny, A.; Taha, T.; Aziz, A.; Azmy, O.; Fakhry, D.; Torky, H., Estradiol and luteinizing hormone concentrations in the follicular aspirate during ovum pickup as predictors of in vitro fertilization (IVF) outcome. *Middle East Fertility Society Journal* **2017,** *22* (1), 27-32.
130. Perry, G. A.; Smith, M. F.; Lucy, M. C.; Green, J. A.; Parks, T. E.; MacNeil, M. D.; Roberts, A. J.; Geary, T. W., Relationship between follicle size at insemination and pregnancy success. *Proceedings of the National Academy of Sciences of the United States of America* **2005,** *102* (14), 5268.
131. Siu, M. K. Y.; Cheng, C. Y., The Blood-Follicle Barrier (BFB) in Disease and in Ovarian Function. *Advances in experimental medicine and biology* **2012,** *763*, 186-192.
132. Hess, K. A.; Chen, L.; Larsen, W. J., The ovarian blood follicle barrier is both charge- and size-selective in mice. *Biol Reprod* **1998,** *58* (3), 705-11.

133. Hu, J.; Zhang, Z.; Shen, W.-J.; Azhar, S., Cellular cholesterol delivery, intracellular processing and utilization for biosynthesis of steroid hormones. *Nutrition & metabolism* **2010,** *7*, 47-47.
134. Eichner R, B. P., Sun TT., Classification of epidermal keratins according to their immunoreactivity, isoelectric point, and mode of expression. *J Cell Biol.* **1984,** *98* (4), 1388-96.
135. Sun, T. T.; Eichner, R.; Schermer, A.; Cooper, D.; Nelson, W. G.; Weiss, R. A., Classification, expression, and possible mechanisms of evolution of mammalian epithelial keratins: a unifying model. *Cancer Cells* **1984,** *1* (Transformed Phenotype), 169-76.
136. Elliott, M. R.; Zheng, S.; Park, D.; Woodson, R. I.; Reardon, M. A.; Juncadella, I. J.; Kinchen, J. M.; Zhang, J.; Lysiak, J. J.; Ravichandran, K. S., Unexpected requirement for ELMO1 in apoptotic germ cell clearance in vivo. *Nature* **2010,** *467* (7313), 333-337.
137. Lee, J.; Park, B.; Kim, G.; Kim, K.; Pak, J.; Kim, K.; Ye, M. B.; Park, S.-G.; Park, D., Arhgef16, a novel Elmo1 binding partner, promotes clearance of apoptotic cells via RhoG-dependent Rac1 activation. *Biochimica et Biophysica Acta (BBA) - Molecular Cell Research* **2014,** *1843* (11), 2438-2447.
138. D'haeseleer, M.; Cocquyt, G.; Cruchten, S. V.; Simoens, P.; Broeck, W. V. D., Cell-specific localisation of apoptosis in the bovine ovary at different stages of the oestrous cycle. *Theriogenology* **2006,** *65* (4), 757-772.
139. Palma, G. A.; Arga; #xf1; araz, M. E.; Barrera, A. D.; Rodler, D.; Mutto, A.; #xc1; ngel; Sinowatz, F., Biology and Biotechnology of Follicle Development. *The Scientific World Journal* **2012,** *2012*, 14.
140. Russell, D. L.; Robker, R. L., Molecular mechanisms of ovulation: co-ordination through the cumulus complex. *Hum. Reprod. Update* **2007,** *13* (3), 289-312.
141. Luisi, S.; Florio, P.; Reis, F. M.; Petraglia, F., Inhibins in female and male reproductive physiology: role in gametogenesis, conception, implantation and early pregnancy. *Hum Reprod Update* **2005,** *11* (2), 123-35.
142. Beg, M.; Meira, C.; Bergfelt, D.; Ginther, O., Role of oestradiol in growth of follicles and follicle deviation in heifers. *Reproduction* **2003,** *125* (6), 847-854.
143. Ginther, O. J.; Bergfelt, D. R.; Kulick, L. J.; Kot, K., Selection of the Dominant Follicle in Cattle: Role of Estradiol1. *Biology of Reproduction* **2000,** *63* (2), 383-389.
144. Aleman-Muench, G. R.; Soldevila, G., When versatility matters: activins/inhibins as key regulators of immunity. *Immunology & Cell Biology* **2012,** *90* (2), 137-148.
145. Roper, L. K.; Briguglio, J. S.; Evans, C. S.; Jackson, M. B.; Chapman, E. R., Sex-specific regulation of follicle-stimulating hormone secretion by synaptotagmin 9. *Nature Communications* **2015,** *6*, 8645.
146. Fukuda, M., Distinct Rab Binding Specificity of Rim1, Rim2, Rabphilin, and Noc2: IDENTIFICATION OF A CRITICAL DETERMINANT OF Rab3A/Rab27A RECOGNITION BY Rim2. *Journal of Biological Chemistry* **2003,** *278* (17), 15373-15380.
147. Südhof, Thomas C., Neurotransmitter Release: The Last Millisecond in the Life of a Synaptic Vesicle. *Neuron* **2013,** *80* (3), 675-690.
148. Mora, J. M.; Fenwick, M. A.; Castle, L.; Baithun, M.; Ryder, T. A.; Mobberley, M.; Carzaniga, R.; Franks, S.; Hardy, K., Characterization and Significance

of Adhesion and Junction-Related Proteins in Mouse Ovarian Follicles1. *Biology of Reproduction* **2012,** *86* (5), 153, 1-14-153, 1-14.
149. Woodruff, T. K.; Shea, L. D., The Role of the Extracellular Matrix in Ovarian Follicle Development. *Reproductive sciences (Thousand Oaks, Calif.)* **2007,** *14* (8 Suppl), 6-10.
150. Da Silva-Buttkus, P.; Jayasooriya, G. S.; Mora, J. M.; Mobberley, M.; Ryder, T. A.; Baithun, M.; Stark, J.; Franks, S.; Hardy, K., Effect of cell shape and packing density on granulosa cell proliferation and formation of multiple layers during early follicle development in the ovary. *Journal of Cell Science* **2008,** *121* (23), 3890.
151. Carnegie, J. A.; Byard, R.; Dardick, I.; Tsang, B. K., Culture of granulosa cells in collagen gels: the influence of cell shape on steroidogenesis. *Biol Reprod* **1988,** *38* (4), 881-90.
152. Asem, E. K.; Carnegie, J. A.; Tsang, B. K., Fibronectin production by chicken granulosa cells in vitro: effect of follicular development. *Acta Endocrinologica* **1992,** *127* (5), 466-470.
153. Luyckx, V.; Dolmans, M.-M.; Vanacker, J.; Scalercio, S. R.; Donnez, J.; Amorim, C. A., First step in developing a 3D biodegradable fibrin scaffold for an artificial ovary. *Journal of Ovarian Research* **2013,** *6*, 83-83.
154. Chiti, M. C.; Dolmans, M. M.; Orellana, R.; Soares, M.; Paulini, F.; Donnez, J.; Amorim, C. A., Influence of follicle stage on artificial ovary outcome using fibrin as a matrix. *Human Reproduction* **2016,** *31* (2), 427-435.
155. Huang, Z.; Wells, D., The human oocyte and cumulus cells relationship: new insights from the cumulus cell transcriptome. *MHR: Basic science of reproductive medicine* **2010,** *16* (10), 715-725.
156. Familiari, G.; Heyn, R.; Relucenti, M.; Nottola, S. A.; Sathananthan, A. H., Ultrastructural Dynamics of Human Reproduction, from Ovulation to Fertilization and Early Embryo Development. In *International Review of Cytology*, Academic Press: 2006; Vol. 249, pp 53-141.
157. Kastrop, P. M. M.; Bevers, M. M.; Destrée, O. H. J.; Kruip Th, A. M., Analysis of protein synthesis in morphologically classified bovine follicular oocytes before and after maturation in vitro. *Mol. Reprod. Dev.* **1990,** *26* (3), 222-226.
158. Crosby, I. M.; Osborn, J. C.; Moor, R. M., Follicle cell regulation of protein synthesis and developmental competence in sheep oocytes. *J. Reprod. Fert.* **1981,** *62*, 575-582.
159. Chand, A. L.; Legge, M., Amino acid transport system L activity in developing mouse ovarian follicles. *Hum Reprod* **2011,** *26* (11), 3102-8.
160. Yamada, M.; Gentry, P. A., Hemostatic profile of bovine ovarian follicular fluid. *Canadian Journal of Physiology and Pharmacology* **1995,** *73* (5), 624-629.
161. Ireland, J. L. H.; Jimenez-Krassel, F.; Winn, M. E.; Burns, D. S.; Ireland, J. J., Evidence for Autocrine or Paracrine Roles of α2-Macroglobulin in Regulation of Estradiol Production by Granulosa Cells and Development of Dominant Follicles. *Endocrinology* **2004,** *145* (6), 2784-2794.
162. Rehman, A. A.; Ahsan, H.; Khan, F. H., alpha-2-Macroglobulin: a physiological guardian. *J Cell Physiol* **2013,** *228* (8), 1665-75.
163. Westwood, M.; Aplin, J. D.; Collinge, I. A.; Gill, A.; White, A.; Gibson, J. M., α2-Macroglobulin: a New Component in the Insulin-like Growth Factor/Insulin-like

Growth Factor Binding Protein-1 Axis. *Journal of Biological Chemistry* **2001,** *276* (45), 41668-41674.
164. Boots, C. E.; Jungheim, E. S., Inflammation and Human Ovarian Follicular Dynamics. *Seminars in reproductive medicine* **2015,** *33* (4), 270-275.
165. Nguyen, P. V.; Kafka, J. K.; Ferreira, V. H.; Roth, K.; Kaushic, C., Innate and adaptive immune responses in male and female reproductive tracts in homeostasis and following HIV infection. *Cellular and Molecular Immunology* **2014,** *11* (5), 410-427.
166. Foulcer, S. J.; Day, A. J.; Apte, S. S., Isolation and Purification of Versican and Analysis of Versican Proteolysis. *Methods in molecular biology (Clifton, N.J.)* **2015,** *1229*, 587-604.
167. Olin, A. I.; Mörgelin, M.; Sasaki, T.; Timpl, R.; Heinegård, D.; Aspberg, A., The Proteoglycans Aggrecan and Versican Form Networks with Fibulin-2 through Their Lectin Domain Binding. *Journal of Biological Chemistry* **2001,** *276* (2), 1253-1261.
168. Bae, D.-H.; Lane, D. J. R.; Jansson, P. J.; Richardson, D. R., The old and new biochemistry of polyamines. *Biochimica et Biophysica Acta (BBA) - General Subjects* **2018,** *1862* (9), 2053-2068.
169. Bastida, C. M.; Cremades, A. n.; Castells, M. T.; López-Contreras, A. s. J.; López-García, C.; Tejada, F.; Peñafiel, R., Influence of Ovarian Ornithine Decarboxylase in Folliculogenesis and Luteinization. *Endocrinology* **2005,** *146* (2), 666-674.
170. Jassil, N. K.; Sharma, A.; Bikle, D.; Wang, X., Vitamin D Binding Protein and 25-Hydroxyvitamin D Levels: Emerging Clinical Applications. *Endocr Pract* **2017,** *23* (5), 605-613.
171. Yousefzadeh, P.; Shapses, S. A.; Wang, X., Vitamin D Binding Protein Impact on 25-Hydroxyvitamin D Levels under Different Physiologic and Pathologic Conditions. *International journal of endocrinology* **2014,** *2014*, 6.
172. Farzadi, L.; Khayatzadeh Bidgoli, H.; Ghojazadeh, M.; Bahrami, Z.; Fattahi, A.; Latifi, Z.; Shahnazi, V.; Nouri, M., Correlation between follicular fluid 25-OH vitamin D and assisted reproductive outcomes. *Iranian Journal of Reproductive Medicine* **2015,** *13* (6), 361-366.
173. Lerchbaum, E.; Obermayer-Pietsch, B., MECHANISMS IN ENDOCRINOLOGY: Vitamin D and fertility: a systematic review. *European Journal of Endocrinology* **2012,** *166* (5), 765-778.
174. Lorenzen, M.; Boisen, I. M.; Mortensen, L. J.; Lanske, B.; Juul, A.; Blomberg Jensen, M., Reproductive endocrinology of vitamin D. *Molecular and Cellular Endocrinology* **2017,** *453*, 103-112.
175. Larsen, M. T.; Kuhlmann, M.; Hvam, M. L.; Howard, K. A., Albumin-based drug delivery: harnessing nature to cure disease. *Molecular and Cellular Therapies* **2016,** *4*, 3.
176. Michelis, R.; Sela, S.; Zeitun, T.; Geron, R.; Kristal, B., Unexpected Normal Colloid Osmotic Pressure in Clinical States with Low Serum Albumin. *PloS one* **2016,** *11* (7), e0159839.
177. Lopez, M. F.; Krastins, B.; Sarracino, D. A.; Byram, G.; Vogelsang, M. S.; Prakash, A.; Peterman, S.; Ahmad, S.; Vadali, G.; Deng, W.; Inglessis, I.; Wickham, T.; Feeney, K.; Dec, G. W.; Palacios, I.; Buonanno, F. S.; Lo, E. H.; Ning, M., Proteomic signatures of serum albumin-bound proteins from stroke patients with and

without endovascular closure of PFO are significantly different and suggest a novel mechanism for cholesterol efflux. *Clinical Proteomics* **2015,** *12* (2), 1-10.
178. Shen, X.; Liu, X.; Zhu, P.; Zhang, Y.; Wang, J.; Wang, Y.; Wang, W.; Liu, J.; Li, N.; Liu, F., Proteomic analysis of human follicular fluid associated with successful in vitro fertilization. *Reprod. Biol. Endocrinol.* **2017,** *15* (1), 58.
179. Kenawy, H. I.; Boral, I.; Bevington, A., Complement-Coagulation Cross-Talk: A Potential Mediator of the Physiological Activation of Complement by Low pH. *Frontiers in Immunology* **2015,** *6*, 215.
180. Gettins, P. G. W.; Olson, S. T., Inhibitory Serpins. New Insights into their Folding, Polymerization, Regulation and Clearance. *The Biochemical journal* **2016,** *473* (15), 2273-2293.
181. Law, R. H. P.; Zhang, Q.; McGowan, S.; Buckle, A. M.; Silverman, G. A.; Wong, W.; Rosado, C. J.; Langendorf, C. G.; Pike, R. N.; Bird, P. I.; Whisstock, J. C., An overview of the serpin superfamily. *Genome Biology* **2006,** *7* (5), 216-216.
182. Ellis, V.; Scully, M.; MacGregor, I.; Kakkar, V., Inhibition of human factor Xa by various plasma protease inhibitors. *Biochim Biophys Acta* **1982,** *701* (1), 24-31.
183. Gans, H.; Tan, B. H., α1-antitrypsin, an inhibitor for thrombin and plasmin. *Clinica Chimica Acta* **1967,** *17* (1), 111-117.
184. Janciauskiene, S.; Welte, T., Well-Known and Less Well-Known Functions of Alpha-1 Antitrypsin. Its Role in Chronic Obstructive Pulmonary Disease and Other Disease Developments. *Ann Am Thorac Soc* **2016,** *13 Suppl 4*, S280-8.
185. Dahlbäck, B.; Villoutreix, B. O., The anticoagulant protein C pathway. *FEBS Letters* **2005,** *579* (15), 3310-3316.
186. Rezaie, A. R., Regulation of the Protein C Anticoagulant and Antiinflammatory Pathways. *Current medicinal chemistry* **2010,** *17* (19), 2059-2069.
187. Danckwardt, S.; Hentze, M. W.; Kulozik, A. E., Pathologies at the nexus of blood coagulation and inflammation: thrombin in hemostasis, cancer, and beyond. *Journal of Molecular Medicine (Berlin, Germany)* **2013,** *91* (11), 1257-1271.
188. Noris, M.; Remuzzi, G., Overview of Complement Activation and Regulation. *Seminars in Nephrology* **2013,** *33* (6), 479-492.
189. Moreau, M. E.; Garbacki, N.; Molinaro, G.; Brown, N. J.; Marceau, F.; ccedil; ois; Adam, A., The Kallikrein-Kinin System: Current and Future Pharmacological Targets. *Journal of Pharmacological Sciences* **2005,** *99* (1), 6-38.
190. Daugherty A; SC., W., book-chapter-quantification-of-atherosclerosis-in-mice.pdf. *Methods Mol Biol.* **2003,** *209*, 293-309.
191. Pendse, A. A.; Arbones-Mainar, J. M.; Johnson, L. A.; Altenburg, M. K.; Maeda, N., Apolipoprotein E knock-out and knock-in mice: atherosclerosis, metabolic syndrome, and beyond. *Journal of Lipid Research* **2009,** *50* (Supplement), S178-S182.
192. Ma, Y.; Wang, W.; Zhang, J.; Lu, Y.; Wu, W.; Yan, H.; Wang, Y., Hyperlipidemia and atherosclerotic lesion development in Ldlr-deficient mice on a long-term high-fat diet. *PloS one* **2012,** *7* (4), e35835.
193. Cheng, C.; Tempel, D.; van Haperen, R.; van der Baan, A.; Grosveld, F.; Daemen, M. J. A. P.; Krams, R.; de Crom, R., Atherosclerotic Lesion Size and Vulnerability Are Determined by Patterns of Fluid Shear Stress. *Circulation* **2006,** *113* (23), 2744-2753.

194. Ku, D. N.; Giddens, D. P.; Zarins, C. K.; Glagov, S., Pulsatile flow and atherosclerosis in the human carotid bifurcation. Positive correlation between plaque location and low oscillating shear stress. *Arteriosclerosis, Thrombosis, and Vascular Biology* **1985,** *5* (3), 293-302.
195. Davies, P. F., Hemodynamic shear stress and the endothelium in cardiovascular pathophysiology. *Nature clinical practice. Cardiovascular medicine* **2009,** *6* (1), 16-26.
196. Bäck, M.; Gasser, T. C.; Michel, J.-B.; Caligiuri, G., Biomechanical factors in the biology of aortic wall and aortic valve diseases. *Cardiovascular Research* **2013,** *99* (2), 232-241.
197. Wang, J. C.; Bennett, M., Aging and Atherosclerosis: Mechanisms, Functional Consequences, and Potential Therapeutics for Cellular Senescence. *Circulation research* **2012,** *111* (2), 245-259.
198. Smith, D. D.; Tan, X.; Tawfik, O.; Milne, G.; Stechschulte, D. J.; Dileepan, K. N., Increased Aortic Atherosclerotic Plaque Development in Female Apolipoprotein E-Null Mice is Associated with Elevated Thromboxane A(2) and Decreased Prostacyclin Production *Journal of physiology and pharmacology : an official journal of the Polish Physiological Society* **2010,** *61* (3), 309-316.
199. Perez-Lopez, F. R.; Larrad-Mur, L.; Kallen, A.; Chedraui, P.; Taylor, H. S., Gender differences in cardiovascular disease: hormonal and biochemical influences. *Reproductive sciences* **2010,** *17* (6), 511-31.
200. Rapundalo, S. T., Cardiac protein phosphorylation: functional and pathophysiological correlates. *Cardiovasc. Res.* **1998,** *38* (3), 559-588.
201. Ardito, F.; Giuliani, M.; Perrone, D.; Troiano, G.; Lo Muzio, L., The crucial role of protein phosphorylation in cell signaling and its use as targeted therapy (Review). *International journal of molecular medicine* **2017,** *40* (2), 271-280.
202. Vidyasagar, A.; Wilson, N. A.; Djamali, A., Heat shock protein 27 (HSP27): biomarker of disease and therapeutic target. *Fibrogenesis & tissue repair* **2012,** *5* (1), 1-7.
203. Park, H. K.; Park, E. C.; Bae, S. W.; Park, M. Y.; Kim, S. W.; Yoo, H. S.; Tudev, M.; Ko, Y. H.; Choi, Y. H.; Kim, S.; Kim, D. I.; Kim, Y. W.; Lee, B. B.; Yoon, J. B.; Park, J. E., Expression of heat shock protein 27 in human atherosclerotic plaques and increased plasma level of heat shock protein 27 in patients with acute coronary syndrome. *Circulation* **2006,** *114* (9), 886-93.
204. Fíla, J.; Honys, D., Enrichment techniques employed in phosphoproteomics. *Amino Acids* **2012,** *43* (3), 1025-1047.
205. Dunn, J. D.; Reid, G. E.; Bruening, M. L., Techniques for phosphopeptide enrichment prior to analysis by mass spectrometry. *Mass Spectrometry Reviews* **2010,** *29* (1), 29-54.
206. van Tilburg, M. F.; Rodrigues, M. A. M.; Moreira, R. A.; Moreno, F. B.; Monteiro-Moreira, A. C. O.; Cândido, M. J. D.; Moura, A. A., Membrane-associated proteins of ejaculated sperm from Morada Nova rams. *Theriogenology* **2013,** *79* (9), 1247-1261.

APPENDICES

Appendix 1. Details on 231 proteins identified in bovine PL and FF with high and low E2 during the pre-ovulatory stage.

Description (* indicates protein was up- or down-regulated in at least one sample)	Accession	Coverage	# Peptides	# unique peptides	Score
*2-acylglycerol O-acyltransferase 3 (Fragment)	E1BN30	2.62	1	1	20.86
Acidic mammalian chitinase	Q95M17	3.18	1	1	34.89
Actin, cytoplasmic 1	F1MRD0	4.80	1	1	33.01
Afamin	G3MYZ3	3.15	2	2	81.25
A-kinase anchoring protein 9 (Fragment)	F1MXF5	0.86	2	1	428.46
Aldehyde oxidase 4	E1BL62	1.57	1	1	105.29
Alpha-1-acid glycoprotein	Q3SZR3	52.48	12	12	1535.16
*Alpha-1-antiproteinase	P34955	15.14	5	5	529.12
Alpha-1B-glycoprotein	Q2KJF1	38.37	10	9	1035.57
Alpha-2-antiplasmin	P28800	16.06	4	3	259.00
Alpha-2-HS-glycoprotein	P12763	25.35	6	6	1390.94
*Alpha-2-macroglobulin	Q7SIH1	45.43	48	47	7776.09
Alpha-amylase	F1MJQ3	4.50	2	2	15.59
Angiotensinogen	Q3SZH5	11.79	3	2	91.25
*Ankyrin repeat and KH domain containing 1	G3MZJ0	0.67	1	1	118.87
Antithrombin-III	F1MSZ6	43.44	14	13	1121.12
*AP complex subunit beta	F6PZ41	3.11	1	1	56.29
AP-2 complex subunit beta	G3X7G4	2.84	1	1	779.71
Apolipoprotein A-I	P15497	63.77	26	26	4696.98
Apolipoprotein A-II	P81644	27.00	4	4	339.84
Apolipoprotein A-IV	F1N3Q7	46.58	16	15	655.00
*Apolipoprotein B	E1BNR0	0.68	2	2	140.79
Apolipoprotein C-III	P19035	16.67	1	1	24.41
*Apolipoprotein R	G3N0S9	8.54	1	1	19.91
*ApoN protein	Q2KIH2	16.54	4	4	110.40
*Asparagine-linked glycosylation 5, dolichyl-phosphate beta-glucosyltransferase homolog (S. cerevisiae)	Q2KIM7	10.49	2	2	28.98
*ATP binding cassette subfamily B member 9	E1BKR0	0.96	1	1	61.08

*B double prime 1, subunit of RNA polymerase III transcription initiation factor IIIB	F1MEB1	0.68	1	1	129.29
BCL2 interacting protein 2	F1N6R4	4.46	1	1	53.24
Beta-2-glycoprotein 1	P17690	13.91	4	4	205.18
Beta-2-microglobulin	P01888	10.17	1	1	15.16
C3 and PZP like, alpha-2-macroglobulin domain containing 8	E1BAA2	0.61	1	1	200.14
C4b-binding protein alpha chain	Q28065	4.59	2	2	50.60
*C8G protein	A8YXZ2	8.86	1	1	10.66
*CAD protein	F1MVC0	0.90	1	1	119.60
Caspase recruitment domain family member 10	F1MW90	1.36	1	1	72.61
*CCDC80 protein	A5PKA3	2.41	1	1	80.34
*Cell adhesion molecule 1	Q2TBL2	4.56	1	1	599.16
Ceruloplasmin	F1N076	29.40	22	22	1539.90
Chaperone activity of bc1 complex-like, mitochondrial	Q29RI0	2.01	1	1	84.33
*Chromosome 14 open reading frame 166 ortholog	Q3T0S7	5.31	1	1	175.46
Chromosome 20 open reading frame 96 (Fragment)	F1N466	5.59	1	1	276.11
Clusterin	P17697	5.24	2	2	116.19
CMP-N-acetylneuraminate-poly-alpha-2,8-sialyltransferase	F1MVI9	2.23	1	1	71.46
Coagulation factor IX	F1MBC5	2.78	1	1	36.96
*Coagulation factor V	F1N0I3	1.83	2	2	37.79
*Coagulation factor XII	F1MTT3	2.78	1	1	14.55
*Coagulation factor XIII A chain	F1MW44	3.96	2	1	89.51
*Cohesin subunit SA-3	E1B9B0	3.43	2	1	363.69
*Complement C1s subcomponent	Q0VCX1	6.39	2	1	27.90
Complement C3	Q2UVX4	50.09	65	1	11912.41
Complement C3	G3X7A5	49.91	65	1	11675.41
complement C3 (Fragment)	E1B805	3.82	4	4	165.08
Complement C5a anaphylatoxin	F1MY85	11.87	15	13	633.38
Complement C8 alpha chain	F1MX87	11.04	4	3	92.83
Complement C8 beta chain	F1N102	12.37	4	3	123.27
complement component 4A	E1BH06	26.88	32	16	1940.14
*Complement component C6	F1MM86	12.88	7	7	256.29
Complement component C7	Q29RQ1	4.15	3	3	50.20
Complement component C9	Q3MHN2	25.36	11	9	700.87
Complement factor B	P81187	32.06	17	17	2031.94
Complement factor H	Q28085	11.73	10	9	766.87

Complement factor I	F1N4M7	12.30	6	6	300.36
*Conglutinin	P23805	11.59	4	4	99.90
Corticosteroid-binding globulin	E1BF81	13.37	3	2	86.85
C-reactive protein	C4T8B4	4.46	1	1	62.37
C-type lectin domain family 1 member A	Q0VCS6	3.96	1	1	85.12
*Cumulus cell-specific fibronectin 1 transcript variant	B8Y9T0	2.73	4	4	139.98
*Cytochrome P450 20A1	Q5E980	2.81	1	1	47.83
*Cytohesin 1 (Fragment)	F1MCV3	3.49	1	1	79.67
*Cytokine receptor like factor 3	E1BCF2	3.19	1	1	33.06
*DDB1 and CUL4 associated factor 5	F1N0J7	1.83	1	1	125.40
DEAH-box helicase 16	E1BF68	2.30	1	1	99.02
*Delta-like protein	E1BDN7	1.40	1	1	71.56
*Dolichyl-diphosphooligosaccharide--protein glycosyltransferase subunit 1	F1MJ36	2.80	1	1	380.50
*Dpy-19 like 4 (Fragment)	F1MJJ1	2.77	1	1	74.83
*DUOXA1 protein	A6H723	4.45	1	1	81.06
*Dynein axonemal heavy chain 11	F1N724	0.22	1	1	198.47
*Dynein heavy chain domain 1	F1MEF7	0.78	1	1	68.05
Dystonin	F1MPT5	0.15	1	1	569.35
*E3 ubiquitin-protein ligase CHIP	F1MUH4	7.95	1	1	21.38
*Endophilin-A2	Q2KJA1	7.07	1	1	78.25
*Engulfment and cell motility 1	F1MQH0	3.30	1	1	115.02
*Epidermal growth factor receptor kinase substrate 8-like protein 1	E1BKS0	2.00	1	1	31.95
*Factor XIIa inhibitor precursor	E1BMJ0	18.80	7	6	341.85
*Family with sequence similarity 81 member A	F1N4N5	4.38	1	1	32.29
*Fas activated serine/threonine kinase	F1N4L0	7.14	1	1	45.88
Fetuin-B	Q58D62	6.20	3	3	90.71
*FGG protein	Q3SZZ9	48.05	16	15	2805.06
*Fibrinogen alpha chain	A5PJE3	38.70	22	22	4967.64
*Fibrinogen beta chain	F1MAV0	58.79	31	30	3584.70
*Fibulin-1	F1MYN5	3.26	1	1	100.67
*Filamin B	E1BKX7	0.91	1	1	188.29
Fragile X mental retardation syndrome-related protein 2	E1B9L5	4.02	1	1	121.87
G1/S-specific cyclin-D1	Q2KI22	5.42	1	1	157.65
*Gametocyte-specific factor 1-like	Q3T026	12.43	1	1	49.67
*Gasdermin B	F1MCQ4	1.99	1	1	9.35
Gelsolin	F1MJH1	12.18	6	5	252.10

Glutathione peroxidase	G3X8D7	7.59	1	1	13.51
Glutathione S-transferase	E1BKD8	10.00	1	1	25.42
*Haptoglobin	G3X6K8	12.47	4	4	123.61
HAUS augmin like complex subunit 3	F1MNN1	1.16	1	1	34.23
*HEAT repeat containing 5B	E1BB26	1.45	1	1	345.14
*HECT domain E3 ubiquitin protein ligase 2	F1N7A0	3.48	1	1	47.44
*HECT, UBA and WWE domain containing 1, E3 ubiquitin protein ligase	E1BNY9	0.16	1	1	114.05
*Hemoglobin subunit alpha	P01966	50.00	5	5	461.90
*Hemoglobin subunit beta	P02070	70.34	10	10	1298.93
Hemopexin	Q3SZV7	48.15	16	16	2252.77
Hepatocyte growth factor activator preproprotein (Fragment)	E1BCW0	10.77	2	2	46.89
Histidine-rich glycoprotein	F1MKS5	18.28	9	5	530.26
Histidine-rich glycoprotein (Fragments)	P33433	14.65	5	1	282.49
*Homeobox D3	E1B856	4.38	1	1	297.84
*Immunoglobulin lambda-like polypeptide 1	F1MLW7	22.65	4	2	313.19
*Immunoglobulin lambda-like polypeptide 1 (Fragment)	G3N2D7	12.93	1	1	28.07
Importin 8	E1B8Q9	0.87	1	1	48.73
*Inhibin alpha chain	P07994	10.28	2	1	44.05
Insulin like growth factor binding protein acid labile subunit(IGFALS) (Fragment)	F1MJZ4	9.18	3	3	115.59
Inter-alpha-trypsin inhibitor heavy chain H1	F1MMP5	22.30	16	15	1046.27
Inter-alpha-trypsin inhibitor heavy chain H2	F1MNW4	18.50	11	10	531.07
Inter-alpha-trypsin inhibitor heavy chain H3	P56652	1.12	1	1	99.98
Inter-alpha-trypsin inhibitor heavy chain H4	F1MMD7	28.28	21	20	1460.66
*Keratin, type II cytoskeletal 7	Q29S21	4.94	2	2	178.36
Kinesin family member 13B	E1BGB0	0.59	1	1	50.27
Kininogen-1	P01044	13.85	7	4	339.99
Kininogen-2	P01045	9.69	5	2	314.99
*KRAS proto-oncogene, GTPase	E1BMX0	6.38	1	1	115.89
*Kruppel like factor 17 (Fragment)	G3N1K6	5.88	1	1	124.69
Leucine rich repeat containing 4C	F1MXH5	3.44	1	1	111.10
*Leucine rich repeat kinase 2	E1BPU0	0.36	1	1	147.56
Leucine-rich alpha-2-glycoprotein 1	Q2KIF2	23.41	6	5	697.42

Leucine-rich single-pass membrane protein 1	A5PK14	9.38	1	1	137.68
L-lactate dehydrogenase B chain	Q5E9B1	5.09	1	1	7.76
*Lumican	Q05443	9.36	2	1	104.51
*Lysine methyltransferase 2C (Fragment)	F1MYZ3	0.19	1	1	57.82
Maltase-glucoamylase	G3MY87	1.31	2	2	46.70
Mitogen-activated protein kinase kinase kinase 5	F1MXH6	0.73	1	1	55.14
*NADH dehydrogenase [ubiquinone] 1 alpha subcomplex assembly factor 4	A4FUH5	9.71	1	1	61.89
*NADH dehydrogenase [ubiquinone] 1 beta subcomplex subunit 11, mitochondrial	Q8HXG5	14.94	1	1	21.41
NADPH-dependent diflavin oxidoreductase 1	Q1JPJ0	3.02	1	1	49.02
*NIMA (Never in mitosis gene a)-related kinase 2	Q2KIQ0	5.22	1	1	17.48
Nuclear factor interleukin-3-regulated protein	Q08D88	2.81	1	1	87.28
Olfactory receptor	E1BDG1	4.13	1	1	2.87
*Ornithine decarboxylase 1	E1BG69	2.49	1	1	68.78
Pantetheinase	Q58CQ9	6.47	2	2	52.55
*Pantothenate kinase 3	Q08DA5	2.43	1	1	71.93
Paraoxonase 1	Q2KIW1	17.18	4	4	109.17
Peptidoglycan recognition protein 2 (Fragment)	E1BH94	5.76	3	3	68.02
Phosphatidylinositol-3,4,5-trisphosphate dependent Rac exchange factor 2	E1BDL7	1.18	1	1	74.79
*Phosphoglycolate phosphatase	Q2T9S4	6.54	1	1	232.07
Pigment epithelium-derived factor	Q95121	31.01	8	7	399.24
*Plasma serine protease inhibitor	Q9N2I2	9.16	2	2	82.95
Plasminogen	P06868	22.29	15	14	1272.51
Primary amine oxidase, liver isozyme	Q29437	25.07	12	11	1069.72
Progesterone immunomodulatory binding factor 1	E1BCF0	0.92	1	1	51.54
Protein AMBP	F1MMK9	17.05	4	4	255.61
Protein HP-20	Q2KIT0	28.80	3	3	762.34
Protein HP-25 homolog 1	Q2KIX7	22.17	3	3	177.58
Protein HP-25 homolog 2	Q2KIU3	40.00	5	5	1012.44
Protein phosphatase 1 regulatory subunit 37	A7Z026	1.72	1	1	38.25
Prothrombin	P00735	40.48	18	17	779.65
*Protocadherin Fat 2 precursor (Fragment)	F1MPF3	0.41	1	1	59.65

PSMD1 protein	A7MBA2	1.05	1	1	149.30
*PTPRR protein	A5PKF8	3.36	1	1	21.91
Pyridine nucleotide-disulfide oxidoreductase domain-containing protein 1	A7YVH9	5.78	1	1	104.19
*Regulating synaptic membrane exocytosis 2 (Fragment)	E1B7V2	1.56	1	1	62.25
Regulating synaptic membrane exocytosis 3	E1BAB7	3.90	1	1	63.55
RELT, TNF receptor	F1N3F7	3.20	1	1	125.55
Retinoic acid induced 1	E1B9X1	1.01	1	1	52.94
Retinol-binding protein 4	P18902	17.49	3	3	158.77
Ribosomal protein S6 kinase C1	E1BB43	1.70	1	1	122.46
*Serglycin (Fragment)	G5E5K5	5.33	1	1	28.09
Serine peptidase inhibitor, Kazal type 5	F1MJH0	1.10	1	1	141.20
Serotransferrin	Q29443	67.90	48	3	10359.71
Serotransferrin	G3X6N3	69.03	49	2	10020.55
Serpin A3-2	A2I7M9	30.66	11	4	2476.77
Serpin A3-4	A2I7N0	27.01	9	2	1486.42
Serpin A3-7	A2I7N3	14.39	9	9	1090.11
Serpin A3-8	A6QPQ2	21.77	8	6	516.68
*Serpin family E member 2	F1MZX2	6.55	2	2	42.36
*Serpin peptidase inhibitor, clade A (alpha-1 antiproteinase, antitrypsin), member 3	G8JKW7	25.24	8	2	1430.95
Serpin peptidase inhibitor, clade A (Alpha-1 antiproteinase, antitrypsin), member 7	Q3SYR0	13.14	4	4	130.93
SERPINA10 protein	A5PJ69	7.96	3	3	81.88
SERPIND1 protein	A6QPP2	19.15	7	6	323.80
*Serum albumin	P02769	35.91	18	18	1669.86
*SH3 domain and tetratricopeptide repeats 1	G3MZW4	0.83	1	1	80.24
SHBG protein	A5PKC2	8.73	2	1	33.21
*Sodium/glucose cotransporter 1-like (Fragment)	G3MXJ0	2.43	1	1	32.29
Solute carrier family 12 member 7 (Fragment)	F1N140	1.65	1	1	25.10
*Sphingomyelin phosphodiesterase 5 (Fragment)	F1N6X9	3.30	1	1	19.12
*SPHK1 interactor, AKAP domain containing (Fragment)	F1MZL5	0.68	1	1	25.46
Superoxide dismutase [Cu-Zn]	A3KLR9	16.60	3	3	25.75
*Suppressor of G2 allele of SKP1	Q2KIK0	5.62	1	1	66.16
*Synaptonemal complex protein 1	E1BLN1	1.90	1	1	41.64

*Synaptotagmin 12	E1BEH9	2.85	1	1	103.23
*TBC1 domain family member 4	E1BPA1	2.00	1	1	172.77
Tetranectin	Q2KIS7	18.32	3	3	156.53
*Titin	F1N757	0.13	2	2	1674.93
*Trans-2-enoyl-CoA reductase, mitochondrial	Q7YS70	6.17	1	1	75.63
Transcription elongation factor A N-terminal and central domain-containing protein 2	A5PKE4	3.85	1	1	20.37
*Transcription factor 7-like 2	G3N0T7	6.53	1	1	116.94
*Transcription initiation factor TFIID subunit (Fragment)	F1MF62	0.48	1	1	268.01
*Transmembrane protein 186	Q5EA03	7.55	1	1	289.96
*Transthyretin	O46375	41.50	5	4	295.47
Tubulin beta-6 chain (Fragment)	G3X7R8	5.08	1	1	76.34
Tyrosine-protein kinase	F1MCX4	0.93	1	1	45.94
Ubiquitin carboxyl-terminal hydrolase 2	Q2KHV7	2.15	1	1	158.76
*Ubiquitin protein ligase E3 component n-recognin 4	G3N0A8	0.40	1	1	118.70
*Uncharacterized protein	E1BPG1	2.67	1	1	47.01
*Uncharacterized protein	F1MI18	13.33	16	15	404.88
Uncharacterized protein	E1BH27	1.44	1	1	144.13
Uncharacterized protein (Fragment)	F1MVK1	15.95	20	5	1479.93
*Uncharacterized protein (Fragment)	G3X6V5	1.12	1	1	242.91
Uncharacterized protein (Fragment)	G3N2S5	2.56	1	1	112.08
Uncharacterized protein (Fragment)	G3N1I8	13.01	1	1	11.29
Uncharacterized protein (Fragment); (Ig-like protein)	G5E513	3.06	1	1	40.37
Uncharacterized protein (Ig-like protein)	F1MH40	6.67	1	1	127.21
Uncharacterized protein (Ig-like protein)	F1MLW8	14.16	3	1	123.85
Utrophin	F1MRT9	0.29	1	1	192.91
*Vacuolar protein sorting-associated protein 28 homolog	E1BIB3	8.60	1	1	90.26
*Versican core protein	F1N6I7	5.95	2	2	91.74
*Vitamin D-binding protein	Q3MHN5	30.17	11	1	1602.50
*Vitamin D-binding protein	F1N5M2	32.07	11	1	1628.97
Vitronectin	Q3ZBS7	7.77	3	3	333.47
Von Willebrand factor A domain containing 3B	E1BB22	0.82	1	1	75.31
*Von Willebrand factor A domain containing 5B1	E1BB39	2.12	1	1	86.25
Xin actin binding repeat containing 2	E1BL04	0.34	1	1	326.21

Zinc-alpha-2-glycoprotein	Q3ZCH5	24.41	5	3	109.60
Zinc finger CCHC domain-containing protein 7	Q2KIN0	1.65	1	1	260.09
*Zinc finger protein 618	E1BJV7	2.71	1	1	73.67
*Zinc finger SWIM-type containing 3 (Fragment)	F1MTI1	2.03	1	1	108.62
*Zona pellucida binding protein 2	Q0VCG8	12.50	1	1	81.07

Appendix 2. Functions and cellular localization of 231 proteins identified in bovine PL and FF with high and low E2 during the pre-ovulatory stage.

Description (* indicates protein was up- or down-regulated in at least one sample)	**Biological Process**	**Molecular Function**	**Cellular Component**
*2-acylglycerol O-acyltransferase 3 (Fragment)	metabolic process	catalytic activity	
Acidic mammalian chitinase	metabolic process	catalytic activity	
Actin, cytoplasmic 1	cellular component organization or biogenesis; cellular process; localization	structural molecule activity	cell part; organelle
Afamin	localization		
A-kinase anchoring protein 9 (Fragment)			
Aldehyde oxidase 4	cellular process; metabolic process	binding; catalytic activity	cell part
Alpha-1-acid glycoprotein			
*Alpha-1-antiproteinase			extracellular region
Alpha-1B-glycoprotein	cellular process; response to stimulus	receptor activity	
Alpha-2-antiplasmin			extracellular region
Alpha-2-HS-glycoprotein	biological regulation	catalytic activity	
*Alpha-2-macroglobulin	cellular process; metabolic process; response to stimulus	binding; catalytic activity	
Alpha-amylase			
Angiotensinogen			extracellular region
*Ankyrin repeat and KH domain containing 1	immune system process; response to stimulus		cell part
Antithrombin-III			extracellular region
*AP complex subunit beta	localization		

AP-2 complex subunit beta	localization		
Apolipoprotein A-I	biological regulation; cellular component organization or biogenesis; cellular process; developmental process; localization; metabolic process; multicellular organismal process; response to stimulus	binding; catalytic activity; transporter activity	extracellular region; macromolecular complex
Apolipoprotein A-II	biological regulation; cellular component organization or biogenesis; metabolic process; multicellular organismal process	binding; catalytic activity; transporter activity	extracellular region; macromolecular complex
Apolipoprotein A-IV	biological regulation; cellular component organization or biogenesis; cellular process; developmental process; localization; metabolic process; multicellular organismal process; response to stimulus	binding; catalytic activity; transporter activity	extracellular region; macromolecular complex
*Apolipoprotein B			
Apolipoprotein C-III			
*Apolipoprotein R	biological adhesion; cellular process; immune system process		
*ApoN protein			
*Asparagine-linked glycosylation 5, dolichyl-phosphate beta-glucosyltransferase homolog (S. cerevisiae)	cellular process; metabolic process		
*ATP binding cassette subfamily B member 9	cellular process; metabolic process	catalytic activity; transporter activity	membrane
*B double prime 1, subunit of RNA polymerase III transcription initiation factor IIIB	cellular component organization or biogenesis; cellular process; metabolic process	binding	cell part; macromolecular complex; organelle
BCL2 interacting protein 2	cellular process; developmental process; metabolic process	catalytic activity	cell part
Beta-2-glycoprotein 1	biological adhesion; cellular process; immune system process		

Beta-2-microglobulin	response to stimulus		macromolecular complex
C3 and PZP like, alpha-2-macroglobulin domain containing 8	cellular process; metabolic process; response to stimulus	binding; catalytic activity	
C4b-binding protein alpha chain	biological adhesion; cellular process; immune system process		
*C8G protein			
*CAD protein	cellular process; metabolic process	catalytic activity	cell part
Caspase recruitment domain family member 10	cellular process		
*CCDC80 protein			
*Cell adhesion molecule 1			
Ceruloplasmin		catalytic activity	macromolecular complex; membrane
Chaperone activity of bc1 complex-like, mitochondrial			cell part; membrane
*Chromosome 14 open reading frame 166 ortholog	cellular process		
Chromosome 20 open reading frame 96 (Fragment)			
Clusterin		binding	cell part; extracellular region; organelle
CMP-N-acetylneuraminate-poly-alpha-2,8-sialyltransferase			
Coagulation factor IX			extracellular region
*Coagulation factor V			
*Coagulation factor XII	metabolic process	catalytic activity	extracellular region
*Coagulation factor XIII A chain	metabolic process	catalytic activity	
*Cohesin subunit SA-3	cellular process	binding	
*Complement C1s subcomponent		catalytic activity	extracellular region
Complement C3	cellular process; metabolic process; response to stimulus	binding; catalytic activity	
Complement C3	cellular process; metabolic process; response to stimulus	binding; catalytic activity	
complement C3 (Fragment)	cellular process; metabolic process;	binding; catalytic activity	

	response to stimulus		
Complement C5a anaphylatoxin	cellular process; metabolic process; response to stimulus	binding; catalytic activity	
Complement C8 alpha chain			
Complement C8 beta chain			
complement component 4A	cellular process; metabolic process; response to stimulus	binding; catalytic activity	
*Complement component C6			
Complement component C7			
Complement component C9			
Complement factor B			
Complement factor H			
Complement factor I			
*Conglutinin	biological regulation; cellular component organization or biogenesis; cellular process; localization; multicellular organismal process	binding	cell part; extracellular region; organelle
Corticosteroid-binding globulin			extracellular region
C-reactive protein			
C-type lectin domain family 1 member A			
*Cumulus cell-specific fibronectin 1 transcript variant	biological adhesion; cellular process	binding	extracellular region
*Cytochrome P450 20A1			
*Cytohesin 1 (Fragment)			
*Cytokine receptor like factor 3		binding	cell part; organelle
*DDB1 and CUL4 associated factor 5	cellular process; metabolic process	binding; catalytic activity	
DEAH-box helicase 16	cellular process; metabolic process	catalytic activity	cell part; macromolecular complex; organelle
*Delta-like protein	developmental process		
*Dolichyl-diphosphooligosaccharide--protein glycosyltransferase subunit 1	cellular process; metabolic process	catalytic activity	cell part; macromolecular complex; membrane; organelle

*Dpy-19 like 4 (Fragment)	cellular process; metabolic process	catalytic activity	cell part; membrane; organelle
*DUOXA1 protein			
*Dynein axonemal heavy chain 11	cellular process	binding; catalytic activity	cell part; macromolecular complex; organelle
*Dynein heavy chain domain 1	cellular process	binding; catalytic activity	cell part; macromolecular complex; organelle
Dystonin	cellular process	binding; structural molecule activity	cell part
*E3 ubiquitin-protein ligase CHIP			
*Endophilin-A2			
*Engulfment and cell motility 1	cellular process	binding	
*Epidermal growth factor receptor kinase substrate 8-like protein 1	biological regulation; cellular component organization or biogenesis; cellular process		Cell part; membrane; organelle
*Factor XIIa inhibitor precursor			extracellular region
*Family with sequence similarity 81 member A			
*Fas activated serine/threonine kinase	cellular process		
Fetuin-B	biological regulation	catalytic activity	
*FGG protein	biological adhesion	binding	extracellular region
*Fibrinogen alpha chain			
*Fibrinogen beta chain	biological adhesion; cellular process	binding	extracellular region
*Fibulin-1	cellular process; developmental process	binding; structural molecule activity	extracellular region; extracellular matrix
*Filamin B			
Fragile X mental retardation syndrome-related protein 2	cellular component organization or biogenesis; cellular process; developmental process; localization; metabolic process; multicellular organismal process	binding; translation regulator activity	cell part; macromolecular complex; organelle; synapse
G1/S-specific cyclin-D1	biological regulation; cellular component organization or biogenesis; cellular process; metabolic process	binding; catalytic activity	cell part; macromolecular complex; organelle

*Gametocyte-specific factor 1-like			
*Gasdermin B	cellular process; developmental process; response to stimulus	binding	
Gelsolin	cellular component organization or biogenesis; cellular process	binding; structural molecule activity	cell part; organelle
Glutathione peroxidase	immune system process; metabolic process; response to stimulus	antioxidant activity; catalytic activity	
Glutathione S-transferase			
*Haptoglobin	metabolic process	catalytic activity	extracellular region
HAUS augmin like complex subunit 3	cellular component organization or biogenesis; cellular process		cell part; organelle
*HEAT repeat containing 5B			
*HECT domain E3 ubiquitin protein ligase 2			
*HECT, UBA and WWE domain containing 1, E3 ubiquitin protein ligase	cellular process; metabolic process		cell part
*Hemoglobin subunit alpha			
*Hemoglobin subunit beta			
Hemopexin			extracellular matrix
Hepatocyte growth factor activator preproprotein (Fragment)	metabolic process	catalytic activity	extracellular region
Histidine-rich glycoprotein	biological regulation	catalytic activity	
Histidine-rich glycoprotein (Fragments)	biological regulation	catalytic activity	
*Homeobox D3			
*Immunoglobulin lambda-like polypeptide 1	immune system process		
*Immunoglobulin lambda-like polypeptide 1 (Fragment)	immune system process		
Importin 8	biological regulation; cellular process; localization; response to stimulus	transporter activity	cell part; organelle
*Inhibin alpha chain	cellular process; developmental process; metabolic process; response to stimulus	binding	extracellular region
Insulin like growth factor binding protein	biological regulation;	binding	

acid labile subunit(IGFALS) (Fragment)	cellular component organization or biogenesis; cellular process; developmental process; locomotion; multicellular organismal process; response to stimulus		
Inter-alpha-trypsin inhibitor heavy chain H1	metabolic process	binding; catalytic activity	
Inter-alpha-trypsin inhibitor heavy chain H2	metabolic process	binding; catalytic activity	
Inter-alpha-trypsin inhibitor heavy chain H3	metabolic process	binding; catalytic activity	
Inter-alpha-trypsin inhibitor heavy chain H4	metabolic process	binding; catalytic activity	
*Keratin, type II cytoskeletal 7			
Kinesin family member 13B	cellular process; metabolic process	binding; catalytic activity	cell part; organelle
Kininogen-1	biological regulation	catalytic activity	
Kininogen-2	biological regulation	catalytic activity	
*KRAS proto-oncogene, GTPase	biological adhesion; cellular process; localization; multicellular organismal process	binding; catalytic activity	
*Kruppel like factor 17 (Fragment)	cellular process; metabolic process	binding	cell part; organelle
Leucine rich repeat containing 4C			
*Leucine rich repeat kinase 2			
Leucine-rich alpha-2-glycoprotein 1			
Leucine-rich single-pass membrane protein 1			
L-lactate dehydrogenase B chain	metabolic process	catalytic activity	
*Lumican	biological regulation; cellular component organization or biogenesis; cellular process; developmental process; locomotion; multicellular organismal process; response to stimulus	binding	
*Lysine methyltransferase 2C (Fragment)			
Maltase-glucoamylase	metabolic process	catalytic activity	

Mitogen-activated protein kinase kinase kinase 5	biological regulation; cellular process; metabolic process; response to stimulus	catalytic activity; signal transducer activity	
*NADH dehydrogenase [ubiquinone] 1 alpha subcomplex assembly factor 4			
*NADH dehydrogenase [ubiquinone] 1 beta subcomplex subunit 11, mitochondrial		catalytic activity	
NADPH-dependent diflavin oxidoreductase 1		binding; catalytic activity	cell part
*NIMA (Never in mitosis gene a)-related kinase 2			
Nuclear factor interleukin-3-regulated protein	cellular process; metabolic process; rhythmic process	binding	cell part; organelle
Olfactory receptor			
*Ornithine decarboxylase 1	biological regulation; cellular process; metabolic process	catalytic activity	cell part
Pantetheinase	cellular process; metabolic process	catalytic activity	
*Pantothenate kinase 3			
Paraoxonase 1		catalytic activity	
Peptidoglycan recognition protein 2 (Fragment)			
Phosphatidylinositol-3,4,5-trisphosphate dependent Rac exchange factor 2	cellular process; metabolic process; response to stimulus	binding; catalytic activity	membrane
*Phosphoglycolate phosphatase	cellular process; metabolic process	catalytic activity	cell part
Pigment epithelium-derived factor			extracellular region
*Plasma serine protease inhibitor			extracellular region
Plasminogen		catalytic activity	
Primary amine oxidase, liver isozyme			
Progesterone immunomodulatory binding factor 1			
Protein AMBP			
Protein HP-20			
Protein HP-25 homolog 1			
Protein HP-25 homolog 2			

Protein phosphatase 1 regulatory subunit 37	immune system process; metabolic process; response to stimulus	binding	
Prothrombin	metabolic process; response to stimulus	catalytic activity	
*Protocadherin Fat 2 precursor (Fragment)	developmental process		
PSMD1 protein	cellular process; metabolic process	catalytic activity	cell part; macromolecular complex; organelle
*PTPRR protein			
Pyridine nucleotide-disulfide oxidoreductase domain-containing protein 1		catalytic activity	
*Regulating synaptic membrane exocytosis 2 (Fragment)	biological regulation; cellular process; multicellular organismal process	binding	cell part; organelle; synapse
Regulating synaptic membrane exocytosis 3	biological regulation; cellular process; multicellular organismal process	binding	cell part; organelle; synapse
RELT, TNF receptor			
Retinoic acid induced 1	cellular process; metabolic process	binding	cell part; organelle
Retinol-binding protein 4	localization		
Ribosomal protein S6 kinase C1	biological regulation; cellular process; metabolic process; response to stimulus	catalytic activity	
*Serglycin (Fragment)			
Serine peptidase inhibitor, Kazal type 5		binding	
Serotransferrin		binding	cell part; macromolecular complex; membrane; organelle
Serotransferrin		binding	cell part; macromolecular complex; membrane; organelle
Serpin A3-2			extracellular region
Serpin A3-4			extracellular region
Serpin A3-7			extracellular region
Serpin A3-8			extracellular region
*Serpin family E member 2			extracellular region

*Serpin peptidase inhibitor, clade A (alpha-1 antiproteinase, antitrypsin), member 3			extracellular region
Serpin peptidase inhibitor, clade A (Alpha-1 antiproteinase, antitrypsin), member 7			extracellular region
SERPINA10 protein			extracellular region
SERPIND1 protein			extracellular region
*Serum albumin	localization		
*SH3 domain and tetratricopeptide repeats 1			
SHBG protein			
*Sodium/glucose cotransporter 1-like (Fragment)	cellular process; localization	transporter activity	
Solute carrier family 12 member 7 (Fragment)	biological regulation; cellular process; localization; multicellular organismal process	transporter activity	
*Sphingomyelin phosphodiesterase 5 (Fragment)			
*SPHK1 interactor, AKAP domain containing (Fragment)	biological regulation; cellular process; response to stimulus	binding	cell part
Superoxide dismutase [Cu-Zn]	cellular process; response to stimulus	antioxidant activity; binding; catalytic activity	cell part; extracellular region
*Suppressor of G2 allele of SKP1	biological regulation; metabolic process		
*Synaptonemal complex protein 1			
*Synaptotagmin 12	biological regulation; cellular component organization or biogenesis; cellular process; multicellular organismal process	binding	membrane
*TBC1 domain family member 4	cellular component organization or biogenesis; cellular process; localization; metabolic process	binding; catalytic activity	cell part
Tetranectin	multicellular organismal process		extracellular region
*Titin	cellular component organization or biogenesis; cellular process;	binding; structural molecule activity	cell part; macromolecular complex;

	developmental process; multicellular organismal process		organelle
*Trans-2-enoyl-CoA reductase, mitochondrial	cellular process; metabolic process	catalytic activity	cell part; organelle
Transcription elongation factor A N-terminal and central domain-containing protein 2	metabolic process	binding	
*Transcription factor 7-like 2			
*Transcription initiation factor TFIID subunit (Fragment)	cellular component organization or biogenesis; cellular process; metabolic process	binding; catalytic activity	cell part; macromolecular complex; organelle
*Transmembrane protein 186			
*Transthyretin	cellular process; metabolic process		
Tubulin beta-6 chain (Fragment)	cellular component organization or biogenesis; cellular process	binding; structural molecule activity	cell part; organelle
Tyrosine-protein kinase			
Ubiquitin carboxyl-terminal hydrolase 2			
*Ubiquitin protein ligase E3 component n-recognin 4			
*Uncharacterized protein			
*Uncharacterized protein			
Uncharacterized protein	cellular process; metabolic process	catalytic activity	
Uncharacterized protein (Fragment)	cellular process; metabolic process; response to stimulus	binding; catalytic activity	
*Uncharacterized protein (Fragment)			
Uncharacterized protein (Fragment)			
Uncharacterized protein (Fragment)			
Uncharacterized protein (Fragment); (Ig-like protein)	biological regulation; cellular component organization or biogenesis; cellular process; immune system process; localization; metabolic process; multicellular organismal process; response to stimulus	binding	extracellular region; macromolecular complex; membrane
Uncharacterized protein (Ig-like protein)	immune system process		

Uncharacterized protein (Ig-like protein)	immune system process		
Utrophin	cellular component organization or biogenesis		
*Vacuolar protein sorting-associated protein 28 homolog	cellular process; localization; metabolic process	binding	cell part; macromolecular complex; membrane; organelle
*Versican core protein	developmental process; multicellular organismal process		extracellular region; extracellular matrix
*Vitamin D-binding protein	localization		
*Vitamin D-binding protein	localization		
Vitronectin	cellular process		
Von Willebrand factor A domain containing 3B			
*Von Willebrand factor A domain containing 5B1			
Xin actin binding repeat containing 2	cellular process	structural molecule activity	cell part
Zinc-alpha-2-glycoprotein			extracellular region
Zinc finger CCHC domain-containing protein 7			
*Zinc finger protein 618	metabolic process	binding	
*Zinc finger SWIM-type containing 3 (Fragment)			
*Zona pellucida binding protein 2			

Appendix 3

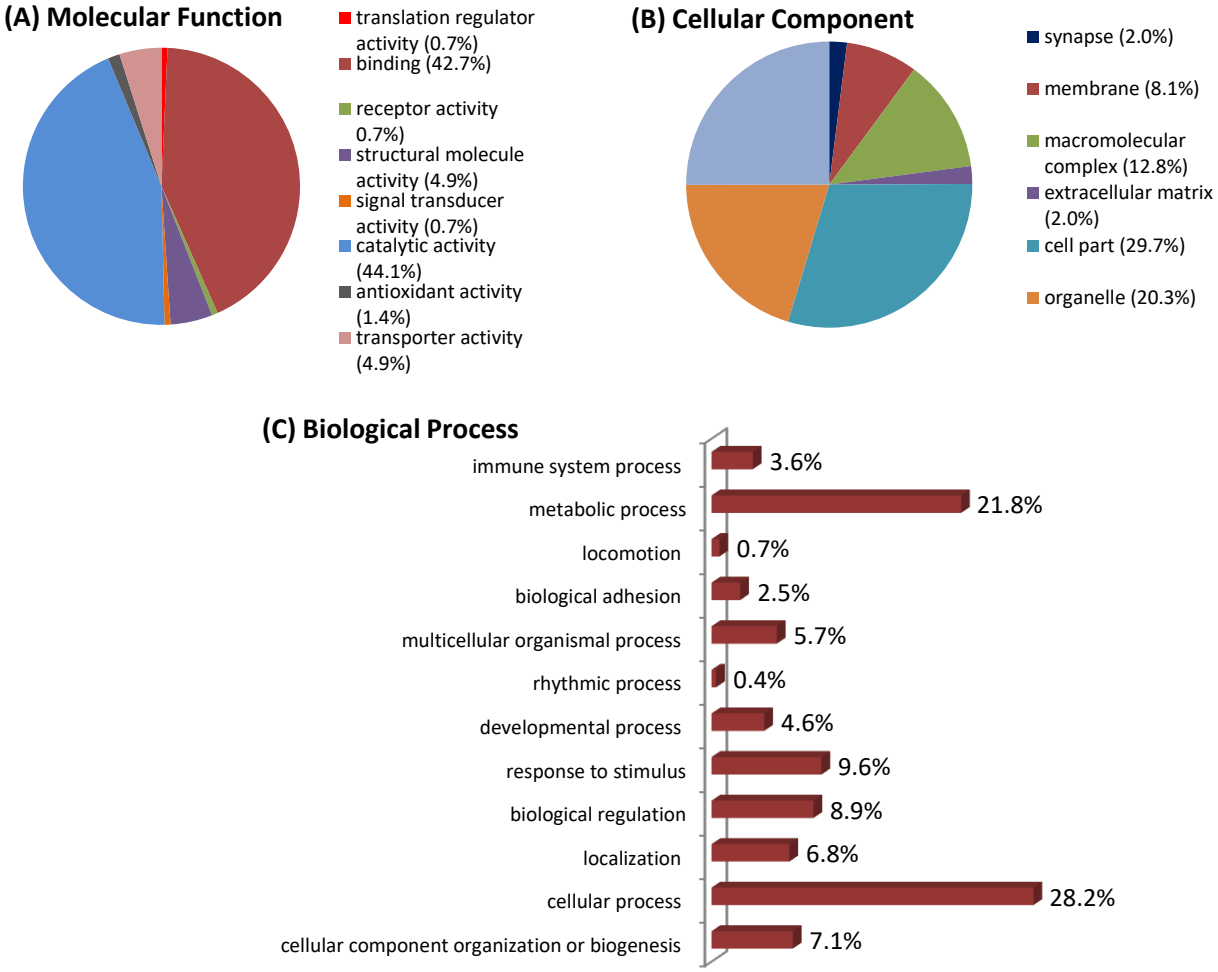

PANTHER analysis of all identified proteins (231 in total) in bovine plasma (PL) and follicular fluid (FF) containing low and high pre-ovulatory E2. Proteins were classified according to (A) Molecular Function (B), Cellular Component, and (C) Biological Processes. The percentages in the different categories are comparable to that from the analysis of only proteins showing expression changes.